IMPROVED DESICCANT COATINGS FOR HEAT AND WATER VAPOUR TRANSFER ON THE MATRIX SURFACES OF AIR-TO-AIR REGENERATIVE WHEELS

A Thesis Submitted to the

College of Graduate Studies and Research

in Partial Fulfillment of the Requirements

for the degree of Master of Science

in the Department of Chemical and Biological Engineering

University of Saskatchewan Saskatoon

By

John Bolster

PERMISSION TO USE

In presenting this thesis in partial fulfillment of the requirements for a Postgraduate degree from the University of Saskatchewan, I agree that the Libraries of this University may make it freely available for inspection. I further agree that permission for copying of this thesis in any manner, in whole or in part, for scholarly purposes may be granted by the professor or professors who supervised my thesis work or, in their absence, by the Head of the Department or the Dean of the College in which my thesis work was done. It is understood that any copying or publication or use of this thesis or parts thereof for financial gain shall not be allowed without my written permission. It is also understood that due recognition shall be given to me and to the University of Saskatchewan in any scholarly use which may be made of any material in my thesis.

Requests for permission to copy or to make other use of material in this thesis in whole or part should be addressed to:

Head of the Department of Chemical Engineering

University of Saskatchewan

Saskatoon, Saskatchewan S7N 5A9

ABSTRACT

Air-to-air energy recovery wheels are now widely used in industry and buildings; however, the effectiveness of water vapor exchange in these regenerative wheels appears to be much lower than may be economically feasible. The purpose of this research is to investigate the feasibility of using agglomerated desiccant particle coatings to improve the performance of regenerative wheels used in HVAC air-to-air heat and moisture exchange and energy recovery applications. Desiccant particles coated on wheels lose most of their water vapor sorption capacity due to the method of coating.

Desiccant agglomerates can be made by mixing starch, fine silica gel particulate, and water within an agglomerating device. The desiccant particle agglomerating process improves the desiccant mass transfer properties by increasing the overall surface area of desiccant particles; and also by creating a much rougher surface that can increase the likelihood of turbulent flow, and therefore, increasing the overall mass transfer rates.

The industrial desiccant coating process involves submerging the desiccant into a coating agent and then applying this mix to the substrate or the matrix of the energy wheel. This process was improved in this research by ensuring the particles are applied after the coating agent is applied to ensure that the agglomerates or desiccant particles are not submerged by the coating material.

Because testing energy wheels under steady state operating conditions has proved to be difficult, time consuming and costly in the past, a small parallel flow test cell is used to measure the transient response of coated substrate aluminum sheets after a step change in the inlet air humidity or temperature. Using a previously developed theoretical model, the time constants for these inlet step change responses are then used to predict the sensible and latent effectiveness of

a regenerative energy wheel coated with the same agglomerated particles, which is rotated at a known operating speed and wheel face velocity. When the new desiccant coatings are used, it is shown that the latent heat effectiveness for a typical wheel could be up to 85%.

It is found that the steady state air flow pressure drop readings for the test cell shows that agglomerated particles coated on the surfaces within the test cell implies some transitional turbulent flow behavior compared to similar substrate surfaces coated in a conventional manner with desiccant particles (e.g. up to 60% higher pressure drop at a channel Reynolds number of 300) in the same test cell. This implied enhanced turbulence flow friction factor in the test cell suggests a somewhat similar enhancement for increased mass and heat transfer coefficients for the test cell or coated wheel matrices.

The transient results for humidity step changes for air flow through the test cell reveals that the adsorption and desorption response time constants are much larger for the agglomerated coated substrate surfaces than the conventional industrial coated surfaces. These data imply much higher moisture or latent heat effectiveness values for wheels coated with agglomerated particles. When the new desiccant coatings are used, it is shown that the latent heat effectiveness for a typical wheel could be better than 80% or 20% higher than currently available typical energy wheels.

With improvements to the desiccant particle agglomerating process, desiccant coating process and particle coating and testing methods, this thesis shows that significant improvements may be practical for the design, testing and operation of regenerative heat and moisture exchange wheels.

ACKNOWLEDGEMENTS

My sincere gratitude goes to my supervisors, Professor Robert W. Besant and Professor Richard W. Evitts. Without their support, knowledge and experience none of this work would have been possible. Their patience and guidance will forever be remembered.

I would also like to thank my committee members for your suggestions and comments on my thesis.

In addition, I would like to thank all of my family and friends for putting up with me while researching and writing this thesis; especially my friend, Aaron Florizone; my wife, Meera Singh; and my parents, Cheryl & Larry Bolster.

DEDICATION

I would like to dedicate this thesis to my loving wife, Meera Singh, without her support this would not have been possible.

TABLE OF CONTENTS

LIST OF TABLES

LIST OF FIGURES

NOMENCLATURE

Latin Letters

A	Place holder constant	
Å	Angstrom	$(10)^{-10}$ meters
B_x or $B(x)$	Bias uncertainty of x	
C	Celsius	
c_p	Specific heat capacity	J/(kg·°C)
N	Number of transfer units for convective heat or moisture transfer	
Pa	Pascals	$kg/(m \cdot s^2)$
P_x or $P(x)$	Precision uncertainty of x	
R^2	Coefficient of determination	
Re	Reynolds number	
t	Time	seconds, s
T	Temperature	°C
U_x or $U(x)$	Uncertainty of x	
v	Face velocity	m/s
V	Voltage reading from the humidity sensors	volts
W	Humidity ratio	$kg_{water}/kg_{dry\ air}$
W^*	Normalized humidity ratio	Dimensionless
W_t^* or $W^*(t)$	Normalized humidity ratio at any time t	Dimensionless
X	Weighting factor for moisture time constants	

Greek Letters

º	Degrees	
Δ	Change in or difference	
ΔW_t	Change in outlet humidity ratio or moisture content at any time t	
ΔW_M	Maximum change in outlet humidity ratio or moisture content for the step change	
ε	Effectiveness or energy wheel effectiveness	
ω	Angular velocity or wheel speed	Radians/s
Ψ	Product of the time constant and angular velocity	$\Psi = \tau\omega$
τ	Time constant	s
τ_m^*	Moisture time constant or the combined final of the weighted moisture time constants	s
Θ	Normalized temperature response	Dimensionless

Subscripts

1 – 2 , k	Integer indexing for time constants or variable for indexing
A	Air or in air
Ads or Adsorption	For or from the adsorption response measurement
CF	Counter Flow arrangement
Des or Desorption	For or from the desorption response measurement
FD	Fully Developed
Final	At the outlet after reaching steady state, i.e. at $t \to \infty$
∞	At infinite time or at steady-state
initial, or 0	At the outlet initially, or at $t = 0$
inlet or in	At the inlet
l	Latent or to do with latent heat energy
m	Moisture or for moisture transfer
M, max	Maximum
min	Minimum
outlet or out	At the outlet
PF	Parallel Flow arrangement
s	Sensible or to do with sensible heat energy
t	At any time t

Other Term Definitions

Term	Definition
Bonding Agent / Bonding Material	Refers to the material used to hold the silica gel within the agglomerates together (i.e. the starch/water solution that is used)
Coating Agent / Coating Material	Refers to the material used to hold the agglomerates to the coating substrate (i.e. the latex paint that is used)
Coating Substrate / Coated Material	Refers to the material that is being coated (i.e. the matrix surface of the energy wheels, or the strips of aluminum foil that were used)

LIST OF ABBREVIATIONS

ASHRAE	American Society of Heating, Refrigerating and Air-Conditioning Engineers
BC	Blank Coating with just latex paint on aluminum foil
CC	Coarse Coating with latex paint and larger agglomerates of silica gel and starch on aluminum foil
FC	Fine Coating with latex paint and finer agglomerates of silica gel and starch on aluminum foil
FCHS	Fine Coating with latex paint and finer agglomerates of silica gel and starch on aluminum foil with Half the Sheets
IAQ	Indoor Air Quality
IC	Industrial Coating of binding agent and silica gel particulates on aluminum foil
LPM	Litres Per Minute
MC	Moisture Content
RH	Relative Humidity
RPM	Rotations Per Minute
SEM	Scanning Electron Microscope

CHAPTER 1 :
INTRODUCTION

There are many different kinds of air-to-air energy recovery systems such as: heat pipes, run-around heat exchangers, thermosiphons, fixed heat and energy plate exchangers, rotary heat and energy (enthalpy) wheels and run-around membrane energy exchanger systems. The latter three may recover both latent and sensible heat energy, whereas the others just recover sensible heat. The difference between the two terms, sensible and latent, do not change the type of energy as they are both heat but sensible heat occurs with a change in temperature whereas latent heat occurs due to a phase change (i.e. due to the heat of vaporization or heat of adsorption). Regenerative energy (enthalpy) wheels now have a large fraction of the market for new commercial buildings for which they mostly recover heat and moisture from exhaust air. Because the volume of ventilation air brought into buildings is large (e.g. about 10 L/s per person or more than $3x10^6$ kg per year per person), it is important to have very effective energy recovery systems to reduce auxiliary energy consumption while maintaining good thermal comfort conditions and high Indoor Air Quality (IAQ) for building occupants. Engineers are concerned with IAQ because IAQ has been shown to have a direct correlation to workplace comfort, health and productivity for occupants. Since people spend about 90% of their time indoors for those in industrial societies, energy recovery using exhaust air is a societal concern (ASHRAE, 2009, 2011a, 2011b). Although there are a wide variety of ambient weather conditions in which buildings operate there is a fairly narrow range of interior conditions for air temperature, humidity and IAQ that lead to increased occupant comfort and productivity (ASHRAE, 2009).

1.1 RESEARCH MOTIVATION AND GOAL

The purpose of this research is to develop a method for desiccant coating that will increase the latent heat energy transfer rate of energy wheels. Energy wheels transfer heat and water vapor between supply and exhaust air while limiting the transfer of air contaminants to a small fraction. In the past energy wheels have not been designed and manufactured for high latent effectiveness, meaning that the desiccant coatings do not transfer a large fraction of water vapor content change available between the ventilation supply air inlet and outlet exhaust air (e.g. latent effectiveness values of 60 to 65% are common for energy wheels). Improving the design and method of desiccant coating on the internal coated surfaces of energy wheels is the main goal of this research.

The physics of energy recovery wheel regeneration is well understood and accurately modeled for energy recovery, but little is known about the design of better desiccant coatings for these wheels. It is the hypothesis of this research that the materials, particles sizes, design and processes for desiccant coating for regenerative energy wheels can be improved to increase the latent effectiveness compared to currently available technology.

1.2 LITERATURE REVIEW

Many areas of engineering were investigated during the course of this research. The following sections present an overview of the research related to desiccant coating and energy wheel performance. Currently fine silica gel or molecular sieve desiccant particles (e.g. 1 to 10 μm size) are used for energy wheel coatings. These particles are immersed or imbedded in a bonding liquid before drying on the substrate coated surface used for the wheel matrix so it is important to understand the different methods of grinding, sizing and agglomerating particles that will very rapidly transfer water vapor in the 1 to 1.5 seconds of time it takes to rotate a

wheel 180°. Current desiccant coatings appear to have their desiccant particles obstructed by coating material and many layers of particles. To help explain why an agglomerated desiccant particle coating was chosen for this research consideration, the relationship between the availability of the exposed desiccant surfaces, diffusion time delays, and convective mass transfer coefficients is needed. In past research energy wheel sensible and latent effectiveness was measured by following the current ASHRAE Standard 84–2008 test procedure (ASHRAE, 2008). Currently these tests are done for certifying the performance of most air-to-air energy recovery devices at a cost of about $10,000 US per test. To obtain laboratory test data while utilizing less resources and time, a new transient test cell and apparatus is used. This transient testing apparatus was used to determine the step change response time constants of the coatings. It will be shown that these time constants for the test cell are directly related to the energy wheel effectiveness when it is operated at a selected rotary speed and face velocity.

1.2.1 MICRON SIZED PARTICULATE

Fine micron sized silica gel particles are a necessary part of the coating process that is being developed because silica gel particles are only available in the 1 to 2 mm size. With them it is possible to significantly increase surface area per unit mass by an order of magnitude, which helps to increase response time and transient sorption moisture capacity for each particle. Agglomerated particles also implies very large pores between bonded particles and rapid water vapor diffusion (Rhodes, 1981).

Grinding fine particles or producing silica gel of very small particle diameter is difficult. According to Ulrich and Vasudevan (2004), there are a few technologies capable of grinding fine powders: Tumbling Ball Mill; Vibrating or Stirred Ball Mill; High Speed Hammer; and Fluid Energy. Due to budget limitations, not all of these are feasible for this investigation

Ball mills are proven to be cost effective means to produce fine powders. Fine micron sized particles are apt to stick together through electrostatic and strong cohesive forces between primary particles. Bulk micron sized particles have a high external particle surface area to volume ratio (Yao, Guangsheng, Fei, & Jun, 2002). Grinding them in a rotating drum or ball mill helps to counter electro-static forces because of the shearing movement among particles (Huang, Zhang, & Zhu, 2009). Circulating powder in a ball mill mixes the air in the drum with the particles and this fluidizes the powder (Huang, Zhang, & Zhu, 2010). The size of grinding media is an important part of the grinding efficiency and the capacity of tumbling ball mills. If the balls are too small they are unable to break the particles that come in contact with them (Bond, 1958; Choi, 2001; Kano & Saito, 1998). Wet ball milling (Mi, 1997) and wet sieving both can help with the development and classification of very tiny silica gel particles, but it has been observed that this method leads to particle caking when the particles are later dried.

Creating tiny agglomerates that are structurally stable during rapid cyclic dry-moist conditions (i.e. 2 to 3 seconds cycle time) is required for this proof of concept study. Starch granules are very small (1 to 150 μm in diameter), tapioca starch, in particular, ranges from 1 to 3 μm (Whistler & Daniel, 2000). When heated to (58.5ºC to 70ºC) the starch gelatinizes (Whistler & Daniel, 2000) and can be used to create a bond between silica gel particles to form agglomerates. It was found that that for large silica gel particles only a small fraction of the internal surface area of silica gel pores is exposed to water and it occurs very slowly (Sun & Besant, 2005); so by increasing the external surface area by grinding and agglomerating these small particles into larger ones it should hasten its moisture absorbance speed for water vapor diffusion within each agglomerated particle.

1.2.2 DESICCANT COATINGS

Desiccant coatings can be used for a variety of applications, including coating ceiling tiles in order to help maintain a steady indoor air relative humidity. Although flat plate membranes are used for moisture transfer in some air-to-air energy exchangers (L.-Z. Zhang, Liang, & Pei, 2008; L.-Z. Zhang & Xiao, 2007), the major use of desiccant coatings is for regenerative wheels. The two most commonly used desiccants are silica-gel and molecular sieve. Most of the details that go into the process of coatings regenerative wheels are proprietary. It has, however, been observed that smaller particle sizes tend to make for a more effective coating; and that the coating material used in the coating process itself inhibits much of the moisture transfer of the desiccant particle (Shang & Besant, 2008). Isotherms for silica gel and molecular sieve, as well as steady-state enthalpy wheel data suggest that silica gel will usually outperform molecular sieve desiccants for regenerative energy (enthalpy) wheel applications (Wang, Besant, & Simonson, 2005).

Shang and Besant (2009a, 2009b), after testing and examining some of the currently used silica gel and molecular sieve desiccant coatings, concluded that it is very likely that the desiccant particles are being limited by being completely submerged in the coating agent during the bonding process. Therefore, the particles near the air-particle interface should be able to respond more quickly to a change in vapor pressure than those several particle layers away from this interface, and by increasing the amount of particle surface area at this interface it should greatly improve the performance of the desiccant coating. Agglomerated particles would greatly improve the surface area of the particles while also decreasing the total amount of the particles being submerged by the coating agent of the coating.

Desiccant particles are internally porous with pore diameters 3 to 100Å and have large internal surface areas relative to the external surface area (e.g. 100 to 10000 times bigger depending on the type of desiccant and particle size). Some desiccants (e.g. molecular sieves) have small pore diameters (e.g. 3 to 10 μm) and others (e.g. silica gel 10 to 100 μm) large. A water molecule has an effective diameter of about 2.8 A so it will diffuse into and penetrate the inner particle's large pores and attach to inner surfaces but the time delay for surface diffusion in small pores will be important when the time delay is longer than 1 second because the energy wheels that rotate at 20 rpm or higher and only have around 1.5 seconds to transfer water vapour. In order to make the desiccant coating more effective for rapid sorption processes the particle should small to give a large surface to volume ratio and the particle pore sizes should be large with respect to the water molecule diameter (e.g. 10 times or more bigger). The use of particle coating material that obstructs the internal pores will reduce the effective internal surface area available for sorption and thus increase the time delay for transient sorption processes as it occurs in most regenerative wheels. Therefore, agglomerated particles will limit the amount of contact the coating agent has with the particles and particles can be bonded in such a way to reduce the amount of obstruction for the water molecule diffusing into and out from the inner pores of the particles. Increased sorption rates may be achieved using agglomerated particles bonded by a single thin layer of coating material placed first on the substrate followed by applying the agglomerated particles onto the coating material or glue, as is presented by this research.

There are other factors that also affect desiccant coating performance due to the deterioration of the coating, such as frosting and dissolution. At very cold ambient air temperatures frosting can be a problem for energy wheels (e.g. below −30ºC) as it will cause uncontrolled

condensation and freezing that can damage the desiccant coating of a wheel (Simonson & Besant, 1998); therefore, it is desirable to create a coating that has potential to avoid deterioration due to frosting and condensation. In the past salts have been used for desiccant coating applications on wheel surfaces. But, due to the salt dissolution that occurs while exposed to high humidity levels, the salt based coatings will deteriorate.

Other coatings or desiccant materials have been investigated including aerogel. Due to its very large surface area per unit mass, aerogel could prove to be a very useful desiccant for some applications, but it is structural frail or weak so it is not likely to be used.

1.2.3 ENERGY WHEEL SORPTION

Energy (enthalpy) wheels typically rotate at 20 to 30 rpm, so the time available for transferring heat and water vapour is only about 1.0 to 1.5 seconds for each flow channel before the wheel rotates 180º and the flow channel is exposed to air flow in the opposite direction at a different temperature and humidity. Equilibrium isotherms of moisture content versus relative humidity for substances don't reveal anything about the rate of absorption or desorption for water vapour. The rates of absorption and desorption depend on the desiccant type, particle size, internal pore size of the particle, coating material and method, and specific surface area of the coatings. Smaller particles increase the particle external surface area to mass ratio, larger internal pore sizes allows for a more rapid diffusion of H_2O molecules into and out of the particle; i.e. silica gel as a desiccant will respond more rapidly than molecular sieve desiccants. A large specific area ratio means a large internal and external surface area per unit dry mass or substrate surface area from which H_2O molecules can attach to surfaces by adsorption or detach by desorption.

The flow channels in currently available energy and dehumidifier wheels are essentially aerodynamically smooth and with Reynolds numbers for the typical range of 600 to 1600. So the flow is laminar in typical wheels. However, for hydraulically or aerodynamically rough surfaces in the air channels the flow would tend to be turbulent for these Reynolds numbers. When this happens the friction factor is no longer that which occurs for laminar flow. That is, it can be 2 to 4 times larger at the same Reynolds number (Colebrook & White, 1937; H. Zhang, Faghri, & White, 1996). This increased friction factor for air flow through the wheel matrix is determined using the pressure drop across the wheel and it implies much larger convective heat and mass transfer coefficients at the same flow rate as that for laminar flow. That is, the convective heat and mass transfer coefficients can increase by a factor of 2 to 3 (Webb & Kim, 2005). This convection benefit is much more important than the pressure drop losses for energy exchangers.

1.2.4 Transient Response and Effectiveness From Energy Wheels

Desiccant coatings are used on energy (enthalpy) wheels, sometimes referred to as rotary regenerative heat and moisture exchangers, and are operated between room and outdoor air temperatures. Desiccant dryer wheels, sometimes referred to as desiccant wheels or rotary dryers, are regenerated at elevated temperatures (100ºC to 200ºC). These wheels are constructed by winding a corrugated material, such as aluminum for enthalpy wheels or plastic for dehumidifier wheels, around a core, forming a porous matrix, through which, the air streams to pass through first at room conditions in one direction and then at outdoor or regenerated air conditions in a counter-flow direction. Enthalpy wheels transfer both heat and moisture between the supply air and exhaust air, while desiccant dryer wheels transfer mainly moisture. Shang and Besant showed that it is important to keep the pore channel sizes consistent or the wheel effectiveness degrades due to uneven air flow distribution (Shang & Besant, 2005a, 2005b).

Testing energy wheels under steady state operating conditions has proved to be difficult, time consuming and costly; however, it is feasible to use a simple parallel flow test and use the transient data to predict the sensible and latent effectiveness of the same wheel at a known operating speed (Abe, Simonson, & Besant, 2006a, 2006b). Equations of heat and moisture transfer can then be used to extrapolate data for similar energy wheels and can be used in the design of the wheels (Abe, Simonson, & Besant, 2006b).

The effectiveness of the design of the wheel also includes the design and effectiveness of the desiccant coating. An analysis was done to determine wheel dynamic characteristics from measured responses of sensors alone and sensors downstream of an energy wheel, if the response time of the wheel is less than the response time of the sensor then that sensor cannot be used to measure transient characteristics of the wheel (Abe, Wang, Simonson, & Besant, 2006; Wang et al., 2005) without modifying the results through analysis. The methods of extrapolation and correlation with humidity wheels and humidity and temperature sensor measurements (Shang & Besant, 2009c), can help for the designing and testing of a novel coating without need for steady-state operating condition tests.

The latent and sensible effectiveness obtained through transient testing has been shown to directly coincide with the same wheel's effectiveness data taken from the steady state testing conditions of ASHRAE Standard 84 (2008), as was shown in recent research by Shang and Besant (2005a, 2005b, 2006a, 2006b, 2008, 2009a, 2009b, 2009c), Wang et al. (Wang, 2005; 2005; 2006), and Abe et. al (Abe, 2005; 2006a, 2006b; 2006a, 2006b; 2006). The transient testing apparatus used to determine the time constants presented by these authors is the same as that presented in this research except a testing cell was used in place of an energy wheel. The benefits of using just a test cell rather than a full energy wheel means that coatings can be

developed and compared prior to manufacturing whole wheels. Thus only coatings that have shown dramatic improvements need to be manufactured and tested via the steady state ASHRAE Standard 84 (2008) method and in so doing much improve the overall latent effectiveness and quality of the energy wheels. This new method of testing and developing coatings could lead to rapid improvement of desiccant coatings whilst saving time and money for the manufacturers.

1.3 THESIS OBJECTIVES

The overall objective of this project is to show that agglomerated desiccant coatings will improve the latent and total effectiveness of regenerative energy (enthalpy) wheels.

The main hypothesis of this research is that micron-sized silica gel agglomerates will outperform, in terms of absorbance and desorbance rate and capacity, current particle systems used in desiccant coatings. This will be proved using experimentally obtained moisture transfer and heat transfer time constants, with response data accurately measured over a range of relative humidity step changes, and face velocities.

1.4 SCOPE AND METHODOLOGY OF PROJECT

The current method of coating desiccant particles on to the substrate surface of regenerative wheels diminishes the equilibrium isotherm water vapour sorption mass transfer by a factor of five compared to the isotherm for the particles alone. By using agglomerates that are bonded on one particle side to the substrate surface and are not completely submerged by the coating agent, the contact area of the desiccant and coating agent being coated to the substrate will be significantly smaller. The sub-objectives for this research will be to increase the rate and total mass of water vapour absorbance or desorbance that occurs within these wheels for each cycle. The main scheme used to improve moisture transport will be the development of a novel

desiccant particle coating comprised of particle agglomerations. The solid particles will be first carefully sized, tested and selected to ensure appropriate moisture transfer for the agglomerate coating. The final particle agglomeration sizes must be sufficiently small (on the order of 5 to 100 μm) so as to not unduly obstruct air flow within the 1 to 2 mm diameter air flow channels of an energy (enthalpy) wheel.

In order to meet the above objective, a set of tasks is required. These tasks are as follows:

1. Devise a method to create particle agglomerates.
    a. All agglomerates must be capable of being subjected to varying humid and dry, and hot and cold conditions without fracturing or being modified in any significant way. Starch will be used in the formation of strong agglomerates.
    b. The agglomerates must be able to be coated onto a substrate (e.g. aluminum foil) and adhere to the surface coating agent.
    c. Larger agglomerate range of 300 to 1000 μm mean particle diameter consisting of small silica gel particles ranging from 1 to 300 μm in particle diameter, with a mean silica gel particle diameter of 70 μm, will first be made and tested.
    d. Agglomerates in the range of 60 to 90 μm diameter consisting of small silica gel particles of less than 50 μm in particle diameter, with a mean silica gel particle diameter of 6 μm, will then be made and tested.
2. Design a testing apparatus for coating
    a. Capable of testing heat and moisture transfer across a coated surface subjected to a volumetric flow rate in between 12 LPM to 200 LPM.

b. The testing cell must be able to test the currently available desiccant coatings and the lab manufactured coatings in a similar geometry and provide adequate face velocities to allow for mainly fully developed air flow across the coating surface.
c. Parallel flow will be used to transiently test the coated surfaces for their response time constants.
d. Capable of taking continuous data with a data acquisition system.

3. Test agglomerates applied in a coating
    a. For each of the particles outlined in 1.c and 1.d.
    b. Analyze the absorbance and desorbance rate in terms of time constants and moisture mass capacity via isotherms; and compare data to a current enthalpy wheel.
    c. Show how the time constants generally related to latent and sensible heat transfer effectiveness.
    d. Determine the uncertainty in the results.

The purpose of the research described in this thesis is to develop a new particle system that will enhance the effectiveness of energy wheels.

1.5 Overview of Thesis

This thesis is subdivided into six chapters. This chapter introduces the topic, outlines a fairly comprehensive literature review and presents the objectives of the research. Chapter 2 describes the agglomerate creation process, coating process, the testing design process and how the coatings were subjectively tested using instrumentation and an experimental test facility. In Chapter 3, steady-state isotherm and pressure drop data is examined. Chapter 4 presents the

transient response experiments that are examined and thoroughly analyzed to give an accurate understanding of the novel coatings used, and how the data gives the sought after time constants. Chapter 5 presents effectiveness correlations with the time constants, and the probable uncertainty that was encountered when deriving these results. Conclusions are then summarized and presented in Chapter 6. Overall recommendations including future work and possible applications are also discussed in Chapter 6.

CHAPTER 2 :
EXPERIMENTAL METHODS

The selection of the testing methods used can ensure accurate data and its analysis. The first step toward making a particle surface coating was to prepare the particles to make agglomerates and then coating the agglomerate particles onto a substrate for testing. After the substrate was coated with particles it was tested in a special apparatus to confirm adequate moisture sorption capacity and rate of sorption for the coated surfaces.

2.1 APPARATUS, EQUIPMENT & MATERIALS

The apparatus and equipment used to prepare a coating comprised of agglomerates consisted of a ball mill, handheld grinder, laser particle size analyzer, agglomerating device, sieves, substrate surfaces, and testing stations for both sorption isotherm data and transient response data. The materials used during the making of coated surfaces were finely ground silica gel particles, starch to bind the silica gel particles into agglomerates, latex spray paint to act as a bonding substance, and aluminum foil sheets that were used as a substrate for the coating.

The desiccant used for the agglomeraes was a silica gel (Silica Gel Desiccant Grade 12, 28-200 mesh, Fisher Scientific, Fair Lawn, NJ, USA) obtained through VWR International, LLC and was a desiccant that is also used for commercial grade chromatography. The specifications for the particles were as follows: DAVISIL® chromatographic silica, average pore size 60Å, pH 7, and particle sized in the range of 75 to 600 μm particle diameter.

The handheld analytical grinder (A11, IKA® Works, Inc., Wilmington, NC, USA) was purchased through VWR International, LLC. This grinder was used to pulverize small (mm sized) particles into micron-sized particles. The analytical grinder in question had an interchangeable blade and two sorts of blades were used during this research, a Stainless Steel

Beater and a Stainless Steel Cutting Blade. This handheld analytical grinder was first used to achieve the particles as listed in Section 1.4 (task 1.c.), and these particles were then used in the creation of the Coarse Coating.

The ball mill (3 Lb capacity ball mill, Pyrocreations.com, Knoxville, TN, US) a device that was intended for the creation black powder for muzzle loading guns. This ball mill operates by rotating steel balls and the purchased powder inside a cylindrical drum. The particle size that a ball mill is able to produce depends on several variables; i.e. the size and hardness of the balls inside the mill, the size of the mill cylinder, the duration of grinding and speed of grinding and the properties of the particles inside the mill being ground. This ball mill was used to achieve the particles as listed in Section 1.4 (task 1.d.), and these particles were then used in the creation of the Fine Coating.

The laser particle size analyzer (Mastersizer S Long Bench Particle Size Analyzer, Malvern Instruments Ltd., Worcestershire, UK) uses laser beam reflection and scatter to analyze the size distribution of a powder giving its mean particle diameter and volumetric size ranges of particles. This device operates in several ways, and depending on the magnification of the lens being used, it gives distributions in different ranges of particle diameters from approximately 1nm to 1 mm. The powders can either be put through the laser particle size analyzer dry or wet. Running the powder through submerged in water gives a more accurate result of the particle diameter distribution as it avoids the particles clinging together. However, if the particles are soluble in water this method is not possible; also if the water has particulate impurities it will skew the results.

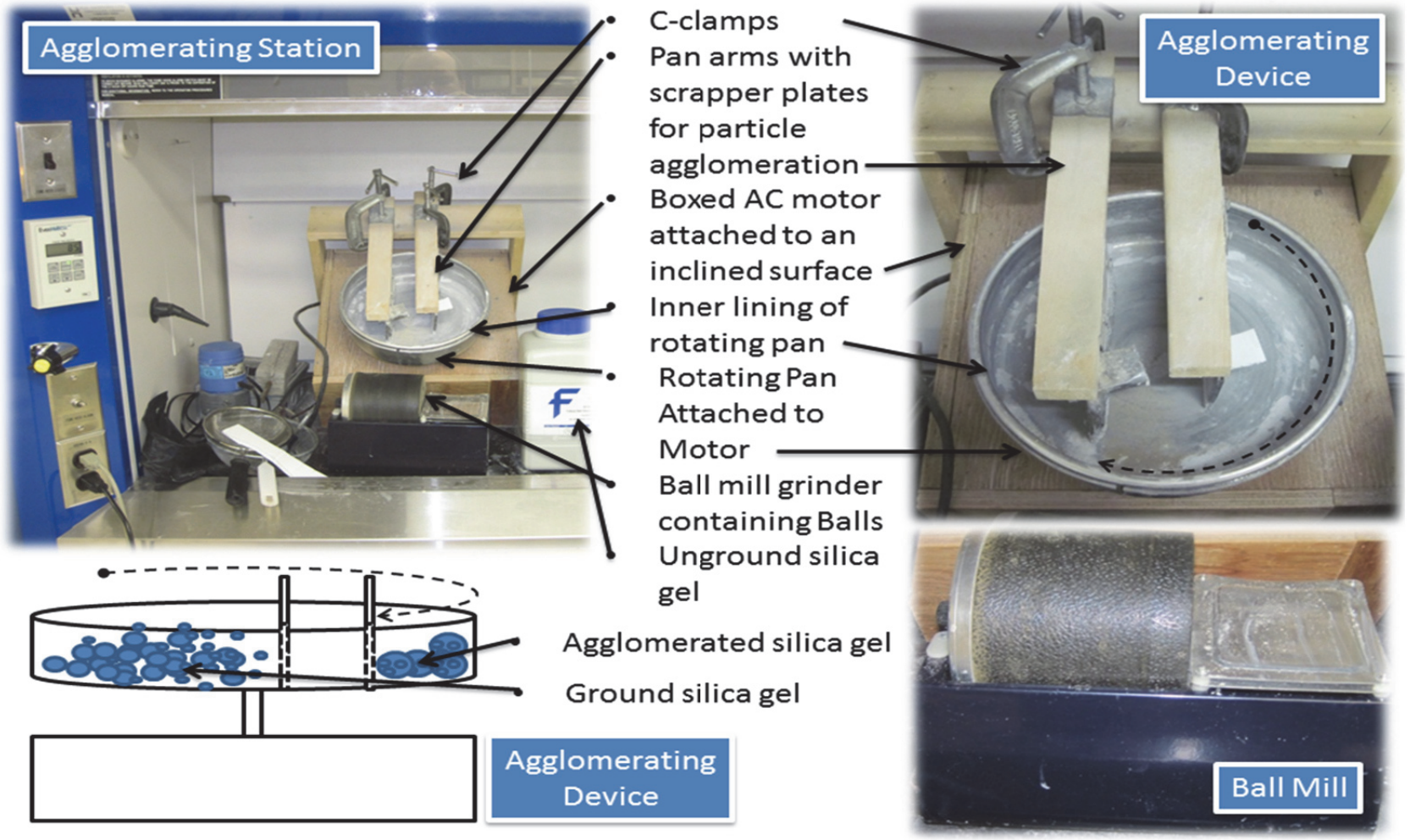

Figure 2.1: The coating area inside a fume hood (top left), where a ball mill (bottom right) grinds silica gel and rotating pan agglomerate processing device (top right, bottom left) agglomerates the silica gel.

The agglomerating device was built based on a method most commonly used for making baking and mineral agglomerates. Figure 2.1 shows an aluminum cylindrical pan with a motor to rotate the pan slowly. Inside the pan with 9 inch diameter, there are two strategically placed scraper plates used to aid the formation of agglomerations and force the granular contents to flow and mix in a particular manner. The scraper plates make contact with the pan along the bottom and one is centered while the other makes contact along the edge as seen in Figure 2.1. This alignment was found to be necessary for effective agglomeration for large numbers of particles, as well as a bonding agent that was used to hold the fine particles together. The agglomerating device was situated inside a fumehood as it is important that very fine powder silica gel is not inhaled.

Sieves were used to size the agglomerated particles and to obtain the range of sizes. Sieves are a mechanical means by which the particles were sorted into desired size ranges. A wide range of sieve sizes were used during this research in order to sort the silica gel and the agglomerates into the desired ranges. The agglomerates for the fine coating were sieved between #230 mesh and #180 mesh (or between 66 to 88 μm).

The particle coating was applied to the aluminum foil sheet specimens in the fumehood. The materials used in this area consisted of a latex spray paint, a particle applicator and a backdrop to protect against spray paint drift. The fumehood was used to contain the fumes of the spray paint. The latex spray paint used was KRYLON® H2O™ Black Sea Latex Aerosol Paint (Krylon Products Group. Cleveland, OH, USA). The applicator used was a simple spice shaker that can be found in most hardware stores. The backdrop was a piece of plastic poster board 1 m by 0.5 m but any size would have worked provided that it fit inside the fumehood and was able to hold 16 substrate specimen strips.

The water vapour sorption isotherm testing used eight closed jars each with a selected saturated salt solution at room temperature, which as a group gave a range of relative humidity from 11% to 97%. An analytical laboratory scale (OHAUS Adventurer™ AR2140, Ohaus Corporation, Pine Brook, NJ, USA) with an accuracy of ± 0.0001 g and a holder for each test sample permitted each test sample to be weighed before and after a known humidity change. The eight jars were prepared so that a sample holder could hang the substrate coated silica gel samples suffixed only to the mass scale. The specimen hanging apparatus consisted of a lid to seal the humidity into the jar, and holder which was able to hold five strips of the same type of coated sample.

The salt solutions used to create a specified humidity at equilibrium in each test jar at room temperature were as follows: Lithium Chloride 11% RH, Potassium Acetate 22% RH, Magnesium Chloride 32% RH, Potassium Carbonate 43% RH, Magnesium Nitrate 52% RH, Sodium Chloride 75% RH, Potassium Chloride 85% RH, and Potassium Sulfate 97% RH.

The coated specimen transient humidity and temperature test cell facility required an air compressor, air pump, two bubblers, connecting air flow tubing, switching device for 180° hand rotation air inlets upstream of the test cell, data acquisition system, and sometimes an air heater as shown in Figure 2.2. The air pump compress consisted of an air dryer (DeVilbiss compressed air dryer, PD35, DeVilbiss Air Power Company, Jackson, TN, USA) and compressed air tank (DeVilbiss air compressor, WAT-5062, DeVilbiss Air Power Company, Jackson, TN, USA), this tank was used as the air source for the transient tests. The dry air within the compressed air tank remained constant at a temperature of 22 to 24°C. The compressed air from the air tank was split into two streams: a heated humid air stream and an ambient temperature dry air stream. On the ambient air side, the mass flow rate was controlled by a mass flow controller (MKS Instruments,

Inc., Andover, MA, USA, Model# 1559A-200L-SV, ±2 L/min,). On the heated and/or humid side a mass flow controller (MKS Instruments, Inc., Model# 1559A-200L-SV, ±2 L/min) was used to move air through an air heating device and humidifier at a desired flow rate. The air heating device was a hot water tube and shell heat exchanger that could warm the air to a temperature between 30 to 40°C. The humidifier consisted of bubblers that were in a parallel flow arrangement with a control valve in order to control the humidity levels in the air to between 70 and 90% RH. Wang et al. (2005) show a different test cell but similar transient test apparatus in Figure 2.3. They (a) show the same flow diagram as Figure 2.2 and (b) show the test section without the test cell with the 180º rotation air inlets. The rapid 180º rotation air inlets allow for a step change in the test cell inlet air conditions to be introduced, with the air streams changing from one flow condition to another.

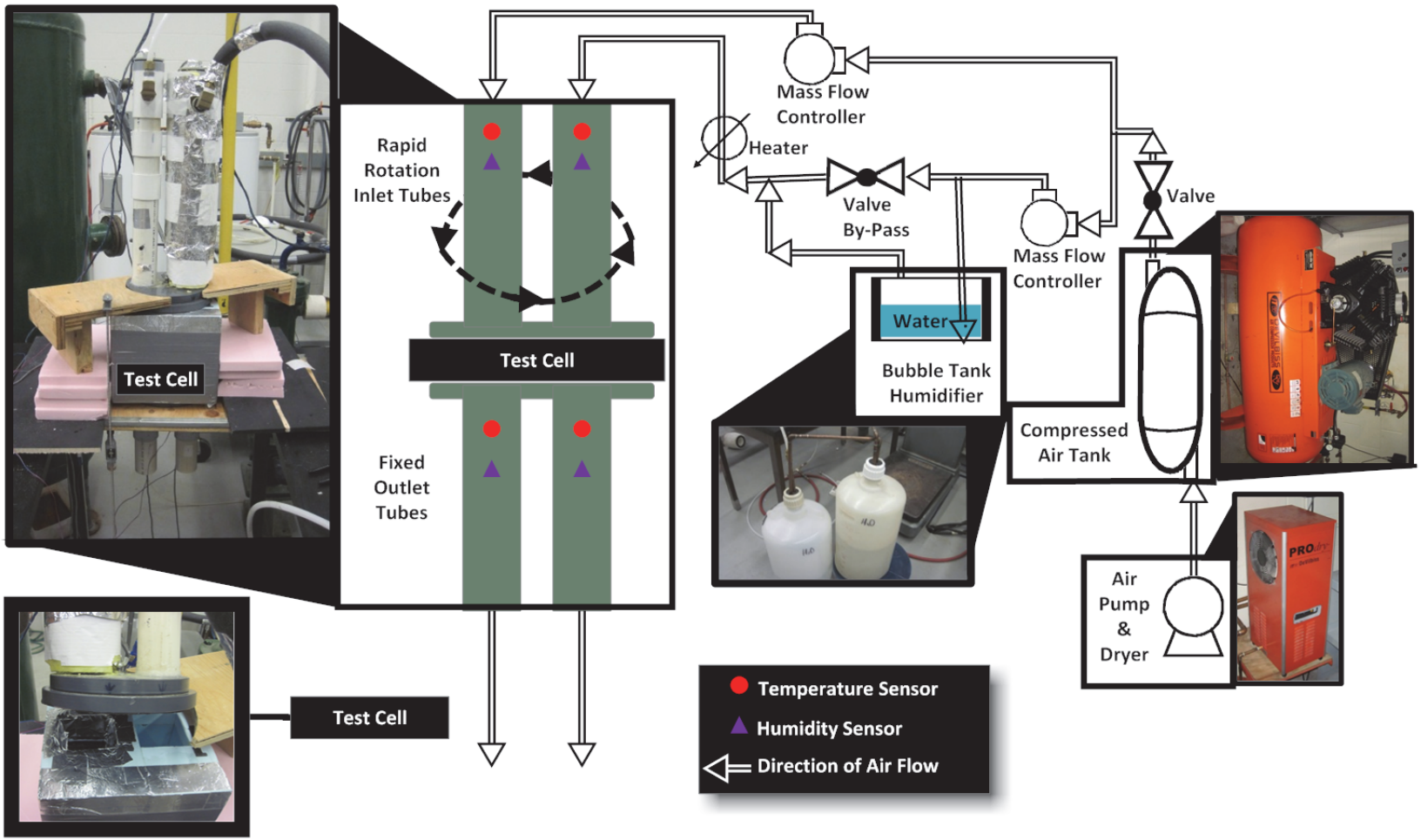

Figure 2.2: Process flow diagram showing the Test Cell used for measuring the transient step response of samples due to a step change in temperature and/or humidity.

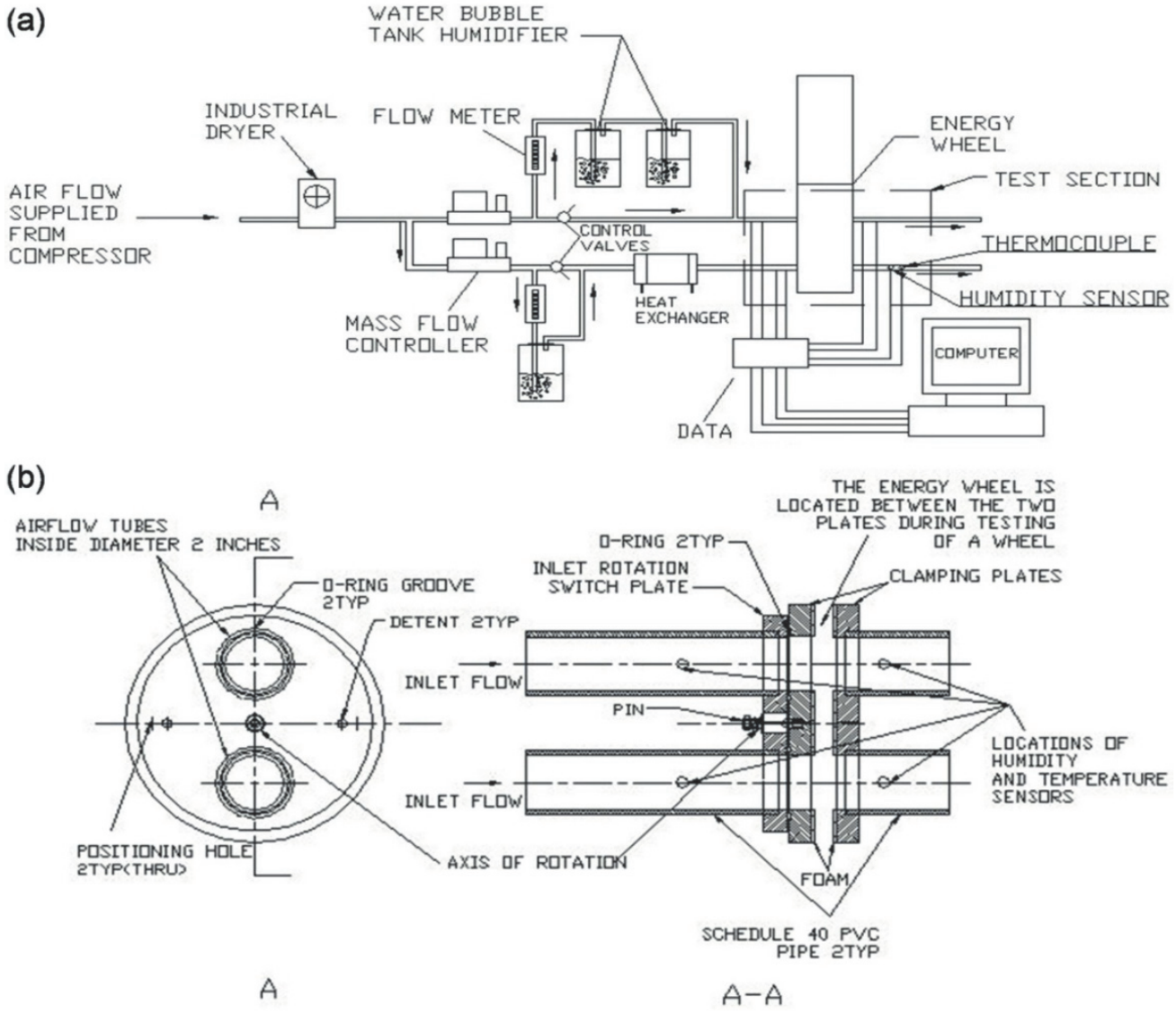

Figure 2.3: Schematic showing (a) air flow tubes, instrumentation, and test wheel, and (b) the test section with its rapid rotation switch plate for the two inlet flow tubes. Reprinted from "Transient Humidity Measurements for Flow Through an Energy Wheel." Wang, Y. H., Besant, R. W., and Simonson, C. J. ©ASHRAE www.ashrae.org. ASHRAE Transactions, no. 111 (2), Annual Meeting, 2005. 353-369. Reprinted with permission.

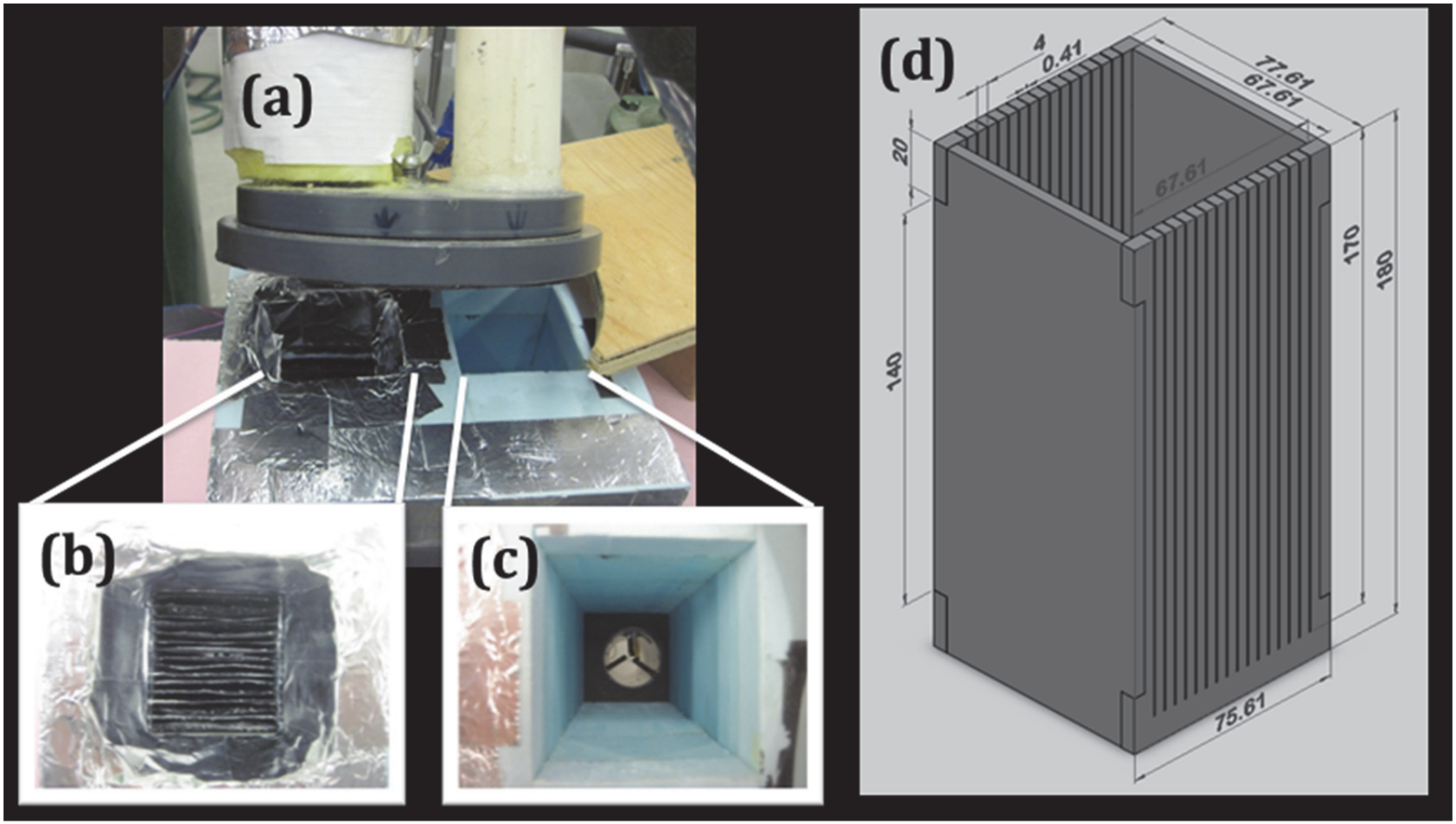

Figure 2.4: Test cell designed to hold 16, equally spaced, coated Sheets: (a) shows the rapid tube rotation piped tubing inlet fits over the test cell; (b) shows how sheets of aluminum foil fit in between the test cell manufactured slits; (c) shows the blank side; (d) shows the device that holds the equally spaced sheets of aluminum foil that fits into the test cell.

The test cell, shown in Figure 2.4(d), is designed to hold 16 equally spaced 8 cm by 17 cm flat sheets of coated or non-coated substrate aluminum sheets. The instrumentation and data acquisition system in Figure 2.2 and Figure 2.3 consists of 4 thermocouples and 4 humidity sensors each connected to a voltage sensor and regulator to ensure proper functionality and all are connected to a computer programmed to monitor with a self-developed virtual instrument for use with LabVIEW^{TM} (National Instruments Corporation, Austin, TX, USA). The data monitoring system included a terminal block (SCXI-1303, National Instruments Corporation, Austin, TX, USA), module (SCXI-1102, National Instruments Corporation, Austin, TX, USA), chassis (SCXI-1000, National Instruments Corporation, Austin, TX, USA), DAQ board (PCI-MIO-16E-4, National Instruments Corporation, Austin, TX, USA), four thermocouples (T Type, constantan copper and nickel) with accuracies of $\pm 0.75\%$ or $\pm 1°C$ and four humidity sensors (Honeywell HIH-4000, Honeywell International, Inc., Morristown, NJ,USA) with accuracies of $\pm 3.5\%\,RH$. A digital pressure probe (TSI DP-Calc™ 8704, TSI Inc., Shoreview, MN, USA) with an accuracy of the greater of $\pm 1\%$ or ± 1 Pa could also, optionally be hooked up across the test cell and was used to determine pressure drop readings in certain testing scenarios.

2.2 Particle Agglomerate Coating Sample Preparation

Creating particle agglomerates was the process used to increase the accessible surface area of a desiccant during short time duration humidity changes. This increase in surface area directly contributed to an increased rate and capacity of moisture sorbance. Part of making an HVAC coating more effective is the incorporation of the agglomerates onto a surface used for moisture transfer. In current industrial applications, desiccants in coatings are usually coated onto the substrate surfaces after being submerged in paint or another coating agent, and then the mixture is applied to the substrate surface and allowed to dry. By not completely submerging the

desiccant before application and ensuring that less volume of the desiccant particles touch the coating agent by using agglomerates, the accessible surface area of the desiccant is increased and thus increases the performance of the coating.

The desiccant was ground to a size fine enough to ensure sufficiently small particles and agglomerates, and, therefore, significantly increased the accessible surface area. At first, the handheld analytic grinder was used, but laser size analysis comparisons revealed that it was inefficient at producing sufficiently small silica gel particulates (see Figure 2.5). This research found the most effective way to acquire particles with a mean particle diameter in the order of one micron is to use a ball grinder with 0.5 inch diameter steel balls. Twenty-eight steel balls and silica gel (28 to 200 Grade Mesh) were added into the cylindrical canister or drum of the rotating ball mill. This 2 L canister, with a rotation speed of 50 to 70 rpm, was filled with approximately 500 mL of grinding balls and 750 mL of silica gel. Each silica gel sample was ground in the ball grinder for a minimum 7 days, and it resulted in an average particulate size of 6 to 7 microns mean particle diameter.

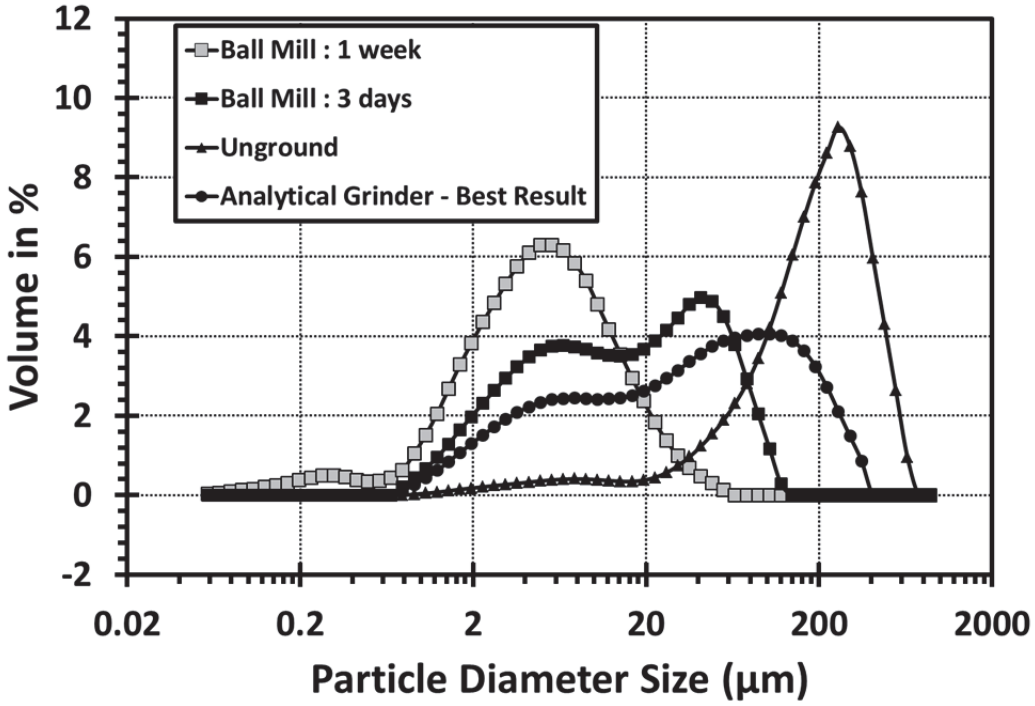

Figure 2.5: Silica Gel particle size distribution using ball mill and analytical handheld grinder methods.

The particle agglomeration process was developed in a series of approximately 200 trials and it was found that the best method to develop consistently sized particle agglomerates was to first make the bonding agent for bonding the particles together in the agglomerates and then to mix it with finely ground silica gel particles in a rotating agglomerate processing machine. The bonding agent was created using a selected mixture of starch and water. Fine ground tapioca starch was selected for this method. To make the bonding agent, reverse osmosis filtered water was heated to approximately 80ºC and then starch was added with a ratio of about 0.5 g starch/mL water. At this concentration, most or all of the starch dissolves into the solution, creating a gel which is more viscous than water. This solution was allowed to cool to room temperature and any remaining starch particulates in the solution sank to the bottom. Then the solution was poured off from the top in order to minimize particle contamination of the solution.

The next part of the process involved using the particle agglomerating device. All that was known to create the agglomerates was the mass ratio of ingredients (5 grams of silica to 2 grams of solution) and the time that was allowed for agglomeration and drying (minimum 2 days). Depending on the size of the agglomerating device, the amounts of each substance may vary. The cooled agglomerate bonding agent and the ground silica gel were added to the agglomerate processing machine in Figure 2.1 being sure to only fill the pan of the machine a maximum of one eighth of the total pan volume. As the machine rotated, the silica gel and bonding agent formed a dough-like material. This material in the rotating pan was continuously scraped by a set of two scrapers while the pan was turning. It is important that the scraping arms make contact with the aluminum rotating pan of the agglomerating device as these arms are essential in the creation of the agglomerates as they create the contact and mixing necessary for the material inside the device to properly ball up. The motor attached to the rotating pan has a variable motor attached which can control the speed at which the pan rotates. After first adding the fine silica gel and the bonding agent the machine should be turned to a fairly high RPM usually to between 20 and 30 rpm, and then after about 5 to 10 min once agglomerates start to form the speed of the machine can be reduced to around 5 rpm. It is important to continue to observe the agglomerates to ensure the speeds being used are creating the desired size of agglomerates. In order for most of the silica to form into agglomerates within in the pan it should be left at a slower rotation for around 1 to 2 hours, or faster rotation will tend to create larger agglomerates which were undesirable for this application. If the agglomerates were getting too large, occasionally they were broken up by hand chopping with another steel plate to reduce the size. The more chopping the finer the agglomerates produced. Scraping, chopping and adding slightly more silica gel continued for about another hour or until the agglomerates began taking the desired shape and

size. Once spherical agglomerates of appropriate size, ranging from 100 to 5000 μm for the coarse agglomerates and between 10 to 1000 μm for the fine agglomerates, were produced within the agglomerate processing pan, the machine was stopped and the agglomerates were left to dry. For complete bonding to occur, the agglomerates were allowed to dry for 2 to 3 days. Then these dry agglomerates were sieved and used in the coating application procedure.

The sieving then took place in order to give a better size for utilization on the inner matrix of a desiccant or energy wheel. Prior to utilizing the ball mill for the fine silica gel, a much coarser silica gel was agglomerated. This silica gel had particles in the range of 1 to 300 μm, therefore it is important to ensure the silica gel alone was being sieved out on the lower end of the sieving process but that the larger particles were not too large. Therefore, in order to accomplish this a #50 and #18 sieve were used, this gives a particles range to in between 297 to 1000 μm which should therefore comprise of mainly the agglomerated particles, and in the next Chapter it will be shown that this was indeed the case. The same reasoning was used to sieve the finer agglomerates used for the FC, in this case though the ground silica gel has a maximum particle size diameter of roughly 50 μm. Therefore, in order to ensure that mainly agglomerated particles were taken from the sieving, #230 and #180 sieves were used; this gives a particle diameter range to in between 66 to 88 μm (where 90% of the particles will fall between these ranges). The next chapter will again verify that the coatings did indeed mainly consist of only agglomerated desiccant particles.

2.3 COATING PROCEDURE

Sample sheets of substrate (aluminum foil) were first cut to size (depending on the experiment that was either 5 sheets of 3 cm by 3 cm or 16 sheets of 8 cm by 17 cm) using a board style paper

cutter for more accurate dimensions; however, sheers and proper measuring would also work. The uniform sheet strips were then placed and adhered with tape to hold them in place on the poster board backdrop. They were coated one side at a time, allowing the first side to dry before coating the other side. These sheets were sprayed as evenly and as lightly as possible using the latex paint, holding the can approximately 0.5m from the aluminum and using short fast bursts of spray to apply. Right after the sheets were coated with the paint, the agglomerate particles were applied so they adhered to the surface of the paint before it dried. Excess particles were applied in order to fully utilize the painted surface as those that were not in contact with the paint were easily falling off once the sheets were finished drying. . This simple method was an easy way to ensure fairly even particle distribution. Once they were dry, the coated sheets were then turned over and the process was repeated on the opposite side. The final step in preparing the sample aluminum sheets coated with the latex paint and silica gel agglomerates was to try to remove as much loose particulate as possible. This was accomplished by brushing the loose particulate off under the fume hood, and then using a can of compressed air to further spray off excess silica gel agglomerates. This ensured that no silica would loosen during the testing and get into the air flow during a test.

2.4 ISOTHERM DEVELOPMENT PROCEDURE

The isotherm testing procedure was fairly simple but involved a lot of repetition. The substrate sheets were aluminum foil sheets of uniform size and weight (before being coated) used with varying coatings, and with no coatings. First, the weight of all 5 of the substrate sheets being tested were taken separately for verification purposes, the weight of the hanging holder was also taken, and then the weights of the sheets and the hanging holder were taken together. Each of the following weights were taken with the cradle holder and the sheets together, as the

cradle holder was tested to ensure that it would had a negligible moisture absorbance. The following steps were repeated for each substrate starting at the lowest 11% RH solution (Lithium Chloride) test and then incrementally increasing the humidity to the highest 97% RH (Potassium Sulfate) test and then back down again, 97% RH to 11% RH.

1. Place the cradle and testing substrate in the jar with the solution.
2. Ensure a seal.
3. Let the moisture sorbance reach equilibrium by allowing the substrates to sorb moisture for at least 24 hours.
4. Weigh the cradle with the substrate.
5. Calculate the moisture sorbance ratio, which is the mass of adsorbate (moisture) divided by the mass of adsorbant (coating).
6. Repeat until all salt solutions have two data points in both ascending and descending order according to their relative humidity equilibrium.

At the end of testing each substrate there were 15 moisture retention data points able to create a sorption equilibrium isotherm with both adsorbance and desorbance and their hysteresis, if it occurs.

This procedure was then used to create isotherms for blank aluminum foil, aluminum foil with just latex paint dried onto both surfaces, and 3 different desiccant coatings applied to aluminum foil. Then similar samples are used in the transient tests outlined in the following section.

2.5 Transient Heat and Moisture Transfer Test Methods and Procedures

The apparatus used to test transient heat and moisture transfer through an energy wheel or through a section of coated aluminum foil sheets is shown in Figure 2.2. Temperature, relative humidity and mass flow rate of the inlet air were controlled for two different flows which

allowed for a controlled step change for the parallel flow going through the coated parallel sheets. The relative humidity was controlled by passing a dry air flow, from the compressed air tank, into a bubbler system where the amount of air flowing through the bubbler was controlled by a mass flow controller with a valve in parallel with the bubble further down the airline. This set up allowed for the amount of dry air to be controlled by the valve which in turn could modify the relative humidity of the inlet supply air. The temperature of the supply air was modified via a shell and tube heat exchanger type apparatus which allowed for the incoming air to be heated or cooled, the temperature could not be controlled to better than ±5ºC but it did allow for the needed step change in temperature.

Accurate data for all temperature and humidity readings were needed on both inlet and outlet of the test cell. The primary test cell is shown in Figure 2.4 consists of parallel evenly spaced sheets being placed inside the slits for testing, but the apparatus allowed for anything that allows a flow through it to be tested, including enthalpy/desiccant wheels. This made two humidity readings and two temperatures for each of the two flows. A total of eight readings were recorded using the data collection system.

For each of the set of sheets prepared, the following procedure was repeated:

1. Take the prepared sheets for the transient tests as outlined earlier and fix them properly into the test cell.
2. Mount the test cell into the testing apparatus and securely clamp it.
3. Turn on air flow at the compressed air tank, to allow for sufficient flow of air into the testing system.
4. Adjust the valve in parallel with the bubblers, on the high humidity and heated side, until readings give a desired relative humidity (usually close to 75% RH), and if

measuring a temperature response also turn on hot water to flow through shell and tube heat exchanger.

5. Monitor readings so as to allow sufficient time for steady state to be reached.
6. Start recording data using the acquisition system, once confident steady state has been reached,
7. Switch the air flows, while making note of and logging the time of the switch. This time is the start time of the temperature and humidity step change.
8. Wait for the system to reach equilibrium, being sure to monitor it closely as the data acquisition system logs data points as the time can vary depending on the coating, the air flow rates and/or the size of the step change applied.
9. Repeat.

Each coating was tested for absorption and desorption (by making the opposite change in the air flow system) at a variety of flow rates, and humidity step changes. Each coated sample in the test cell or energy wheel was tested in the same manner.

2.6 Chapter Summary

This chapter outlined the methodology that is used during the testing phase of this thesis. This includes all of the apparati outlined in Figures 2.1 to 2.4. It then discussed how the particle agglomerates can be made from silica gel particulate and coated using a latex paint. Isotherm data collection methods as well as transient testing procedures are then outlined and discussed.

CHAPTER 3 :
PARTICLE AGGLOMERATES, COATING EQUILIBRIUM ISOTHERMS AND PRESSURE DROP DATA AT STEADY STATE CONDITIONS

The purpose of this chapter is to present and analyze the data for the agglomerated particles and the steady state water vapor sorption isotherm for the desiccant particles and coatings and air pressure drop readings for the coated sheets in the test cell. First the coating particles are presented and analyzed for particle and agglomerate size distributions using the laser particle size analyzer. Then the isotherms of these different coatings on aluminum foil substrates are compared. Finally the steady state air pressure drop data for the test cell with three different coated sheets mounted are compared.

3.1 AGGLOMERATE PARTICLES AND COATINGS

Four different coatings were of importance: the first are large sized (300 to 1000 μm) agglomerated particles, the second were small sized (approximately 60 to 90 μm) agglomerated particles, the third coating was obtained from a current industrial manufacturer, and finally the fourth was a blank aluminum foil coated with a black latex paint. When compared under a scanning electron microscope (SEM), these coatings appeared to be very different as shown in Figure 3.1.The blank coating latex paint showed a few tiny silica gel particles which did not change the sorption results. The industrial coating was much more uniform particle size and distribution than the laboratory coatings CC and FC. Although not visible in Figure 3.1 the industrial coating was saturated by the coating material that was used to bond the desiccant particles to the substrate. Figure 3.2 shows this type of coated substrate in cross-section. The two other laboratory coatings (CC and FC) were prepared for this research by placing the particles on top of the wet paint. Although not as uniform as the IC, the particles appeared to be free from the

coating paint because the paint and the particles appear with different shades of grey in the SEM photos. The laboratory coating process led to large variations in particle size and distribution. Qualitatively these SEM photos affirm that the coatings used throughout this research has left a much more desiccant-exposed surface area by leaving the majority of the desiccant not covered by the coating material. Regarding the industrial coating, Shang and Besant (2009a, 2009b) say that the coating material is very clearly seen in cross-section and that the way this material is applied to the desiccant it will limit the mass transfer, and near the aluminum foil it will respond even slower due to the particles being entrapped by the coating agent. The cross-sectional SEM view shows desiccant particles coated onto both sides of aluminum foil sheets. When the coating material covers the desiccant particles, it slows the moisture adsorption and limits the total amount of sorption that can occur. So, by limiting the amount of coating agent covering the particles, the sorption rate increases and the total mass of water vapor sorption that can occur increases while the wheel rotates.

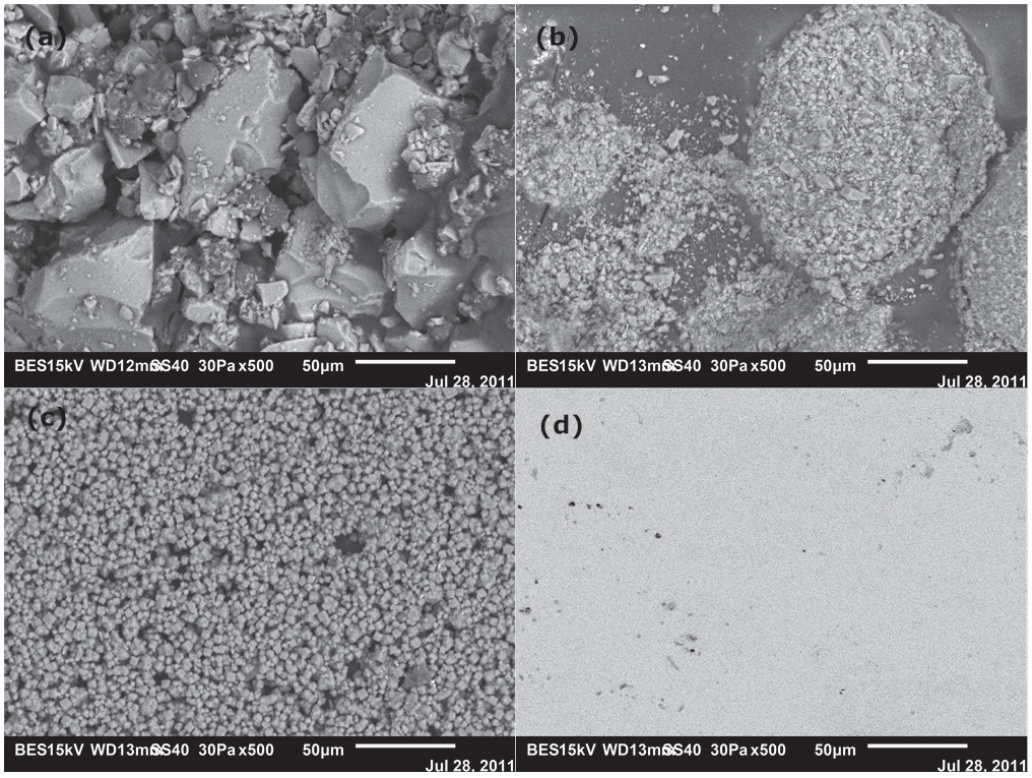

Figure 3.1: SEM Photos of (a) Coarse particle Coating, CC, with large mean particle diameter agglomerates bonded by a latex paint on aluminum foil (b) Fine particle Coating, FC, with fine mean particle diameter agglomerates bonded by a latex paint on aluminum foil (c) Industrial Coating, IC, typical molecular sieve or silica gel particles bonded on a thin sheet of aluminum foil (d) Blank Coating, BC, with latex paint on aluminum foil.

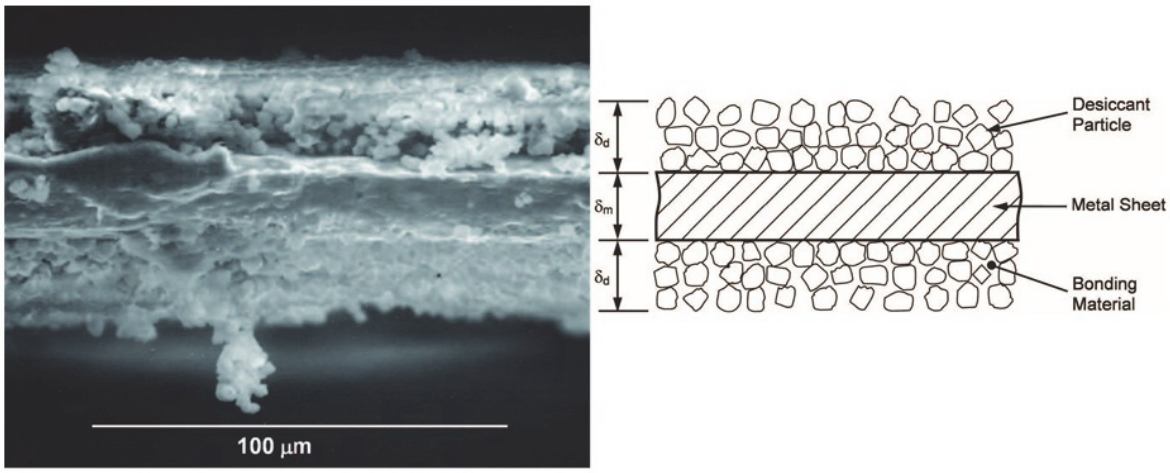

Figure 3.2: Cross-sectional SEM Photos of an Industrial Coating, IC, typical silica gel particles bonded on a thin sheet of aluminum foil. Reprinted/Adapted from "Effectiveness of Desiccant Coated Regenerative Wheels from Transient Response Characteristics and Flow Channel Properties - Part I. Development of Effectiveness Equations." Shang, W., and Besant, R. W. ©ASHRAE www.ashrae.org. HVAC&R Research, no. 15 (2), March, 2009: 329-346. Reprinted/Adapted with permission.

Comparing the small sized particles for the laboratory coating and the coarse laboratory coating, the photos show that the large sized particles in the coating, as expected, is comprised of much larger size particles within the agglomerates, and that the finer coating agglomerates are comprised of much smaller particles than that in even the industrial coating. The reason for this difference with the results obtained from Figure 2.5 is that the laser analyzer used for particle diameter predicts the mean particle diameter measurement based on total volume percentage, therefore, the actual number of particles is not accurately known. Obtaining the mean diameter based on the number of particles would result in a much different outcome. Next this investigation looks at what sort of effect this might have on the quantitative moisture sorption tests conducted not only on these three coatings, but also on a separate blank latex painted surface.

3.2 STEADY-STATE MOISTURE CONTENT ISOTHERMS

The equilibrium sorption properties of the silica gel particles and the desiccant coatings are both of direct interest for energy wheels because they imply the maximum change in moisture content that can occur between any two inlet temperature and humidity conditions. Figure 3.3 shows a typical isotherm for silica gel particles, while Figure 3.4 shows a typical silica gel coating isotherm, Shang and Besant (2009a) made the following comment regarding these figures, "These graphs show that the particles alone behave differently than the coatings, i.e. they*, the coatings in Figure 3.4,* have significantly lower moisture contents and lower gradients of moisture content for the typical range of operating conditions for energy wheels. In addition, the changes in these isotherms are likely to be very small for energy wheels (e.g. 1ºC to 5ºC) but more significant for dehumidifier wheels (e.g. 20ºC to 50ºC) because they are subjected to large temperature changes."

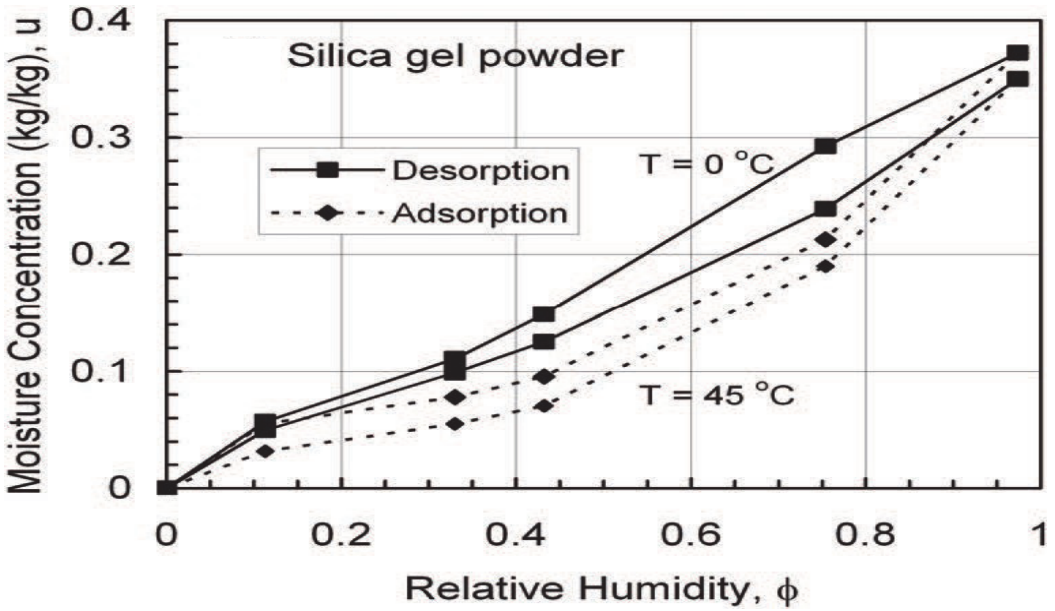

Figure 3.3: Silica Gel Equilibrium Isotherm Data, with mass of moisture adsorbed vs. relative humidity data. Reprinted/Adapted from "Effectiveness of Desiccant Coated Regenerative Wheels from Transient Response Characteristics and Flow Channel Properties - Part I. Development of Effectiveness Equations." Shang, W., and Besant, R. W. ©ASHRAE www.ashrae.org. HVAC&R Research, no. 15 (2), March, 2009: 329-346. Reprinted/Adapted with permission.

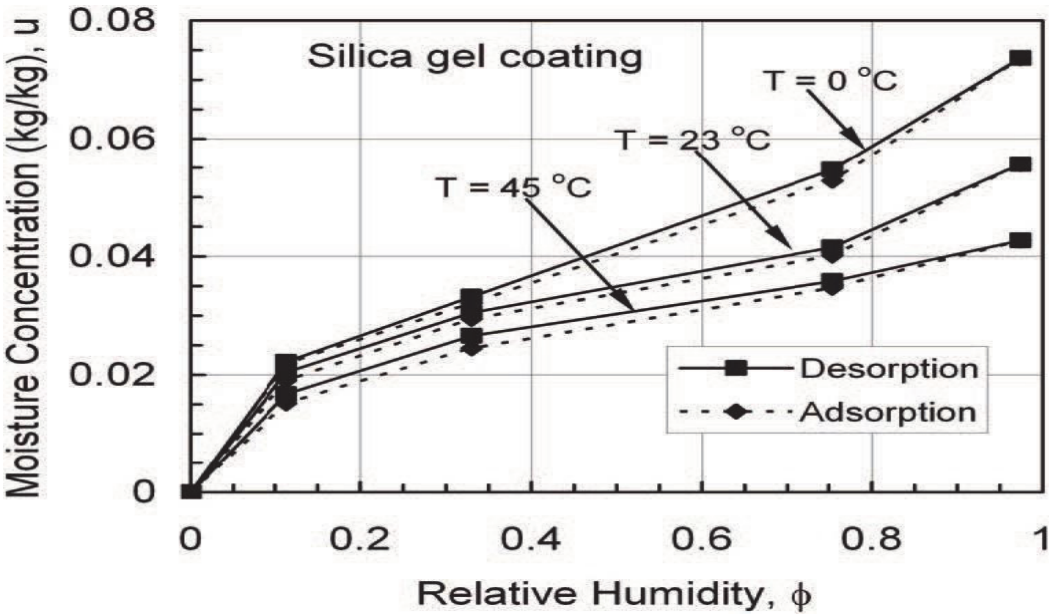

Figure 3.4: Silica Gel Industrial Coating* Equilibrium Isotherm Data, with mass of moisture adsorbed vs. relative humidity data. *Note: This industrial coating was not that same as the one used in this research. Reprinted/Adapted from "Effectiveness of Desiccant Coated Regenerative Wheels from Transient Response Characteristics and Flow Channel Properties - Part I. Development of Effectiveness Equations." Shang, W., and Besant, R. W. ©ASHRAE www.ashrae.org. HVAC&R Research, no. 15 (2), March, 2009: 329-346. Reprinted/Adapted with permission.

Figure 3.5 shows the steady-state isotherms taken during this research. Using the salt solutions and methods outlined in section 2.4, the total adsorption for the coatings was lower than the silica gel isotherm in Figure 3.3 for all of the coatings save the fine coating but significantly higher than the coatings presented in Figure 3.4. The fine coating had significantly lower mass than all the other coatings, but with the agglomerated particles it was able to hold more than the silica gel alone based on the mass of water adsorbed per unit mass of dry coating, probably due to less coating agent and more agglomerates increase the total adsorbable surface area of the coating. The coarse coating weighs the most of the coatings but performs very similar to the silica gel isotherms in Figure 3.3. There was more paint than silica gel agglomerates surfaces exposed for the large particles leading to this decrease in the mass of adsorbable moisture or maybe the large particles were too big. The industrial coating and the blank coating have very similar isotherms, and, therefore, it may be possible that the coating material was the limiting factor in the industrial coating.

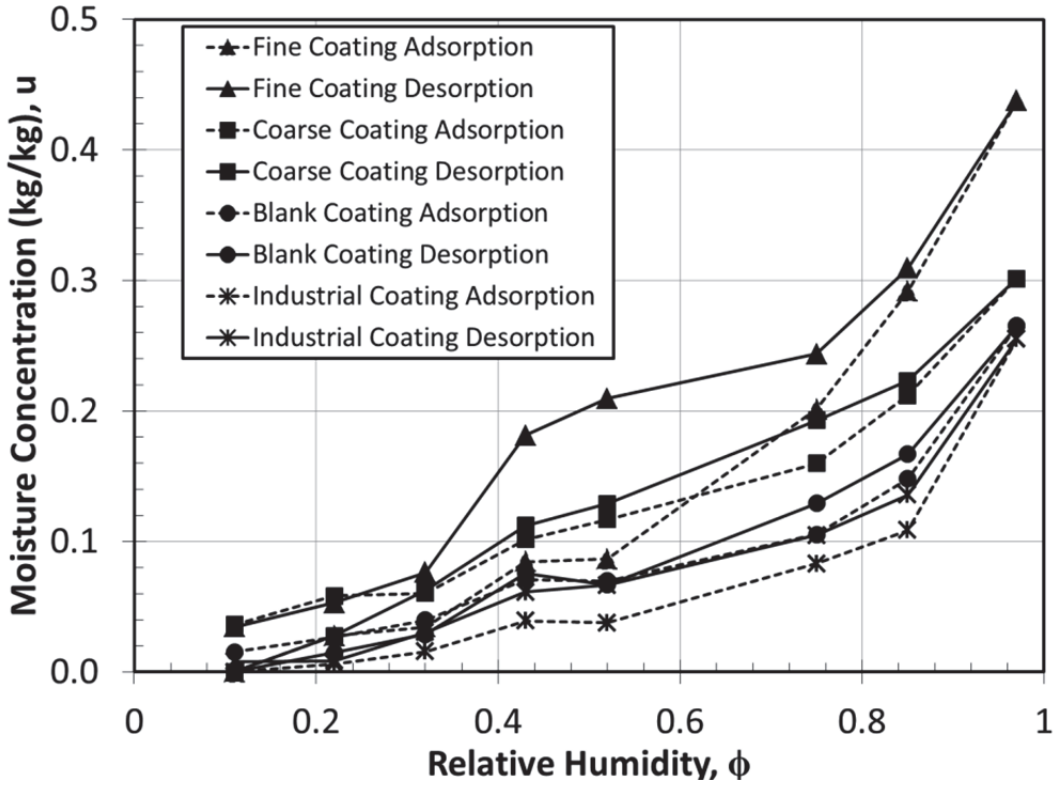

Figure 3.5: Steady State Isotherm Data, i.e. mass of moisture adsorbed per unit mass of dry coating vs. relative humidity.

3.3 Pressure Readings and Turbulent Flow

Due to the roughness of the surface of the coarse coating (CC), it was suspected that the air flow is actually tripping into a developing channel turbulent flow. It has been shown that for very rough surfaces air flow can actually become turbulent at fairly low Reynolds numbers (Colebrook & White, 1937; H. Zhang et al., 1996). This was important because as air flow becomes turbulent, the heat and mass transfer convection coefficients increase, which means energy wheels may become even more effective at transferring energy when the flow channel surfaces are very rough rather than smooth air flow channel surfaces which have been the norm in the industry in the past.

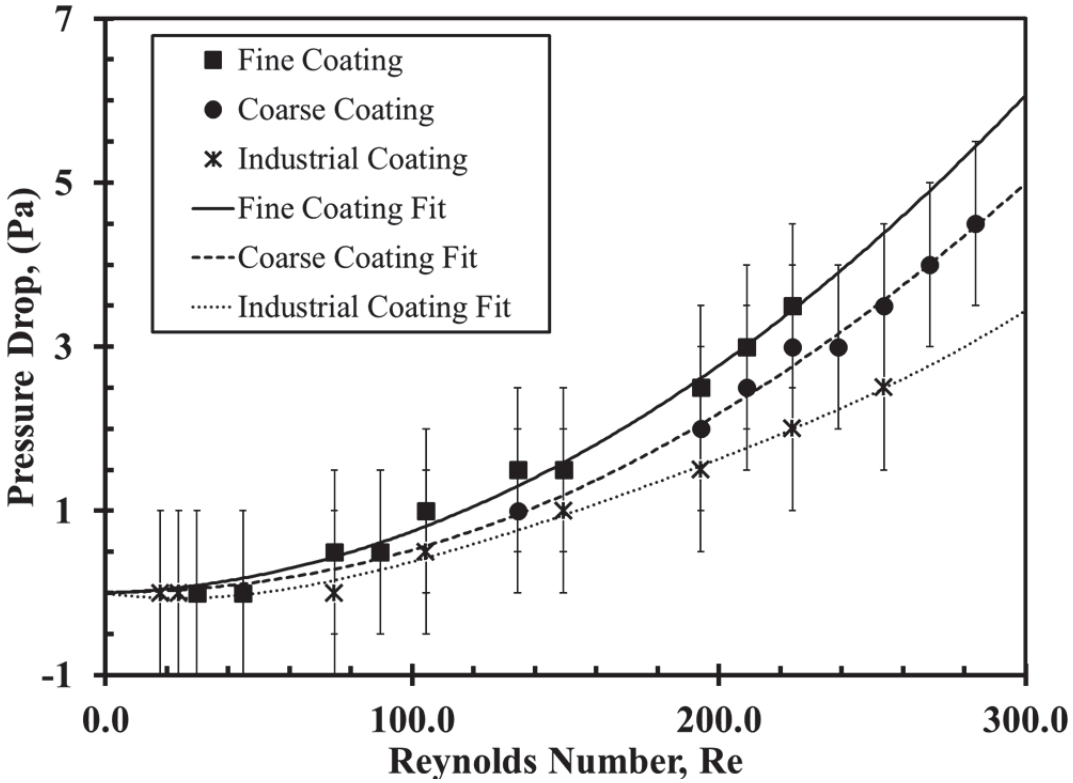

Figure 3.6: Pressure drop measured across the test cell vs. the Reynolds number for 3 different coatings (Fine Coating, Coarse Coating, and Industrial Coating) at a variety of face velocities ranging between 0.04 m/s and 0.68 m/s.

Pressure drop readings were taken to see if the air flows are turbulent for some coatings (CC, FC, and IC) but remaining laminar for others. Figure 3.6 shows the final results. These data show promise as both the FC and the CC exhibit higher pressure drop readings at the same Reynolds numbers, implying that the convection coefficients will be increased due to the change in flow type from laminar to turbulent. With an increase in the convective heat transfer coefficient and the convective mass transfer coefficient, the rate of sensible heat transfer and the rate of sorption will be significantly increased (Incropera, Bergman, & Lavine, 2011).

3.4 Chapter Summary

Chapter 3 presents and analyzes experimental steady state and equilibrium data. It describes how agglomerated particles can be made using a combination of water, silica gel and starch

inside of a rotating pan which serves as an agglomerating device. These agglomerates were then coated onto a substrate (aluminum foil) using a coating agent (latex paint). Two tests were then conducted. The first, an isotherm equilibrium test, is developed using a combination of one of four different coatings (CC, FC, IC, and BC) and a sheet of aluminum foil put into a series of varying relative humidity chambers. The mass of moisture per mass of coating or the moisture concentration was plotted verses the relative humidity. This gives us an understanding as to how much moisture each coating can hold at steady state conditions; the fine coating (FC) was able to obtain a higher moisture concentration, the coarse coating (CC) holds slightly less moisture concentration than the FC; and the two other coatings, the industrial coating (IC) and the blank latex paint coating (BC), also obtain a fairly high moisture concentration close to the CC but significantly lower than the FC. This implies that per mass the FC coating is able to obtain a higher moisture concentration and can perform well on a regenerative energy wheel. The next steady state experiment was taken at the end of the transient tests done in the next chapter. A pressure reading is taken for three different coatings (FC, CC, and IC) at various face velocities in the transient testing apparatus after reaching steady state flow conditions. The FC and CC both had higher and steeper curves for the pressure data as a function of face velocity meaning that the friction factor is 2 to 4 times higher than that of the IC, perhaps implying that turbulent flow and an increase in mass transfer rate is obtained but further data is needed.

CHAPTER 4 :
RESULTS & DISCUSSION FOR TIME CONSTANT DATA

The purpose of this chapter is to analyze the data and present the time constant results for the test cell fitted with various substrate coated sheets. Both responses will be examined and compared in this chapter. First the response from the humidity measurements were converted to humidity ratios, and normalized. The time constants and the uncertainties were then taken from curve fitting the data to equations from transient responses from past work and a new correlation for how these time constants were dependent on face velocity was developed for each of the coatings. This process was then repeated for the same coatings but by looking at the temperature response data. All the correlations were compared in the conclusion of the chapter. This data is then used in the next chapter to predict to the theoretical latent and sensible effectiveness.

4.1 Transient Moisture Sorbance with Humidity Response

Transient response experiments were performed on several different coatings, each with different response characteristics. The experimental test facility, shown in Figure 2.2, was used to measure the humidity transient response at the test cell outlet after a step change in the inlet humidity for the air flowing through the test with substrate coated sheets. When considering the transient response of desiccant coated surfaces, it is important to reduce inaccuracies caused by biased or noisy data. Figure 4.1 shows a typical sensor voltage that was obtained for the humidity. The small voltage cyclic variations near the lowest sensor voltage were caused by the compressor starting and stopping.

There are several types of error that will occur when recording sensor data. Errors will occur due to the sensor calibration which is used to determine the sensors bias error for steady state measurements. Errors may occur due to the location of the sensor in the test cell which leads to a

sensor bias in location error because the sensor does not measure the bulk mean property (e.g. humidity) at the outlet. Errors will occur during dynamic changes in property conditions because the sensor has a delay in its response after a very rapid change in outlet conditions. Finally, errors will occur because the sensor analog electrical signals are amplified and digitized and this process can result in both bias and precision errors.

Sensor steady-state bias errors are accounted for by calibration. Sensor location errors are minimized by good test cell design. Sensor transient response errors can be accounted for by transient testing of the sensors (Wang et al., 2005). Recording equipment errors can accounted for by direct testing but most often the manufacturer of this equipment gives any bias and precision errors in their voltage measurements and these are usually very small relative to the other errors.

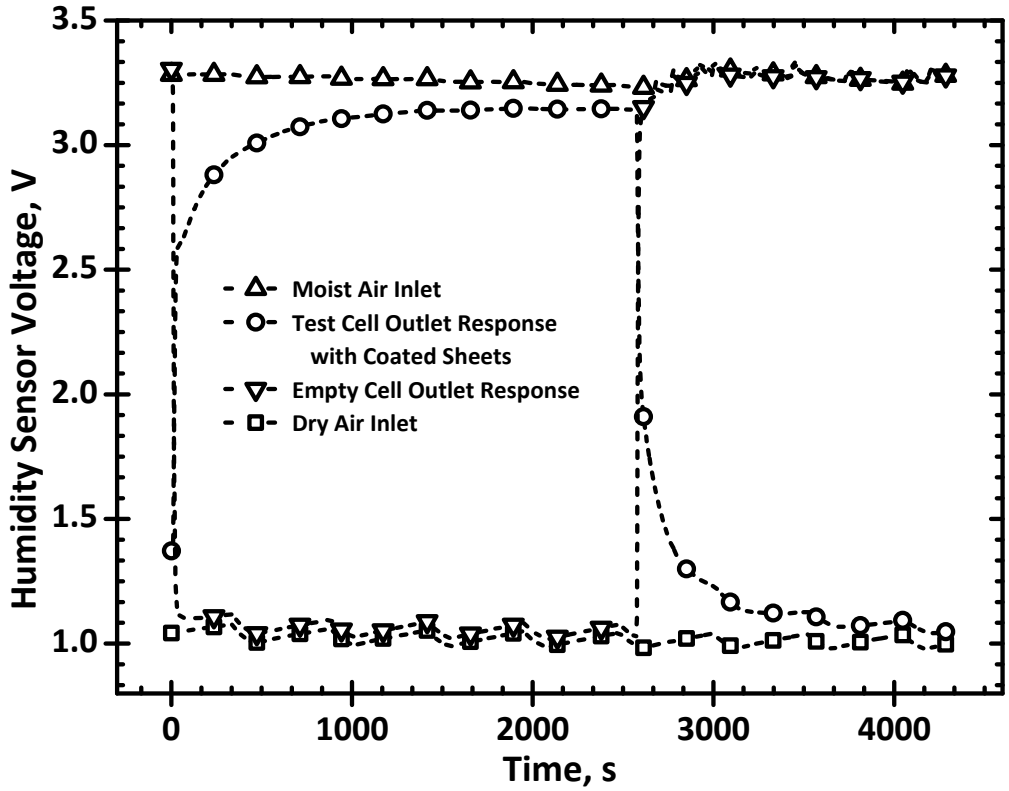

Figure 4.1: Humidity sensor voltage data for four sensors, one for each inlet and outlet, a test cell containing substrate sheets with a coarse coating, CC, agglomerated sample with first a step change in dry air to humid air at t=0.5, and then back again at t=2600s, and opposite step changes across an empty cell. Humid air at 75% RH and 22ºC, dry air at 5% RH and 22ºC, and both with an air face velocity, *v*, of 0.341 m/s and a Reynolds number of 149 for flow through the channels.

The humidity sensors give a reading that corresponds to the sensor calibration % RH as seen in the appendix Table C.1. Figure C.1 shows the steady-state or equilibrium calibration that was used for each humidity sensor in order to obtain an accurate relative humidity. Using the manufacturers predetermined correlations as well the data from the calibration the error due to the accuracy of the instruments can be obtained. As one can see by looking at the data there are another two types of error that are introduced into the system that will affect the precision of our results.

These errors are mostly due to the electrical noise when taking measurements with analog and/or digital electronic sensors as well as the actual fluctuations in both the dry and humid air due to the setup and the impossibility of keeping them 100% constant.

4.1.1 NORMALIZING THE HUMIDITY RESPONSE DATA

The following equation was used to normalize the data:

$$W_t^* = \frac{\Delta W_t}{\Delta W_M} = \frac{W_{out,t} - W_{initial}}{W_{final} - W_{initial}} \qquad 4.1\text{–}1$$

where

W_t^* = normalized humidity ratio at any time t

ΔW_t = the change in outlet humidity ratio or moisture content at any time t

ΔW_M = the maximum change in outlet humidity ratio or moisture content for the step change

and

$W_{out,t}$ = measured humidity ratio or moisture content at the outlet at any time t

$W_{initial}$ = measured humidity ratio or moisture content at the outlet initially, or at $t = 0$

W_{final} = measured humidity ratio or moisture content at the outlet after reaching steady state, i.e. at $t \to \infty$

Equation 4.1–1 shows how the raw data was normalized. The equation takes the humidity ratio at any time and subtracts the inlet relative humidity and then divides by the maximum difference from inlet to outlet for that time period. This normalization has a two-fold purpose; it makes the data comparable to other data regardless of the magnitude of the step change in relative humidity, and it tends to also nullify fluctuations of the humidity ratio at the inlet air because only the difference between the inlet and outlet was calculated.

Figure 4.2 shows the normalized data from Figure 4.1 for both the adsorption and desorption. When looking at this figure, it becomes apparent that the humidity response levels are much slower for the coarse particle coatings than the industrial coating in Figure 4.2. This shows that the coarse particle coating adsorbs or desorbs a greater mass of water than the fine coating and it takes much longer for the coating to become saturated or desaturated. In other words the slower response means that the coating is actually performing better; it has a greater time constant and overall better effectiveness. This phenomenon will be more closely examined in the next section dealing with how the time constants were obtained from the normalized data and what that will mean in terms of increasing the effectiveness of the wheel.

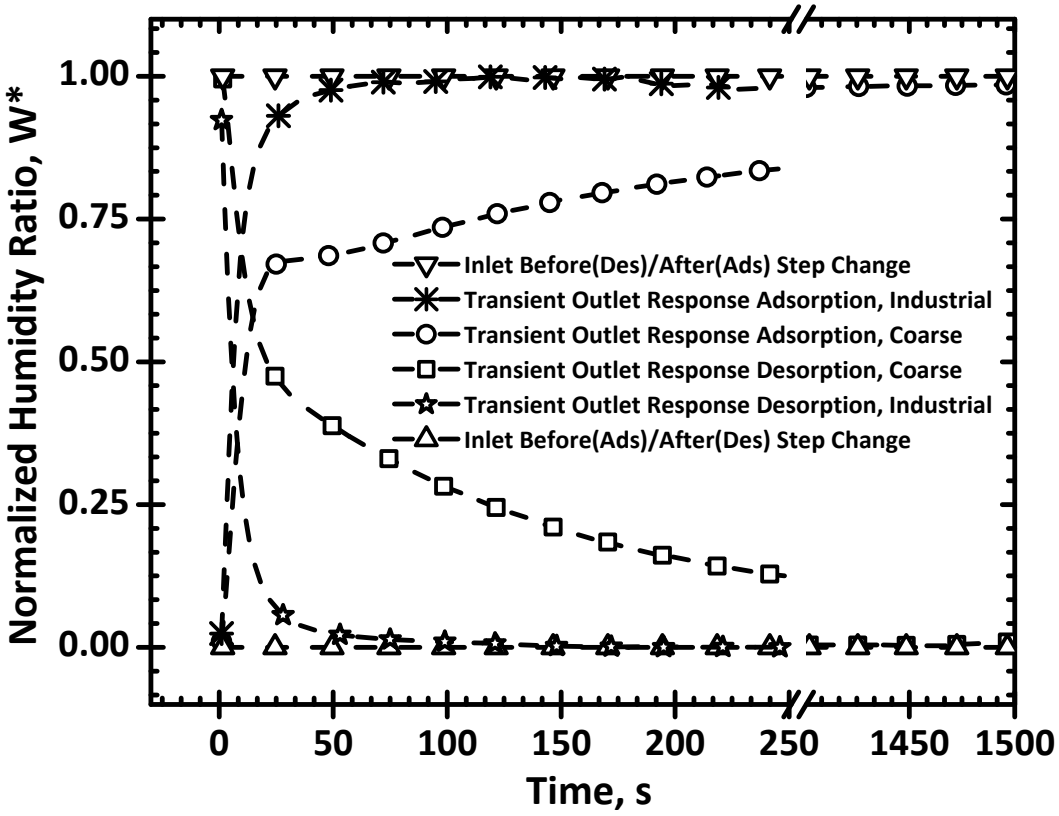

Figure 4.2: Normalized transient humidity data across a test cell containing a coarse coating agglomerated sample or an industrial coating sample with a step change, or as seen for the adsorption and desorption processes. Moist air at 75% RH and 22ºC to, dry air at 5% RH and 22ºC, and air an air face velocity, *v*, of 0.341 m/s and a Reynolds number of 149.

4.1.2 TIME CONSTANT ANALYSIS FROM HUMIDITY RESPONSE

Shang and Besant (2009a, 2009b) show the time constants play a very important role for regenerative wheels. The time constants were obtained by curve fitting normalized data. The curve fitting process starts with the equations that were needed and what they signify. In the simplest case, the curve fit had only one time constant, τ_m^*, being used to represent $W^*(t)$ or represented as W_t^*.

These equations with one time constant are as follows, respectively, for adsorption and desorption:

$$W_{t,\,\text{Adsorption}}^* = \left(1 - e^{\frac{-t}{\tau_m^*}}\right) \qquad 4.1\text{–}2$$

$$W_{t,\,\text{Desorption}}^* = \left(e^{\frac{-t}{\tau_m^*}}\right) \qquad 4.1\text{–}3$$

The curve fit is better using two time constants, $\tau_{m,1}$ and $\tau_{m,2}$, with each time constant corresponding with a weighting factor $X_{m,1}$ and $X_{m,2}$.Physically using two time constants also is more accurate due to the two dominating factors during the sorption processes. While the first, faster, time constant is more representative of the effective diffusion and sorption that occurs at or close to the air-particle interface; the second, much larger time constant is thought to be a consequence of the water vapor having very slow effective diffusion furthest from the air-particle interface and closest to the aluminum foil after the initial boundary becomes more saturated (Shang & Besant, 2009a).

Equations with two time constants for adsorption and desorption, respectively, are:

$$W^{*}_{t,\ \text{Adsorption}} = X_{m,1,\text{Ads}}\left(1 - e^{\frac{-t}{\tau_{m,1,\text{Ads}}}}\right) + X_{m,2,\text{Ads}}\left(1 - e^{\frac{-t}{\tau_{m,2,\text{Ads}}}}\right) \qquad 4.1\text{–}4$$

$$W^{*}_{t,\ \text{Desorption}} = X_{m,1,\text{Des}}\left(e^{\frac{-t}{\tau_{m,1,\text{Des}}}}\right) + X_{m,2,\text{Des}}\left(e^{\frac{-t}{\tau_{m,2,\text{Des}}}}\right) \qquad 4.1\text{–}5$$

Where,

$$X_{m,1} + X_{m,2} = 1; 0 \le X_{m,1} \le 1; 0 \le X_{m,2} \le 1 \qquad 4.1\text{–}6$$

$$\tau_{m,1} > 0; \text{and } \tau_{m,2} > 0 \qquad 4.1\text{–}7$$

Combining the time constants together, a weighted time constant was obtained:

$$\tau^{*}_{m} = X_{m,1}\tau_{m,1} + X_{m,2}\tau_{m,2} \qquad 4.1\text{–}8$$

The overall moisture time constant, τ^{*}_{m}, is the weighted time constant for latent heat effectiveness of energy wheels. Due to the weighting factors properties of $X_{m,1} > X_{m,2}$ the overall moisture time constant is dominated by the first moisture time constant, $\tau_{m,1}$. It could also be noted that slowly rotating desiccant drying wheels will use a long period for sorption but rapidly rotating energy wheels, will only have 1 to 2 seconds to respond, therefore, all both the first and overall moisture time constants will be given for each coating.

Figure 4.3 shows examples of the curve fits that were obtained through MatLab™, and the relevant equations that were used for the process are also shown in the figure.

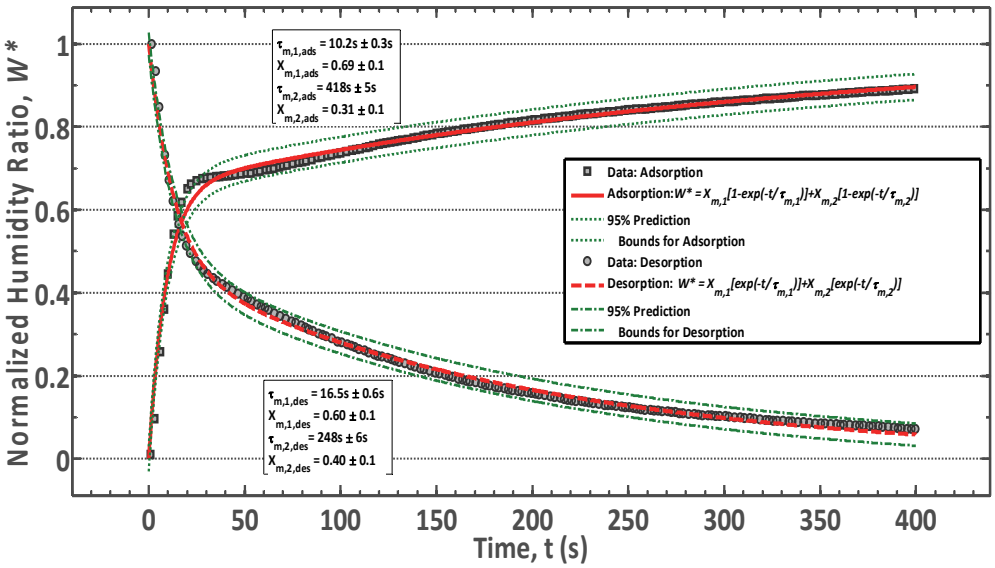

Figure 4.3: Curve fitted data of normalized transient humidity data at two points across a test cell containing a coarse coating, CC, agglomerated sample with a step change for both adsorption and desorption. Humid air at 75% RH and 22ºC to, dry air at 5% RH and 22ºC, and air an air face velocity, *v*, of 0.341 m/s and a Reynolds number of 149.

4.1.3 Uncertainty of the Time Constants taken from Humidity Response

Wang et al. (2005) shows that each humidity sensor had two uncertainties associated with a step change, one for the sensor first time constant, $B(\tau_{m,1}) \le \pm 13\%$, and another for the sensor second time constant, $B(\tau_{m,2}) \le \pm 30\%$, as these uncertainties were biased for transient measurements. This bias, B, when combined with the precision data for an experiment gives the total uncertainty at the 95% confidence level.

$$U = \sqrt{B^2 + P^2} \qquad 4.1\text{–}9$$

Wang et al. (2005) shows that each uncertainty in the bias, B, remains quite low if not negligible compared to the precision uncertainty, P, with curve fits of greater than $R^2 \ge 0.99$. And for this case it can be shown that the sensor bias is almost negligible compared with the error associated with the precision of the curve fit, e.g. the best curve fit obtained was obtained

with CC and a face velocity of 0.0683 m/s which would give $B(\tau_{m,1}) \leq \pm 0.1$ s and an $B(\tau_{m,2}) \leq \pm 3$ s for the sensors, and the uncertainty due to precision was $P(\tau_{m,1}) \leq \pm 0.5$ s and an $P(\tau_{m,2}) \leq \pm 31$ s. Using equation 4.1–9, it follows that $U(\tau_{m,1}) \leq \pm 0.51$ s and $U(\tau_{m,2}) \leq \pm 31.1$ s. For this case where P is much less than $P_{average}$ it is still the case that B has barely an effect on the uncertainty and becomes even more negligible for the majority of the cases. Therefore, the total uncertainty used is just what is obtained from the confidence bounds of the curve fits in the prior section 4.1.2 and is calculated as follows:

$$\left|U(\tau_m^*)\right| = \left[\left|P(\tau_{m,1}) \cdot X_{m,1}\right| + \left|P(X_{m,1}) \cdot \tau_{m,1}\right|\right] + \left[|P(\tau_{m,2}) \cdot X_{m,2}| + |P(X_{m,2}) \cdot \tau_{m,1}|\right] \qquad 4.1\text{–}10$$

Where all of the unknowns can be gathered directly from the curve fits obtained from MatLab™.

4.1.4 TIME CONSTANTS FROM TRANSIENT HUMIDITY RESPONSE

After examining all the different test data, calculating their respective time constants with MatLab™ and equations 4.1–4 to 4.1–8, Table B.1 and Table B.2 show all the numerical values of the three previously explained τ_m^*'s with the uncertainty as explained in the previous chapter. The data in Table B.1 was then used to produce the graphs found in this and the following section, along with corresponding error bars.

The resultant overall moisture time constant, τ_m^*, from equation 4.1–8 was then plotted against the measured face velocity for each coating. It is clear that for adsorption and for desorption; the trends of the time constants of the newly agglomerated, CC and FC, coatings are much higher than the industrial coating, IC. Both the fine coating with half the sheets, FCHS, and the blank coating, BC, give results similar to the IC (see Appendix Figure B.1 and Figure

B.2). Although the BC is not considered a true blank as it was just tested to determine the role that coating agent, latex paint, plays in the sorption of moisture. It is also worth noting that both the FC contain about a third of the mass of the other coatings. If the FC was closer in mass to the CC, resulting observations could be much better for this coating, therefore, it is important that all of these coatings be studied in more detail, i.e. for equal coating mass per unit area, fraction of the surface area completely covered by desiccant particles, and higher flow channel Reynolds number.

Figure 4.4 shows the transient moisture time constant, τ_{m}^{*}, data of CC, FC and IC obtained from MatLab™ curve fits plotted against the known face velocity of the air flowing across the sheets for both the adsorption and desorption process. It is shown that for all three of the most important coatings tested, the adsorption and desorption curves are very close together. This means that there is virtually no difference between the sorption processes.

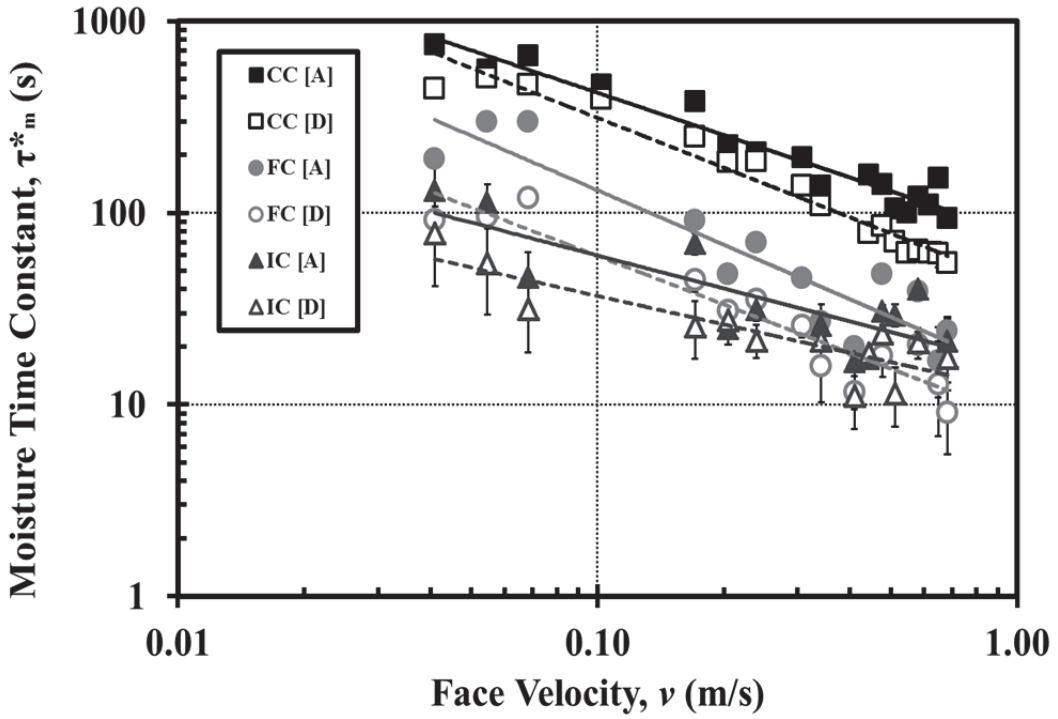

Figure 4.4: Transient moisture time constant, τ_m^*, from the transient humidity data of CC, FC and IC obtained from MatLab™ curve fits plotted against the known face velocity, *v*, of the air flowing across the sheets for both the adsorption and desorption process.

In Figure 4.5 only the first time constant, $\tau_{m,1}$, was looked at. It is important to note that the most prominent time constant in τ_m^* is the first time constant, $\tau_{m,1}$, and it is thought to be a consequence of air diffusion resistance(Wang, 2005). Wang showed that the second time constant is at least an order of magnitude greater than the first one perhaps because of a slow diffusion process of water molecules and this is also observed in this thesis. The correlation of the first time constant is almost the same as the overall moisture transfer time constant, because the first is always weighted more heftily than the second in equations 4.1–4 to 4.1–8. Nonetheless it is still important to calculate the overall moisture transfer time constant as this gives a more accurate representation of the process as most authors have demonstrated (Abe, 2005; Abe, Simonson, Besant, et al., 2006a, 2006b; Shang & Besant, 2009a, 2009b; Wang et al., 2005).

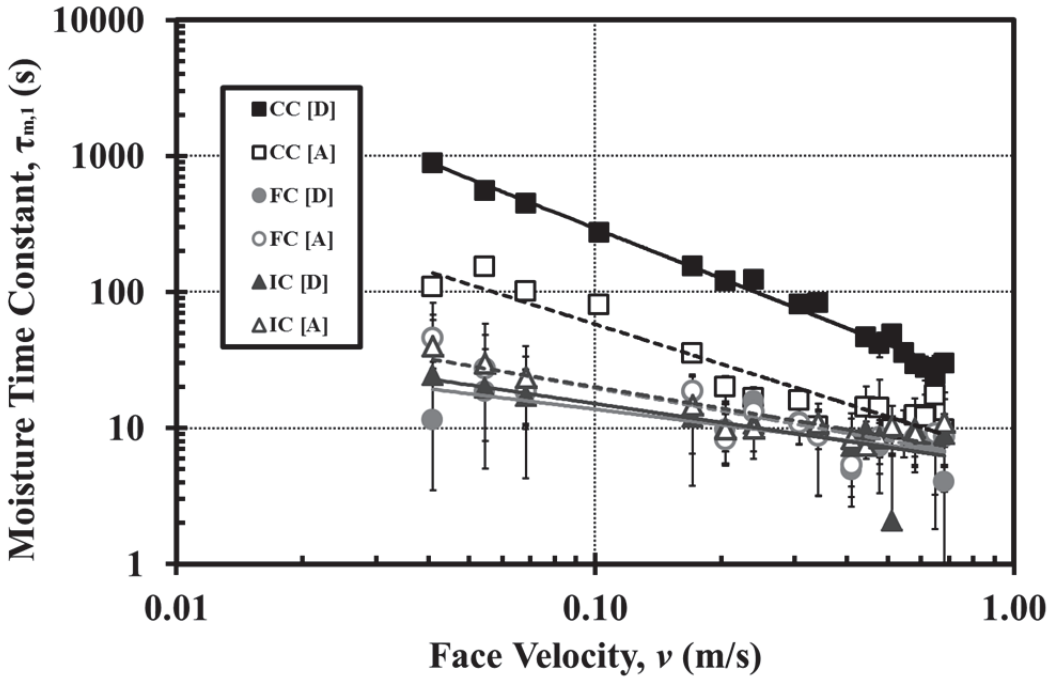

Figure 4.5: Only the first unweighted time constant, $\tau_{m,1}$, from the transient humidity data of CC, FC and IC obtained from MatLab™ curve fits plotted against the known face velocity, v, of the air flowing across the sheets for both the adsorption and desorption process.

4.1.5 Equation Approximations for the Various Coatings from Humidity Response Data: Time Constants as a Function of Face Velocity

It was shown from the aforementioned work (Abe, 2005; Abe, Simonson, Besant, et al., 2006a, 2006b; Shang & Besant, 2009a, 2009b; Wang et al., 2005) that it is more accurate to represent the overall moisture time constant, τ_m^*, as a function of two time constants, $\tau_{m,1}$ and $\tau_{m,2}$, from the equations 4.1–4 to 4.1–8, and, therefore, the results from Figures 3.18 and 3.19. The resultant time constants of τ_m^* in seconds are presented as power functions of face velocity in m/s, v, below. These correlations are useful in order to quantify and compare the relative difference in these specific results or results with same testing procedure and apparatus.

While doing the curve fits it was noticed that in general all the data follows a similar slope on a log-log plot, meaning that in order to fit the data, a common exponent was chosen to yield

more accurate comparative results. To obtain a common exponent, Excel™ was used in order to give rough approximations as to an average slope that could best fit all the data across the various utilized face velocities, (see Appendix B Figures B.1 & B.2, and Tables B.7 & B.8). With an average of the exponents from these least square functions done by using an Excel™ power equation curve fit, as well as by some manual trial and error in order to reduce the overall coefficient of determination, R^2, a common exponent power of -0.9 was found to give the best fit for all of the coatings time constants as functions of face velocity. Therefore, this more accurate representation for the coatings with common exponents was derived, and can be graphically seen in Figures 4.7 & 4.8. This goodness of these fit is, therefore, only dependent on one curve fitting constant, (i.e. the constant in front of the independent variable of face velocity, *v*). Not only is the fit presented here more universally applicable but it also offers higher values of the least square residuals squared, R^2, for most of the curve fits of the experimental time constants result from the coating testing procedure.

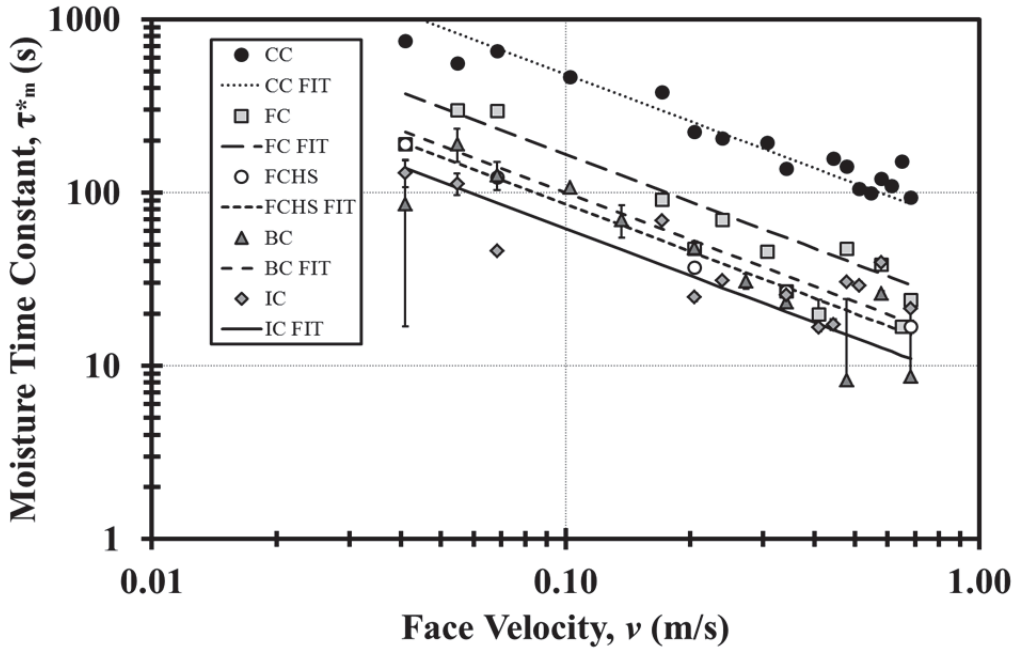

Figure 4.6: Transient moisture time constant, τ^*_m, data of all the coatings obtained from MatLab™ curve fits plotted against the known face velocity, *v*, of the air flowing across the sheets for the **adsorption** process. The best fit lines are power fits obtained through MatLab™ with a common power or slope on the log-log graph.

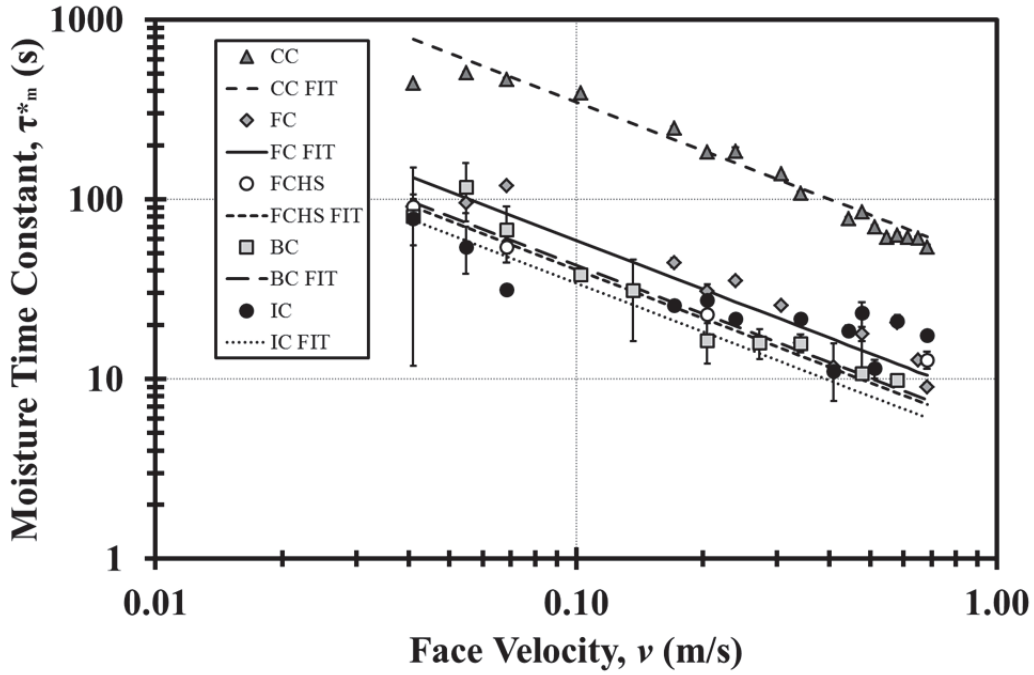

Figure 4.7: Transient moisture time constant, τ^*_m, data of all the coatings obtained from MatLab™ curve fits plotted against the known face velocity, *v*, of the air flowing across the sheets for the **desorption** process. The best fit lines are power fits obtained through MatLab™ with a common power or slope on the log-log graph.

A least square function with a MatLab™ power equation correlation that has common exponents for all sorption processes and coatings is used in Tables 4.1 & 4.2 for both adsorption and desorption respectively. It is also clear by these values and visually for the Figure 4.8 that the curve fits for both sorptions are more closely related and also give much more precise and accurate fits, as is the case for all the coatings but namely for the CC, FC and IC. It is also clear that the desorption process for all of the coatings has a smaller time constant than for the adsorption meaning that none of the coatings are able to release moisture or water vapour as fast as they can adsorb it; which physically makes sense since it is fairly common that a material will have a different rate of adsorption and desorption and in this case the silica gel agglomerates tend to have a faster rate of adsorption than its desorption process.

Table 4.1: Overall moisture time constants, τ_m^* in seconds, presented as power functions of the face velocity, v, in m/s, as taken from adsorption moisture response data. Least squared approximations taken from MatLab™ with common power exponents as taken from Figure 4.11

CC:	$\tau_m^* = 48.84v^{-0.9}$	$R^2 = 0.883$	4.1–11
FC:	$\tau_m^* = 17.06v^{-0.9}$	$R^2 = 0.759$	4.1–12
FCHS:	$\tau_m^* = 10.73v^{-0.9}$	$R^2 = 0.997$	4.1–13
IC:	$\tau_m^* = 7.441v^{-0.9}$	$R^2 = 0.747$	4.1–14
BC:	$\tau_m^* = 9.441v^{-0.9}$	$R^2 = 0.619$	4.1–15

Table 4.2: Overall moisture time constants, τ_m^* in seconds, presented as power functions of the face velocity, v, in m/s, as taken from desorption moisture response data. Least squared approximations taken from MatLab™ with common power exponents as taken from Figure 4.12

CC:	$\tau_m^* = 34.94v^{-0.9}$	$R^2 = 0.843$	4.1–16
FC:	$\tau_m^* = 6.999v^{-0.9}$	$R^2 = 0.810$	4.1–17
FCHS:	$\tau_m^* = 5.124v^{-0.9}$	$R^2 = 0.989$	4.1–18
IC:	$\tau_m^* = 4.286v^{-0.9}$	$R^2 = 0.702$	4.1–19
BC:	$\tau_m^* = 5.851v^{-0.9}$	$R^2 = 0.829$	4.1–20

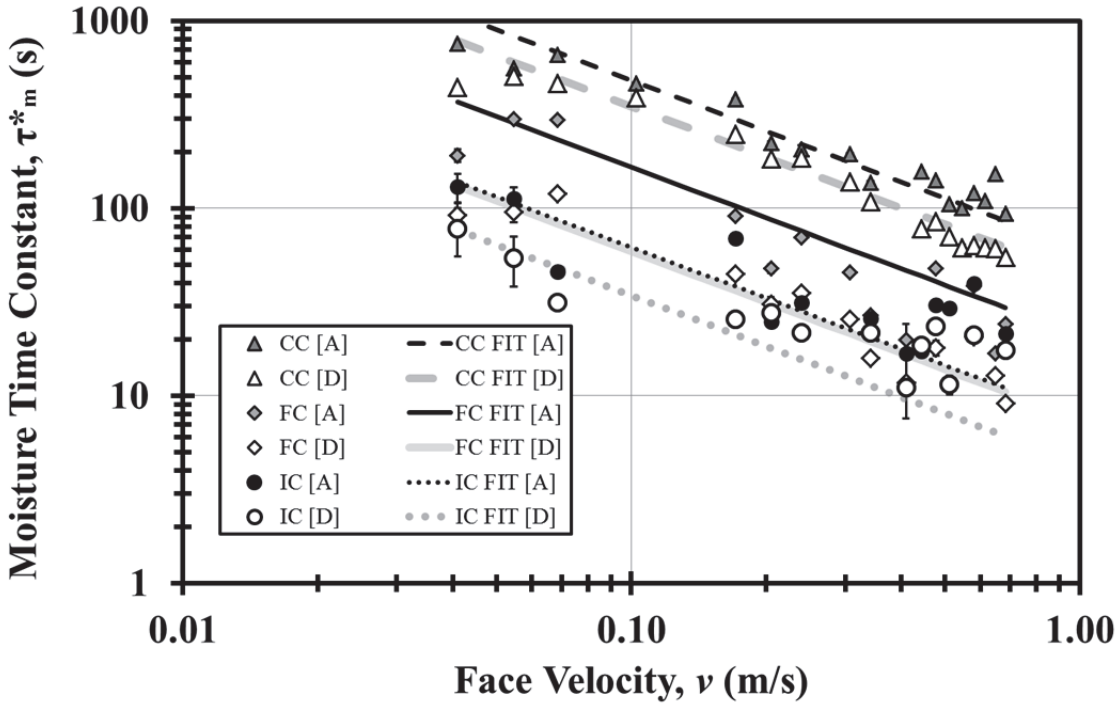

Figure 4.8: Transient moisture time constant, τ^*_m, data of CC, FC and IC obtained from MatLab™ curve fits plotted against the known face velocity, v, of the air flowing across the sheets for both the adsorption and desorption process. The best fit lines are power fits obtained through MatLab™ with a common power or slope on the log-log graph.

In the next section these time constants were calculated by the temperature response data, and then they were compared to one another in the following section. In Chapter 5 the equations obtained here were used to determine a latent or moisture effectiveness with a theoretical energy wheel rotating at certain angular velocities and for a range of various face velocities, more closely relating those that are actually used for practical purposes.

4.2 Transient Moisture Sorbance with Temperature Response

The same transient response experiments performed in the last section were also monitored for a temperature change due to sorption. Again this response varies from coating to coating and the same experimental test facility described by Figure 2.2 was used to measure the transient

response of the temperature downstream of a step change in the inlet humidity of air flowing across a test cell obtaining a certain coating.

An example of the raw data taken from the temperature sensor is shown in Figure 4.9. The temperature sensors gave a reading in degrees Celsius (ºC), but this reading was inconsistent from sensor to sensor, therefore, the readings were calibrated with a reference temperature and humidity to give more accurate readings. The temperature sensor readings as taken from the data in Table C.1, correspond to a specific relative humidity percentage and air at 24ºC as referenced from the calibration environment chamber. Figure C.2 shows the calibration temperature offset in ºC that was used for each thermocouple's reading in reference to the set temperature and respective humidity of the environment calibration chamber. Using the data from the calibration, an approximate error due to the accuracy of the instruments was obtained. As one can see by the data there are also another two types of error that are introduced into the system that will affect the precision of our results.

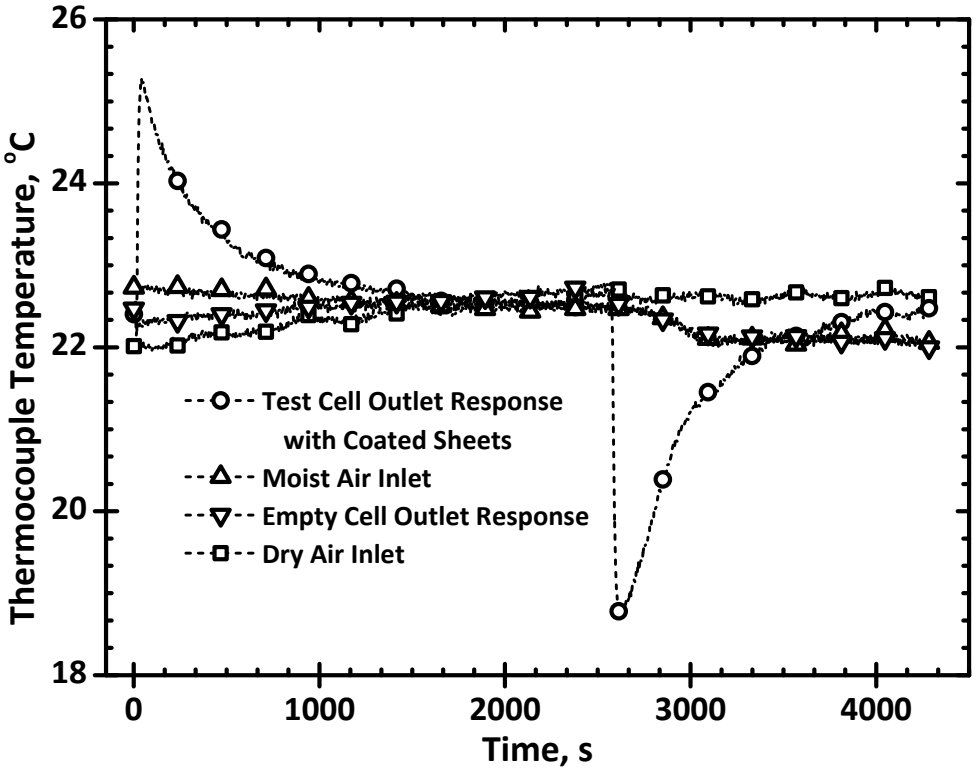

Figure 4.9: Raw transient temperature data in ºC at four points across a test cell containing a coarse coating, CC, agglomerated sample with first a step change in dry air to moist air, and then back again, and opposite step changes across an empty cell. Moist air at 75% RH and 22ºC to, dry air at 5% RH and 22ºC, and air an air face velocity, *v*, of 0.341 m/s and a Reynolds number of 149.

These thermocouples, like the humidity sensors, also introduced two more errors in precision due to the electrical noise when taking measurements with analog and/or digital electronic devices as well as the actual fluctuations in local temperature of both the dry and the wet air due to the setup and the impossibility of keeping them 100% constant.

4.2.1 NORMALIZING THE TEMPERATURE RESPONSE DATA

The following equation was used to analyze the data:

$$\Theta_t = \frac{\Delta T_t}{\Delta T_M} = \frac{T_{out,t} - T_{inlet}}{\Delta T_M} \qquad 4.2\text{–}1$$

where

Θ_t = normalized and dimensionless temperature response at time equal to t due to sorption

ΔT_t = the change in temperature at time equal to t

$T_{out,t}$ = measured temperature at the outlet at time equal to t

T_{inlet} = measured temperature at the inlet where the sensors are corrected so that at $t = 0$, $T_{out,0} = T_{inlet}$

ΔT_M = the maximum change in outlet temperature due to sorption

and

$$\Delta T_M = \frac{h_{ads} \Delta W_M}{c_{pa}} \qquad 4.2\text{–}2$$

where

h_{ads} = the heat of adsorption, which was estimated at the heat of vaporization for water, as these two will be relatively close in value

ΔW_M = the maximum change in the outlet's humidity ratio as $t \to \infty$

c_{pa} = the heat capacity of the air

Equation 4.2–1 shows how the raw data was normalized for temperature across the time for the run. The equation takes the temperature at any one point and subtracts the inlet constant temperature at 24º Celsius and then divides by the maximum possible change in temperature due to sorption. For this normalization it is assumed that the heat of adsorption is equal to the heat of vapourization, and although this assumption is not correct it should be very close. And because the same normalization is applied to each of the coatings the difference in these values will be negligible when comparing the data to other data referenced in the same manner. In other words, these curves may only suit for comparing data analyzed in the same manner, which in this

research study is all of the relevant data. It should also be noted that this assumption only affects the magnitude of the peak of the analyzed data and not the actual response used for obtaining the time constants. This normalization is again twofold in purpose, to make the data comparable to other data regardless of the magnitude of the step change in relative humidity, because the difference is taken with the humidity step change being used to determine the maximum temperature; and to also nullify the fluctuation of the relative humidity in the air because as the inlet fluctuates so too does the response and only the difference between the inlet and outlet temperatures is of concern.

Figure 4.10 shows how the temperature normalization was applied to Figure 4.9 for both the adsorption and desorption response giving the CC in the test cell and also for the same conditions on an IC. When looking at these figures it becomes apparent that the temperature response levels are much greater for the coarse coatings normalized than for the .industrial coating, this is in accordance with the humidity response obtained in the previous section that shows that the coarse coating is adsorbing or desorbing a greater volume and that it takes much longer for the coating to become saturated with liquid during the adsorption process and also that it takes longer for the liquid to fully reach desaturation during the desorption process. The amount of volume being adsorbed or desorbed is in direct correlation to the magnitude and duration of the response. Although not performed in this research, integration across the temperature response data should correlate directly to the amount of moisture each of the coatings was adsorbing or desorbing via these respective processes. When looking at the next section these details are discussed and the resulting time constants taken from this data were used to determine the overall coating effectiveness.

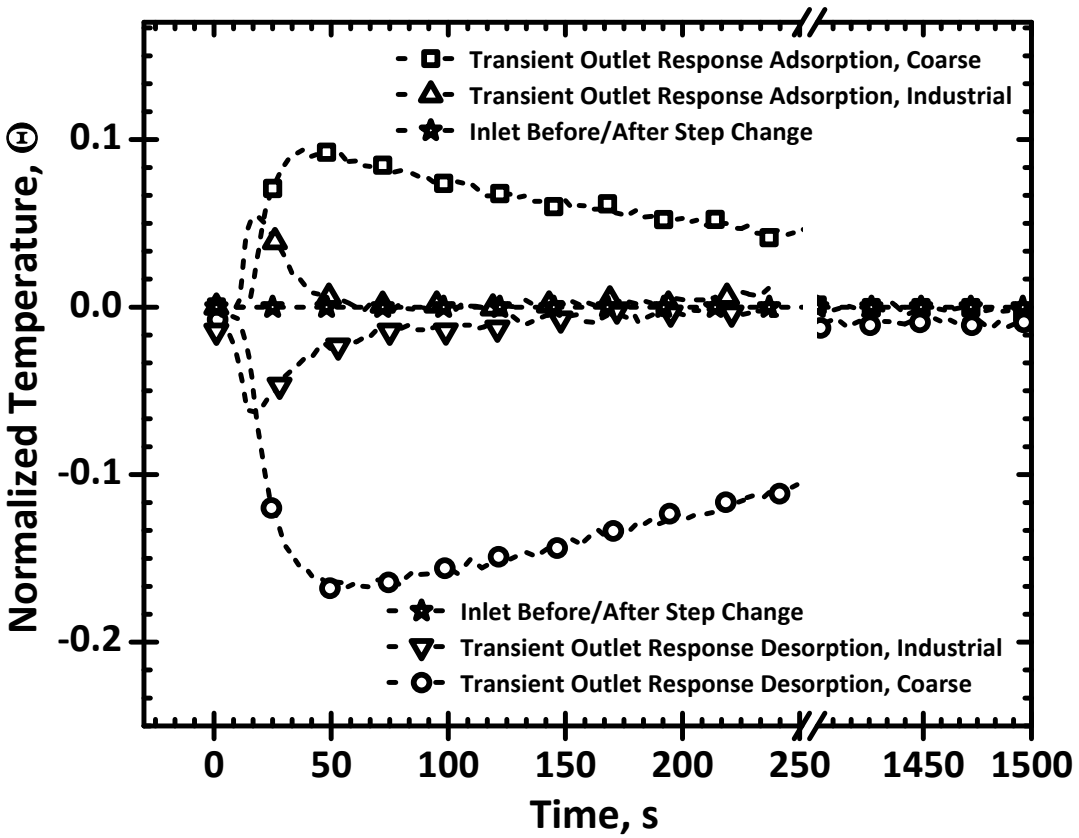

Figure 4.10: Dimensionless transient temperature data at two points across a test cell containing a coarse coating, CC, agglomerated sample with a step change in wet air to dry air, or as seen for the adsorption process. Wet air at 75% RH and 22ºC to, dry air at 5% RH and 22ºC, and air an air face velocity, *v*, of 0.36 m/s and a Reynolds number of 159.

4.2.2 TIME CONSTANT ANALYSIS FROM TEMPERATURE RESPONSE

The temperature response after a step change in humidity is represented by two time constants: the time constant for latent effectiveness, τ_m^*, and the time constant for sensible effectiveness, τ_s. Shang and Besant (2009a, 2009b) shows, respectively for adsorption and desorption, these equations as:

$$\Theta_{t,Adsorption} = +\left| e^{\frac{-t}{\tau_{s,ads}}} - e^{\frac{-t}{\tau^*_{m,ads}}} \right| \qquad 4.2\text{–}3$$

$$\Theta_{t,Desorption} = -\left| e^{\frac{-t}{\tau_{s,des}}} - e^{\frac{-t}{\tau^*_{m,des}}} \right| \qquad 4.2\text{–}4$$

Where $\Theta_{t,Adsorption,Max}$ and $\Theta_{t,Desorption,Min}$ are peaks for adsorption and desorption curves as fitted by the equations above. These peaks represent the total amount of moisture that can be sorbed into the coatings, the higher the peak the greater amount of heat released or absorbed by the phase change or the moisture into or from the desiccant coating.

Figure 4.11 shows examples of the curve fits that are obtained through MatLab™, and the relevant equations that are used for the process are also shown in the figures.

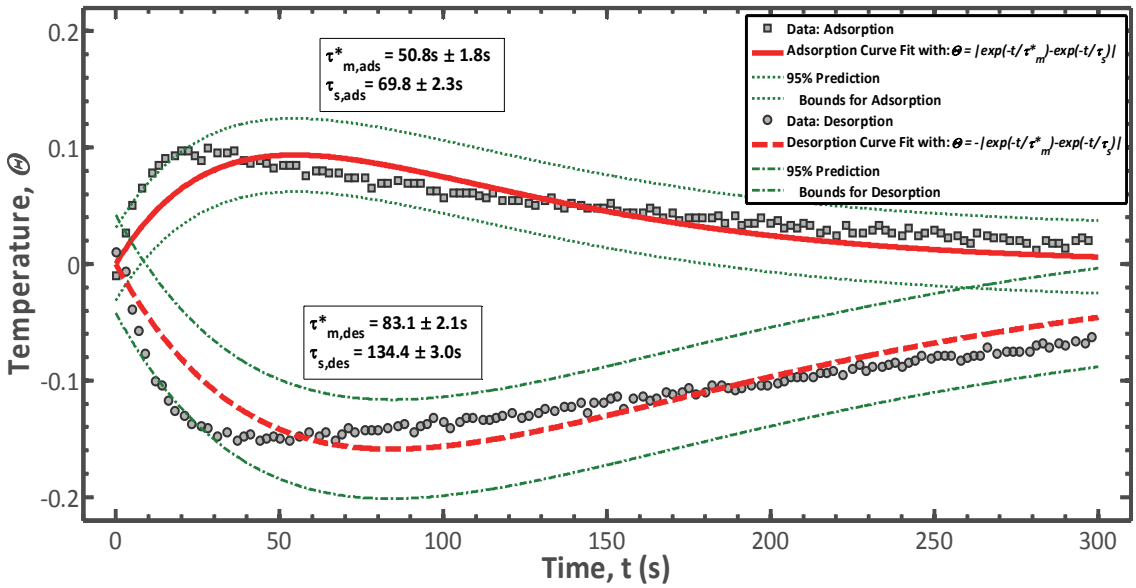

Figure 4.11: Curve fitted data of dimensionless transient temperature data at two points across a test cell containing a coarse coating, CC, agglomerated sample with a step change in dry air to wet air, or as seen for the adsorption process. Wet air at 75% RH and 22ºC to, dry air at 5% RH and 22ºC, and air an air face velocity, *v*, of 0.36 m/s and a Reynolds number of 159.

4.2.3 Uncertainty of the Time Constants taken from Temperature Response

Abe, Wang, et al. (2006) shows that each thermocouple has, like the humidity sensors, two biases associated with it, one for the first time constant, $B\left(\tau_m^*\right) \le \pm 30\%$, and one for the second time constant, $B\left(\tau_s\right) \le \pm 15\%$, as the same thermocouples are used. This bias, B, when

combined with the total precision of the curve fits at the 95% confidence level, P, gives the total root sum square uncertainty, U, as:

$$U = \sqrt{B^2 + P^2} \qquad 4.2\text{–}5$$

Abe, Wang, et al. (2006) shows that each uncertainty in the bias, B, remains quite low if not negligible compared to the offset P with curve fits of greater than $R^2 \geq 0.99$. And for this case it can be shown that the thermocouple bias is almost completely nullified as compared with the error associated with the precision of the curve fit, e.g. the best curve fit and, therefore, the smallest value of P obtained was obtained with CC and a face velocity of 0.055 m/s which would give $B\left(\tau_m^*\right) \leq \pm 0.045$ s and an $B\left(\tau_s\right) \leq \pm 0.033$ s for the thermocouple response and the uncertainty due to precision was $P(\tau_m^*) \leq \pm 7.08$ s and $P\left(\tau_s\right) \leq \pm 8.89$ s. Using equation 4.2–5, the resulting errors are obtained as $U\left(\tau_m^*\right) \leq \pm 7.08$ s and $U\left(\tau_s\right) \leq \pm 8.89$ s. For this case where P is much less than $P_{average}$ it is still the case that B has no significant effect on the uncertainty and becomes even more negligible for the majority of the cases. Therefore, the total uncertainty used is just what is obtained from the confidence bounds of the curve fits in the prior section 4.2.2 and is calculated as follows:

$$\left|U\left(\tau_m^*\right)\right| = \left|P\left(\tau_m^*\right)\right| \qquad 4.2\text{–}6$$

and

$$\left|U\left(\tau_s\right)\right| = \left|P\left(\tau_s\right)\right| \qquad 4.2\text{–}7$$

Where all of the unknowns can be gathered directly from the curve fits obtained from MatLab™.

4.2.4 TIME CONSTANTS FROM TRANSIENT TEMPERATURE RESPONSE

After examining all the different testing scenarios, calculating their respective time constants with MatLab™ and equations 4.2–3 to 4.2–7 the following tabulated data was resultant (see Appendix Tables B.3 to B.6). It is also clear that in Figure 4.12 with plotting the time constants versus the face velocities for each of the different coatings, that the trends of the time constants of the newly agglomerated, CC and FC coatings are much higher than the industrial coating, IC and that blank coating give negligible results as most of the peaks observed are very minute.

In Figure 4.13 the maximum peaks of each of the functions is plotted, and another trend is observed. It is clear that although the time constants are the most important factor when dealing with effectiveness the overall moisture that is transferred is also reflected in the height of the peaks. For the most part as the peak is greater, the time constants are also greater, but for BC and IC, even when the time constants are greater than those of other coatings, i.e. FC at high flowrates has a lower time constant than that of the BC at low flowrates but the amplitude of the peak or the amount of moisture transferred is much greater than that of the BC. This amplitude, therefore, needs to be investigated further.

It is also seen from Figure 4.14 plotting the resultant τ_s as a function of air face velocity, that the sensible time constant is also a power function of face velocity. The plots of these sensible time constants should be almost identical, in terms of magnitude and degree of change, from coating to coating due to the dissipation of heat by the aluminum foil; however, this is not the case and that although not as great of a difference as seen in the moisture time constant there is still the same general trend between the coatings. This implies that some of the coatings can also dissipate and absorb sensible heat energy as well as latent heat energy.

The overall moisture time constant for adsorption and desorption, $\tau^*_{m,ads}$ and $\tau^*_{m,des}$, are the main factors associated with the latent heat effectiveness of the energy wheels, and the sensible time constant for adsorption and desorption, $\tau_{s,ads}$ and $\tau_{s,des}$, are the main factors associated with the sensible heat effectiveness of the energy wheels. For energy wheels where the overall heat transfer is of greatest importance, both high τ_s and τ^*_m are useful and lead to increased effectiveness, however, for dehumidifier wheels it is important to also keep τ_s low in order to pass highest level of moisture but the lowest amount of heat energy. Although the τ_s was high for this research, this would be significantly lowered by replacing the aluminum foil used for testing with an ABS plastic as is the case with most industrial manufactured desiccant drying wheels. Therefore, the effectiveness of this research will be correlated to results of energy wheels in the next section, rather than desiccant drying wheels, although the drying wheels may be a more significant application for this type of coating, it was not tested for this case as aluminum foil was used as the coated substrate.

In the next section the time constants τ_s and τ^*_m were presented as functions of face velocity for each coating, but these simple correlations were only helpful in order to quantify the relative difference in these specific results or results with same testing procedure and apparatus.

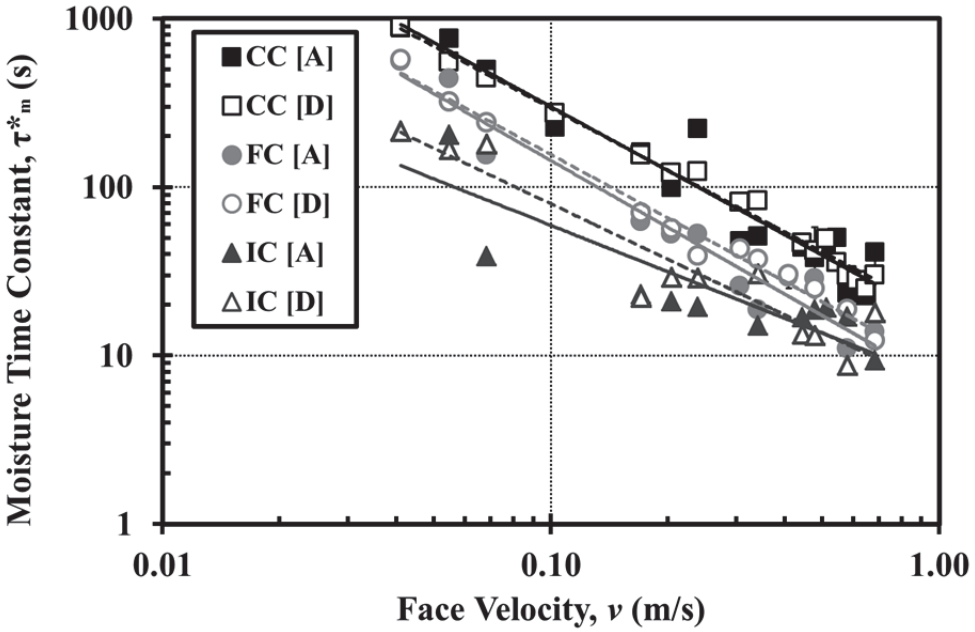

Figure 4.12: Moisture time constant, τ_m^*, obtained from the transient temperature response data of CC, FC, and IC obtained from MatLab™ curve fits plotted against the known face velocity, *v*, of the air flowing across the sheets for the adsorption and desorption processes. The best fit lines are power fits obtained through Excel™.

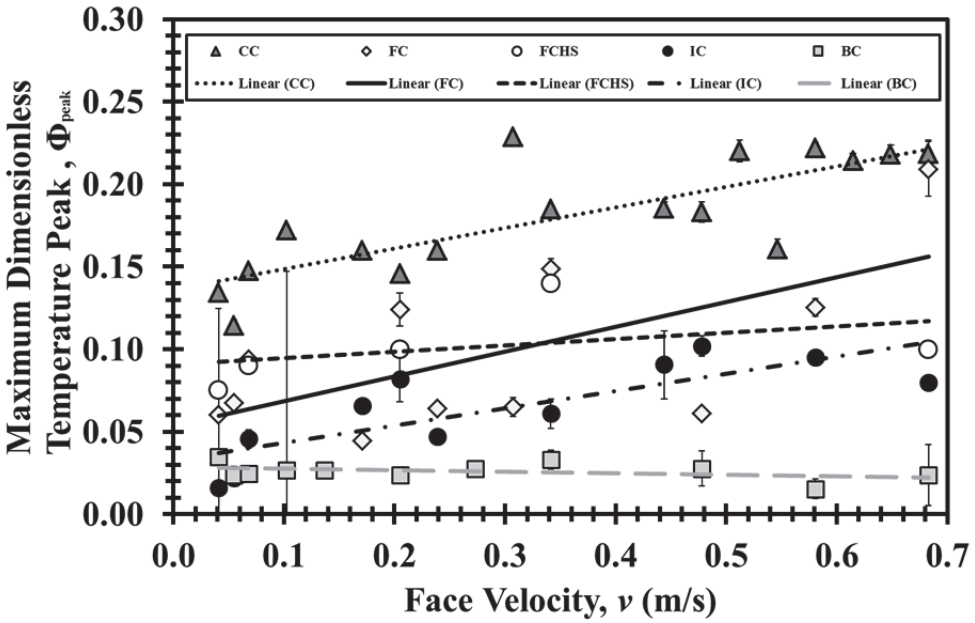

Figure 4.13: The maximum dimensionless temperature peaks, Φ_{peak}, obtained from the transient temperature response data as analyzed by the MatLab™ curve fits plotted against the known face velocity, *v*, of the air flowing across the sheets for the adsorption process. The best fit lines are power fits obtained through Excel™.

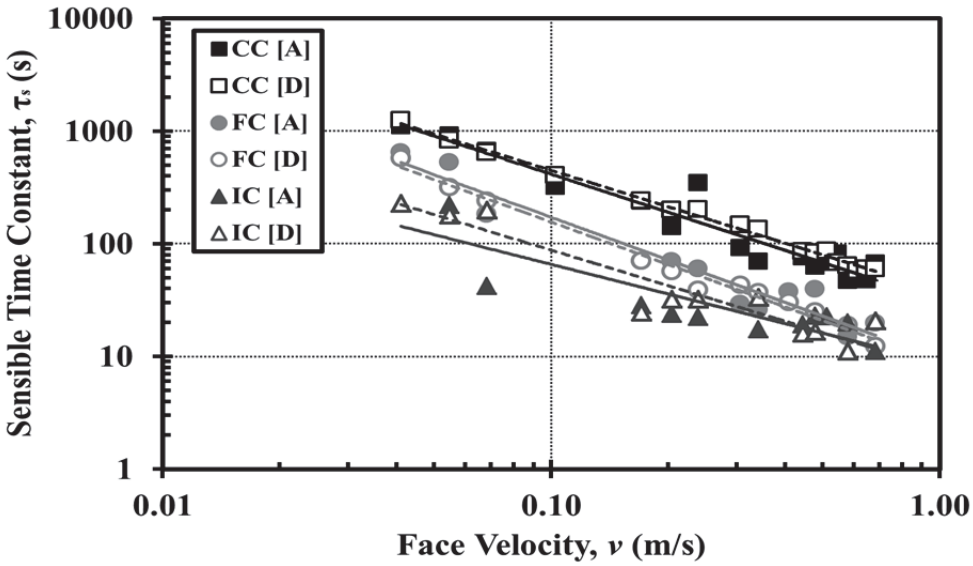

Figure 4.14: Sensible time constant, τ_s, obtained from the transient temperature response data of CC, FC, and IC obtained from MatLab™ curve fits plotted against the known face velocity, *v*, of the air flowing across the sheets for the adsorption and desorption processes. The best fit lines are power fits obtained through Excel™.

4.2.5 Equation Approximations for the Various Coatings from Temperature Response Data: Time Constants as a Function of Face Velocity

It was shown from the aforementioned work (Abe, 2005; Abe, Simonson, Besant, et al., 2006a, 2006b; Shang & Besant, 2009a, 2009b; Wang et al., 2005) that it is not only possible to represent the overall moisture time constant, τ_m^*, as a function of two time constants, $\tau_{m,1}$ and $\tau_{m,2}$, from the humidity response and the equations 4.1–4 to 4.1–8, but also from the temperature response data and equations 4.2–1 to 4.2–7 if moisture is being sorbed by the coating. These equations, which when combined with the error of the MatLab™ curve fits, are able to determine the moisture time constant, τ_m^*, as well as the sensible heat time constant, τ_s. The resultant time constants of τ_m^* in seconds are presented as power functions of face velocity, *v*, in m/s in Tables B.9 & B.10 which were taken from Figures B.3 & B.4. These correlations are useful in order to qualitatively compare the relative difference. In order to better quantify these

differences a best fit slope on a log-log plot for all the coatings can be taken and used to determine a best fit exponent for the power functions. Therefore, a more accurate representation for the coatings with common exponents was derived, and can be graphically seen in Figures 4.15 & 4.16.

With these figures a common power exponent of -1.2 was chosen that gives the best possible fit for all of the coatings. The fits obtained using this for the calculation of all the time constant functions gives the best possible fit as a function of face velocity for all the coatings, while maintaining a constant exponent. The goodness of these fits is, therefore, only dependent on the constant in front of the independent variable of face velocity, *v*. Not only is the fit presented here more universally applicable but it also offers higher values of the coefficient of determination, R^2, for most of the curve fits of the experimental coating results. Tables 4.3 & 4.4 show the according correlations and analyzing the data in this manner will help to ensure that the effectiveness correlations in the next part, Chapter 5, were more conducive for comparative purposes. These tables also show that for these functions the R^2 remains very high, and at a 95% confidence level the error remains relatively low, this confirms that using this type of fit to determine the time constant as a function of face velocity will be very effective and useful for the next chapter.

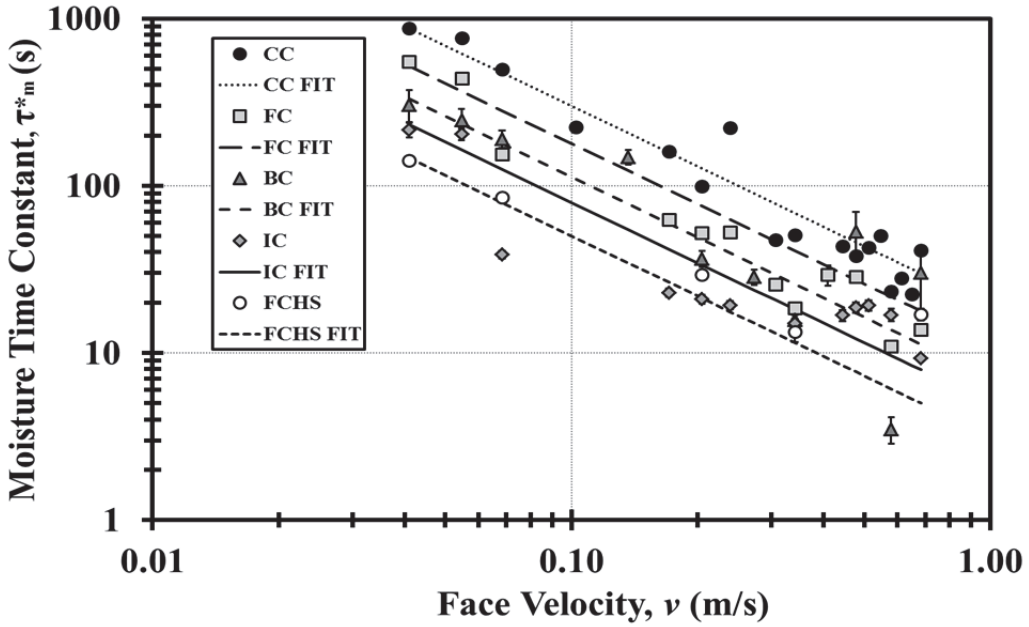

Figure 4.15: Moisture time constant, τ_m^*, obtained from the transient temperature response data of all the coatings obtained from MatLab™ curve fits plotted against the known face velocity, *v*, of the air flowing across the sheets for the **adsorption** process. The best fit lines are power fits obtained through MatLab™ with a common power or slope on the log-log graph.

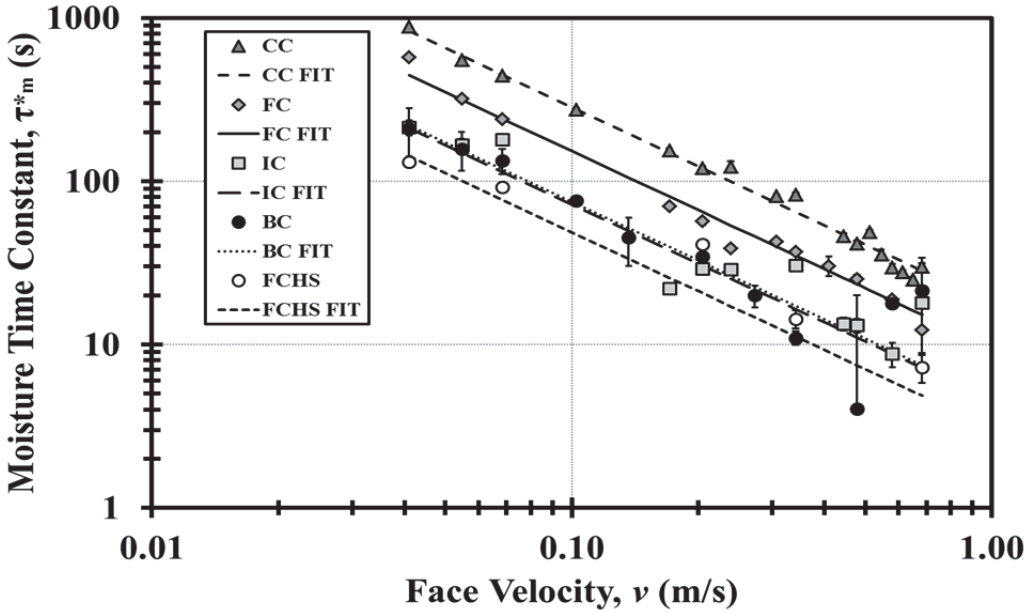

Figure 4.16: Moisture time constant, τ_m^*, obtained from the transient temperature response data of all the coatings obtained from MatLab™ curve fits plotted against the known face velocity, *v*, of the air flowing across the sheets for the **desorption** process. The best fit lines are power fits obtained through MatLab™ with a common power or slope on the log-log graph.

Table 4.3: Overall moisture time constants, τ_m^* in seconds, presented as power functions of the face velocity, *v*, in m/s, as taken from **adsorption** temperature response data. Least squared approximations taken from MatLab™ with common power exponents as taken from Figure 4.15

CC:	$\tau_m^* = 18.9v^{-1.2}$	$R^2 = 0.993$	4.2–8
FC:	$\tau_m^* = 11.3v^{-1.2}$	$R^2 = 0.931$	4.2–9
FCHS:	$\tau_m^* = 3.18v^{-1.2}$	$R^2 = 0.978$	4.2–10
IC:	$\tau_m^* = 5.02v^{-1.2}$	$R^2 = 0.848$	4.2–11
BC:	$\tau_m^* = 7.14v^{-1.2}$	$R^2 = 0.935$	4.2–12

Table 4.4: Overall moisture time constants, τ_m^* in seconds, presented as power functions of the face velocity, *v*, in m/s, as taken from **desorption** temperature response data. Least squared approximations taken from MatLab™ with common power exponents as taken from Figure 4.16.

CC:	$\tau_m^* = 17.9v^{-1.2}$	$R^2 = 0.999$	4.2–13
FC:	$\tau_m^* = 9.66v^{-1.2}$	$R^2 = 0.998$	4.2–14
FCHS:	$\tau_m^* = 3.084v^{-1.2}$	$R^2 = 0.917$	4.2–15
IC:	$\tau_m^* = 4.56v^{-1.2}$	$R^2 = 0.978$	4.2–16
BC:	$\tau_m^* = 4.75v^{-1.2}$	$R^2 = 0.981$	4.2–17

Figure 4.17 shows that the correlations for both the adsorption and desorption process for each of the CC, FC, and IC are very close to the same, though for the adsorption it is slightly higher. This observed increase in the moisture time constant for the adsorption, $\tau_{m,adsorption}^*$, over the moisture time constant for the desorption, $\tau_{m,desorption}^*$, is the case for all the calculated functions of the moisture time constant with respect to the face velocity. In other words, for each coating, at equal face velocities for the adsorption and desorption processes, then the moisture time constant will be greater for the adsorption than for the desorption process (i.e. $\tau_{m,adsorption,Coating}^* > \tau_{m,adsorption,Coating}^*$). This is the case with all the coatings and for the equations taken for the time constant as a function of face velocity for both the temperature response and humidity response and confirms that the adsorption process does in fact transfer more moisture

than that for the desorption process, and again this physically makes sense for the responses to behave as such.

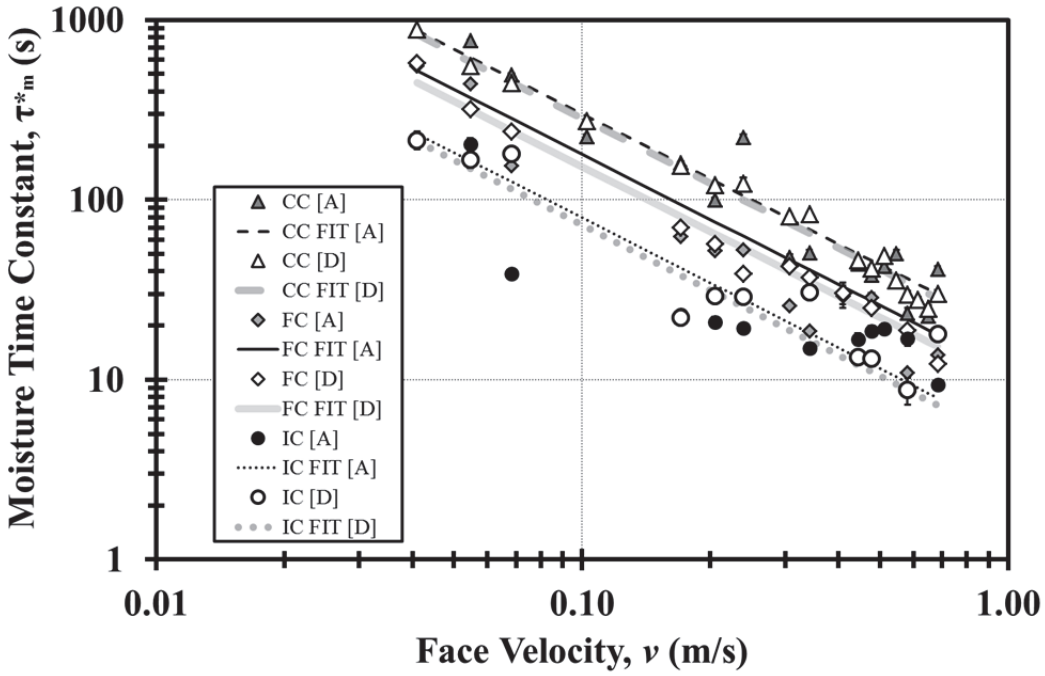

Figure 4.17: Moisture time constant, τ_m^*, obtained from the transient temperature response data of CC, FC, and IC obtained from MatLab™ curve fits plotted against the known face velocity, *v*, of the air flowing across the sheets for the adsorption and desorption processes. The best fit lines are power fits obtained through MatLab™ with a common power or slope on the log-log graph.

The sensible time constant was also obtained from the temperature response data. This can be taken due to the fact that the heat dissipation after the moisture has been fully adsorbed or desorbed bringing the temperature back to that of the incoming air flow. The sensible time constant was only calculated as a function of face velocities for the three most important coatings examined during this research. Tables 4.5 & 4.6 show how these functions were represented with a common exponent of -0.9 as was the case for all of the moisture time constants taken as functions of face velocities for the humidity response data. Because all the time constants can be obtained fairly accurately with a common exponent for all three to the time constants obtained for each coating this means that all the time constants behave in relatively the same physical

manner for each coating and response as when compared to one another. These functions for the sensible time constants were plotted in Figure 4.18 and the curve fits appear to follow the data very closely as a good value of R^2 was calculated.

Table 4.5: Overall sensible time constants, τ_s in seconds, presented as power functions of the face velocity, v, in m/s, as taken from **adsorption** temperature response data. Least squared approximations taken from MatLab™.

CC:	$\tau_s = 59.58v^{-0.9}$	$R^2 = 0.934$	4.2–18
FC:	$\tau_s = 31.24v^{-0.9}$	$R^2 = 0.836$	4.2–19
IC:	$\tau_s = 12.40v^{-0.9}$	$R^2 = 0.900$	4.2–20

Table 4.6: Overall sensible time constants, τ_s in seconds, presented as power functions of the face velocity, v, in m/s, as taken from **desorption** temperature response data. Least squared approximations taken from MatLab™.

CC:	$\tau_s = 55.69v^{-0.9}$	$R^2 = 0.990$	4.2–21
FC:	$\tau_s = 24.98v^{-0.9}$	$R^2 = 0.967$	4.2–22
IC:	$\tau_s = 12.51v^{-0.9}$	$R^2 = 0.956$	4.2–23

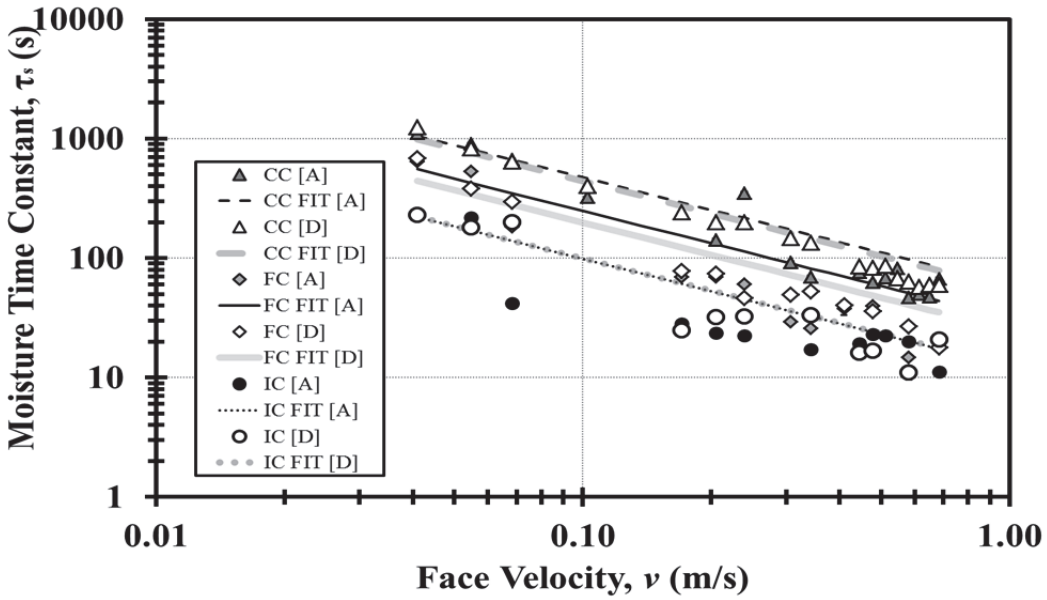

Figure 4.18: **Sensible** time constant, τ_s, obtained from the transient temperature response data of CC, FC, and IC obtained from MatLab™ curve fits plotted against the known face velocity, v, of the air flowing across the sheets for the adsorption and desorption processes. The best fit lines are power fits obtained through MatLab™ with a common power or slope on the log-log graph.

In the next section the moisture time constants for each of the three most important time constants were compared for each of the different response data (i.e. both temperature and humidity response, as well as for adsorption and desorption response for each).

4.3 Comparison of Temperature Response and Humidity Response Analyses

Figure 4.19 shows both the τ_m^* obtained from the moisture response of the moisture adsorption and desorption curve fits and those obtained from the temperature response of the moisture adsorption and desorption for each of the coatings versus the respective face. Although these two have very similar magnitudes for the range of the face velocities shown, there are still significant differences when comparing those obtained through the humidity response and temperature response and also for adsorption and desorption.

Firstly, due to the differences in the slopes, the uncertainty going outside of the shown bounds will become far too great especially if comparing temperature response data to humidity response data. Therefore, τ_m^* obtained through either of the response methods cannot be compared to one of a different response but must be compared to the results obtained through the same response. It is also worth noting that the equations used to simulate the response of the temperature-obtained time constant are in much closer agreement with the experimental results

The adsorption process always produces significantly higher time constants than that of the desorption process. The reason for this discrepancy between the sorption processes can be explained due to ink bottle theory. This theory explains a difference in adsorption and desorption due to a change in density of the porous desiccant that occurs during desorption and thus limits the total capacity of the desiccant (Naumov, 2009). Ink bottle theory explains the hysteresis that occurs in equilibrium isotherms, also seen in the previous chapter, and as this hysteresis affects

the capacity of the desiccant for each of the sorption processes, it in turn will affect the time constants that are obtained. Therefore, τ_m^* obtained through either of the response methods cannot be compared to one of a different response but must be compared to the results obtained through the same response. However, it is good to note that all of the equations for CC are higher than those for FC and those for FC, save one, are higher than those for IC. It is also worth noting that the equations used to simulate the response of the humidity obtained time constant is in much closer agreement with the experimental results. The next chapter will investigate how these time constant functions of face velocity could affect the latent effectiveness of the energy wheels being used.

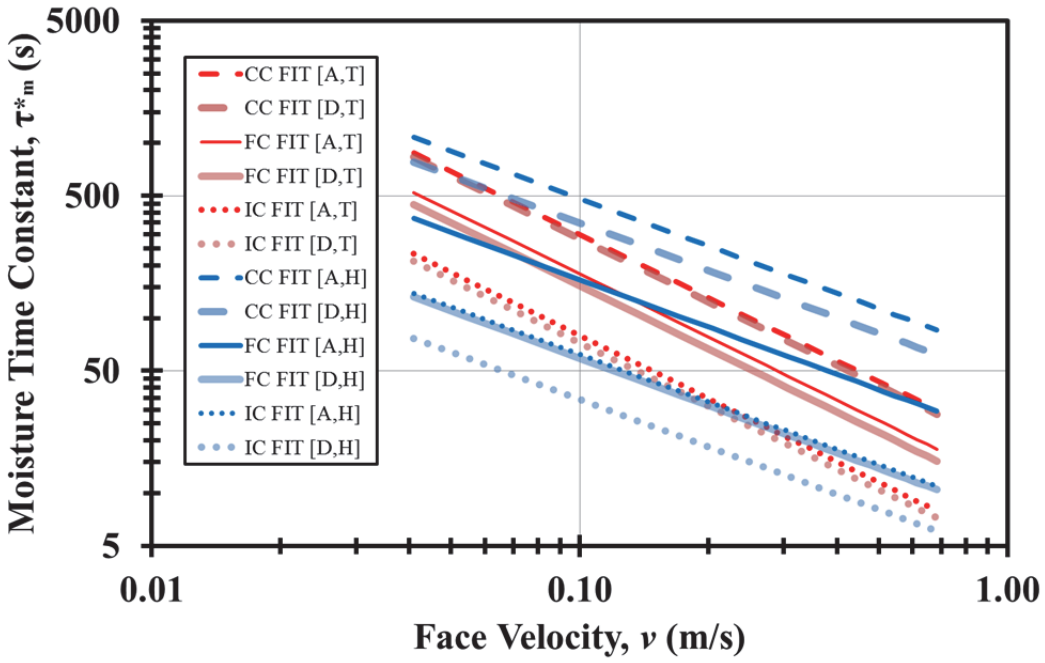

Figure 4.19: Function lines of the moisture time constant, τ_m^*, for adsorption, [A,x], and desorption, [D,x], obtained from the transient temperature, [x,T], and humidity, [x,H], response of CC, FC, and IC as a function of face velocity, v, obtained from MatLab™ fits.

4.4 CHAPTER SUMMARY

Chapter 4 presented and analyzed experimental transient system data for each of the 5 coatings: the coarse coating (CC), the fine coating (FC), the fine coating with half the sheets or mass of coating (FCHS), the industrial coating (IC) and the blank coating with just latex paint (BC). The response data taken at different flow rates (or face velocities) for each of the various coatings were normalized for both the humidity response and the temperature response. The normalized response data for the humidity ratio was then used to calculate two weighted moisture time constants from curve fitting their respective function found in past papers. These weighted time constants were then used to calculate the total moisture time constant, τ_m^*, and it is plotted as a function of face velocity for each coating for both adsorption and desorption responses. The normalized data for the temperature response was then used to calculate the total moisture time constants, τ_m^*, and sensible time constants, τ_s, directly from the curve fits; and both of these were plotted as a function of face velocity for each coating for both adsorption and desorption responses.

All of these functions or correlations are of an exponential nature and appear to consistently show that the CC gives much higher time constants than all the other coatings, with the FC functions plotted slightly below the curves for CC, while the remaining three, FCHS, IC, and BC, are significantly lower time constant curves. In the previous section in Figure 4.19 it is shown exactly how these moisture time constants (being the most important for a desiccant coating) vary between the coatings and for each of the responses. Also the mass of the total desiccant coating plays a significant role in how the response behaves and, therefore, how much the coating is sorbing. Perhaps if the total mass of the FC coating was equal to that of the CC and IC (both of which are very similar or about three times the mass of the FC), much better time

constant results would have been seen, as doubling the mass made a huge impact as was the case for the FC versus the FCHS. Because the goal of this research is to develop an energy wheel coating with increased time constants obtained from transient testing results, it is evident that both the CC and FC coatings have significant improvement over the IC.

CHAPTER 5 :
RESULTS & DISCUSSION FOR IMPLIED EFFECTIVENESS

In this chapter, the objective was to establish a theoretical and implied relationship between the step response time constants and the effectiveness of an energy wheel coated with the same coating as the surfaces used in the test cell. The predicted effectiveness of an energy wheel implies a number of assumptions which were presented in the recent research by Shang and Besant (2005a, 2005b, 2006a, 2006b, 2008, 2009a, 2009b, 2009c), Wang et al. (Wang, 2005; 2005; 2006), and Abe et. al (Abe, 2005; 2006a, 2006b; 2006a, 2006b; 2006). The equations for the effectiveness of a function of the time constant are then presented. Both the CC and FC were compared to the IC while the FCHS and the BC were disregarded. Only examining the relative difference between the time constants obtained from each of these 3 coatings, it will be shown how these differences could affect the coatings latent effectiveness. These time constant functions of face velocities are also analyzed given similar parameters to those used in past experiments.

Parallel flow and counter flow energy wheel arrangements were both presented, however, in applications such as university, office and industrial buildings, only the counter flow wheels are used. Therefore, only the counter flow arrangement equations were used for comparisons of the CC, FC and IC coatings. The effectiveness is then shown for all the coatings and compared for both the results from the humidity response data and the temperature response data. Comparisons between the effectiveness of the IC, FC and CC coatings on wheels at various rotational speeds were made. The uncertainty within these relationships are shown, however, it should be noted that these uncertainties were calculated in terms of the 95% confidence that the mean of the

steady state ASHRAE Standard 84 tests (2008) would fall into the associated error for each of the coatings.

5.1 Effectiveness and Time Constants Correlations

Effectiveness of energy wheel can be broken down into two subcategories, one for sensible heat and one for latent heat, and when combined will give a total effectiveness for the wheel. The term effectiveness in relation to heat exchangers is defined as the ratio of the energy that the exchanger is capable of exchanging to the maximum possible energy that could be exchanged given an infinite surface area for heat transfer. Or in other words for a parallel or counter flow energy wheel, the effectiveness is defined as the ratio of the *net energy* to the *maximum possible energy* (Abe, Simonson, Besant, et al., 2006a, 2006b). Relationships for effectiveness for energy wheels can depend on a number of factors, however, most of these factors were assumed to be constant for comparison purposes. The only factors that were changed in terms of parameters that affect effectiveness are the time constants for respective coatings. These equations were taken from Shang and Besant (2009a, 2009b), and assume the time constants obtained through this research were taken under the same wheel configuration and assumptions given in those papers. These assumptions are as follows:

1. The same energy wheel was used for both transient tests and steady state tests, and the time constant transient results were used in place of those from Shang and Besant (2009a, 2009b).
2. The supply and exhaust mass flow rates were equal and flow through equal area of the energy wheel, therefore, for every 180º of wheel rotation each flow channel could pass from exhaust to the supply and vice versa with no leakage in air transfer occurring.

3. Each flow channel inside a wheel matrix would have the inlet air go through a series of cyclic step changes corresponding to the wheel rotation.
4. The energy wheel rotates at a constant angular speed, ω, greater than 5 rpm.

5.1.1 PARALLEL FLOW AND COUNTER FLOW ENERGY WHEEL EFFECTIVENESS EQUATIONS

Shang and Besant (2008) show that the corresponding sensible and/or latent heat effectiveness for an energy wheel in a parallel flow arrangement with equal supply and exhaust flow rates and fully developed flow profiles in each channel can be expressed as:

$$\varepsilon_{k,FD-PF} = \frac{\omega\tau_k}{\pi} \bullet \frac{\left(1-e^{-\pi/\omega\tau_k}\right)^2}{\left(1-e^{-2\pi/\omega\tau_k}\right)} \qquad 5.1\text{–}1$$

As well, basic heat exchanger theory gives

$$\varepsilon_{k,FD-PF} = \frac{1}{2} \bullet \left(1-e^{-2N}\right) \qquad 5.1\text{–}2$$

where τ_k is the time constant of concern, ω is the wheel's angular velocity in rad/s, and N is the number of transfer units for convective heat or moisture transfer. Equating 5.1–1 and 5.1–2 gives:

$$N = \frac{1}{2}\ln\left[1 - \frac{2\omega\tau_k}{\pi} \bullet \frac{\left(1-e^{-\pi/\omega\tau_k}\right)^2}{\left(1-e^{-2\pi/\omega\tau_k}\right)}\right] \qquad 5.1\text{–}3$$

It is also noted that for latent effective k=m and for sensible effectiveness k=s. Since the number of transfer units, N, does not depend on flow direction the effectiveness for an energy wheel in a counter flow arrangement with fully developed flow profile can be expressed as:

$$\varepsilon_{k,FD-CF} = \frac{N}{1+N} \qquad 5.1\text{–}4$$

The following figures show how a general Ψ_k can relate to the effectiveness for any corresponding flow arrangements, and shows that as the Ψ_k increases the effectiveness increases. Where $\Psi_k = \omega\tau_k$ and implies that ω or τ_k need to increase in order to increase the effectiveness.

The next two sections apply these, assumptions and equations, to the transient results obtained in Chapter 4; and the last section of this chapter compares these results for the different coatings.

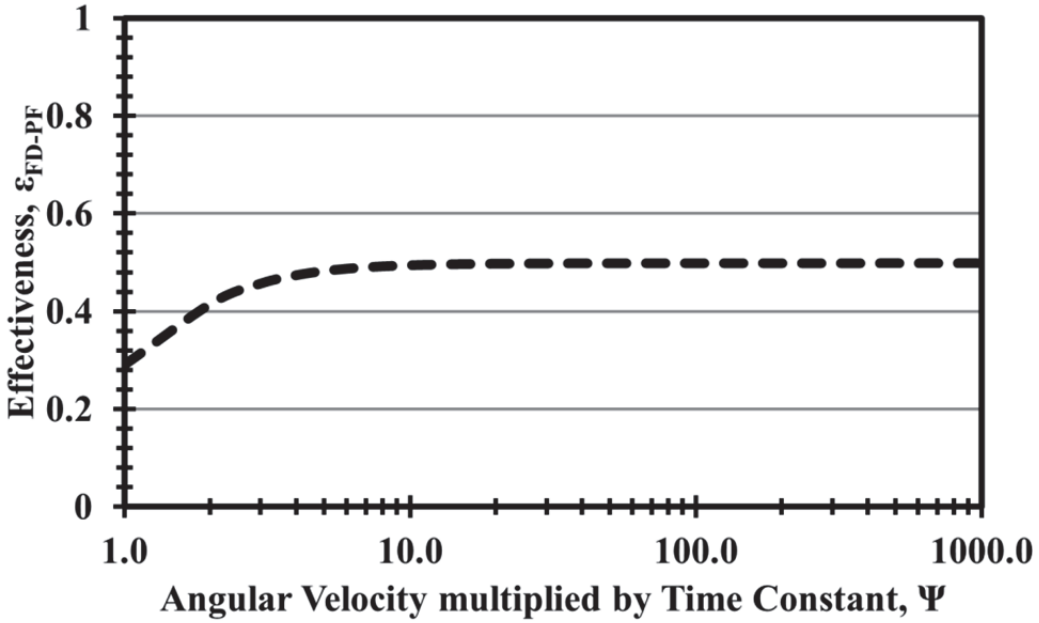

Figure 5.1: Fully developed **parallel** flow energy wheel effectiveness, $\varepsilon_{k,FD-PF}$, as a function of the time constant multiple by the wheel speed in radians, $\Psi_k = \omega\tau_k$.

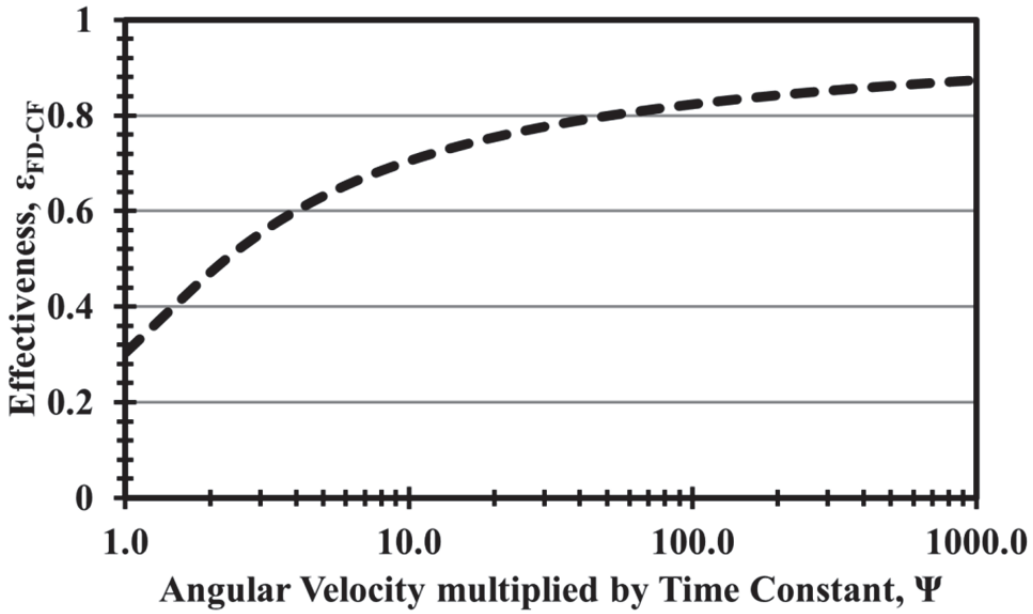

Figure 5.2: Fully developed **counter** flow energy wheel effectiveness, $\varepsilon_{k,FD-CF}$, as a function of the time constant multiple by the wheel speed in radians, $\Psi_k = \omega\tau_k$.

5.2 Simulated Effectiveness Comparisons for Counter Flow Energy Wheels

If a parallel flow arrangement is used, the effectiveness from Figure 5.1 and Figure 5.2 is very limited. Therefore, in most energy wheel applications, a counter flow scheme is used. This section will look at how 3 different coatings compare under certain situations, and will estimate the amount of improvement the newly developed coating might have over the ones currently being used. The blank coating is used to show how the latex paint as a coating agent might react as a desiccant. Half the sheets are tested to give an idea of how the total mass of the coating might affect the energy wheel. Only the coarse coating, fine coating and industrial coatings are of importance for these effectiveness results, as neither the blank coating or the fine coating with half the sheets are relevant for these predictions.

5.2.1 EFFECTIVENESS WITH TIME CONSTANT FUNCTIONS FROM HUMIDITY RESPONSE

After calculating the functions with the humidity response in Section 4.1.5, using the equation 5.1–4 and applying the aforementioned assumptions for the energy wheel the following results for the theoretical effectiveness are calculated and summarized in Figure 5.3:

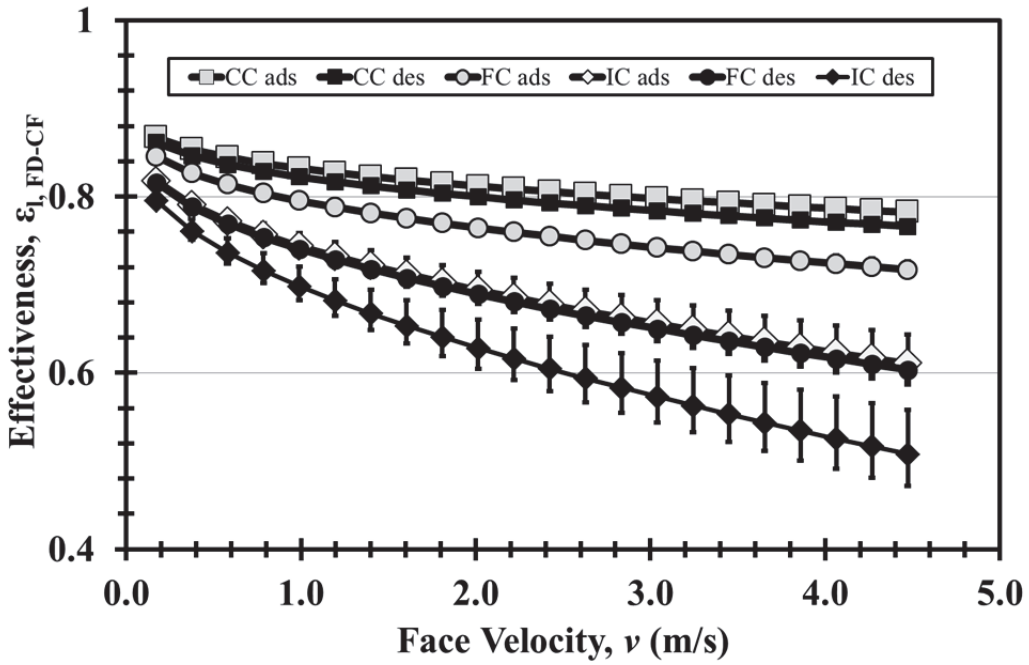

Figure 5.3: Latent effectiveness as a function of face velocity (m/s), v, as found from the **humidity desorption** and **adsorption** response results for only the CC, FC and IC coatings. At an operating wheel speed of 20 rpm.

In Figure 5.3 the latent effectiveness was calculated for a range of face velocities both ones that were tested and for face velocities of greater than 1 m/s they were extrapolated from the equations given in Table 4.1 and Table 4.2. It was assumed that the energy wheel would rotate at 20 rpm as is the case for most HVAC applications. The uncertainties that are plotted are at the 95% confidence level for those curve fits, but it is clear that both the CC and FC have much better curve fits and, therefore, the results are more accurate. It is also the case that the error gets larger as the effectiveness drops; this is discussed further in Section 5.3. Due to the CC and FC having a much higher time constants (and, therefore, effectiveness) the predictions for

effectiveness should be more accurate as well. The predictions made are strictly to determine where the mean of the samples should fall with 95% confidence if tested in a steady state system with the coatings on an energy wheel; it does suggest that the deviations of the sample would not be greater than the error shown.

5.2.2 Effectiveness with Time Constant functions from Temperature Response

After calculating the functions with the temperature response in Section 4.2.5, using the equation 5.1–4 and applying the aforementioned assumptions for the energy wheel the following results for the theoretical latent and sensible effectiveness at operating wheel speed of 20 rpm were calculated and summarized in Figure 5.4 and Figure 5.5, respectively:

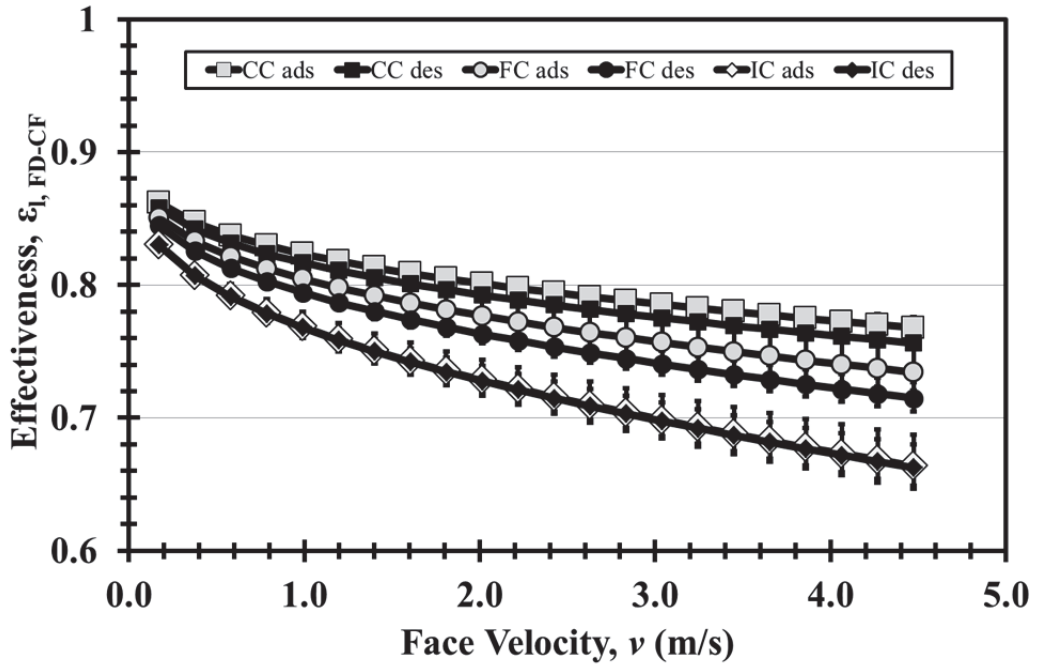

Figure 5.4: **Latent** effectiveness as a function of face velocity (m/s), v, as found from the **temperature desorption** and **adsorption** response results for only the CC, FC and IC coatings. At an operating wheel speed of 20 rpm.

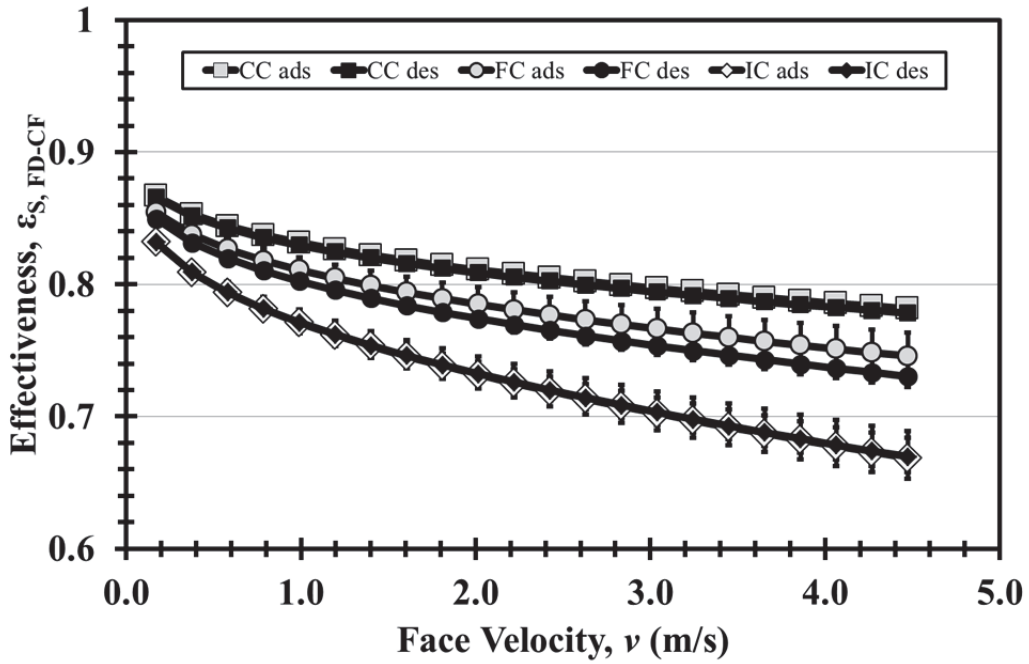

Figure 5.5: **Sensible** effectiveness as a function of face velocity (m/s) , *v*, as found from the **temperature desorption** and **adsorption** response results for only the CC, FC and IC coatings. At an operating wheel speed of 20 rpm.

In Figure 5.4 and Figure 5.5 the latent and sensible effectiveness was calculated and plotted, respectively, for a range of face velocities both ones that were tested and for face velocities of greater than 1 m/s they were extrapolated from the equations given in Tables 4.3 to 4.6. It was assumed that the energy wheel would rotate at 20 rpm as is the case for most HVAC applications. The uncertainties that are plotted are at the 95% confidence level for those curve fits, but it is clear that both the CC and FC have much better curve fits and, therefore, the results are pretty accurate. It is also the case that the error gets larger as the effectiveness drops; this is discussed earlier in section 5.2.2 and further in Section 5.3. The temperature response data gives values for adsorption and desorption that are much closer together than those from the humidity response, and it is more likely that they would tend to be relatively close together as the amount of mass adsorbed or desorbed are close as well as the rates of sorption are similar for both. The sensible and latent effectiveness behave in the same manner for each coating with the face

velocities. For an energy wheel this trend is exactly what the engineers are trying to accomplish by increasing both sensible and latent effectiveness with changing the desiccant coating from an IC to a FC or CC, means that the total energy exchanged is significantly higher and precisely the purpose of the wheel. However, with a desiccant wheel it is best to keep the sensible time constant (and, therefore, effectiveness) very low so as only to transfer moisture from one air stream to the other. This can be accomplished by replacing the aluminum foil substrate with plastic or some other material to limit the heat transfer, as is the case with most desiccant wheels. And again it should be stated that the predictions made are strictly to determine where the mean of the samples should fall with 95% confidence if tested in a steady state system with the coatings on an energy wheel, it does not suggest that the deviations of the sample would not be greater than the error shown.

Also due to the discrepancies between this method of collecting the time samples from the humidity response data and that of taken them from the temperature response data, it is not certain which provides more accurate results to the actual performance of the energy wheels and should be looked into further. The data is not averaged across both methods as this produces a much larger confidence band than what is shown. It is important to note that although these are not accounted for, the difference between CC, FC and IC would be significant. One of the primary reasons FC does not perform as well as CC is due to the mass difference in the coating samples that are tested, and as it was observed with FCHS the mass can make a significant difference in how coatings respond; therefore, future work is needed to ensure that a FC sample more closely resembles that of the CC and the IC samples.

5.2.3 Effectiveness Variations by Wheel Speed for each of the Agglomerated Coatings

The two coatings, CC and FC, were analyzed at 3 different rpm speeds (5, 10, and 20) and compared to the IC coating at the most utilized wheel speed in the current industry of 20 rpm. First the effectiveness of the CC was looked at for both humidity and temperature response and compared to the IC response for both cases, as shown below in Figure 5.6 and Figure 5.7, respectively:

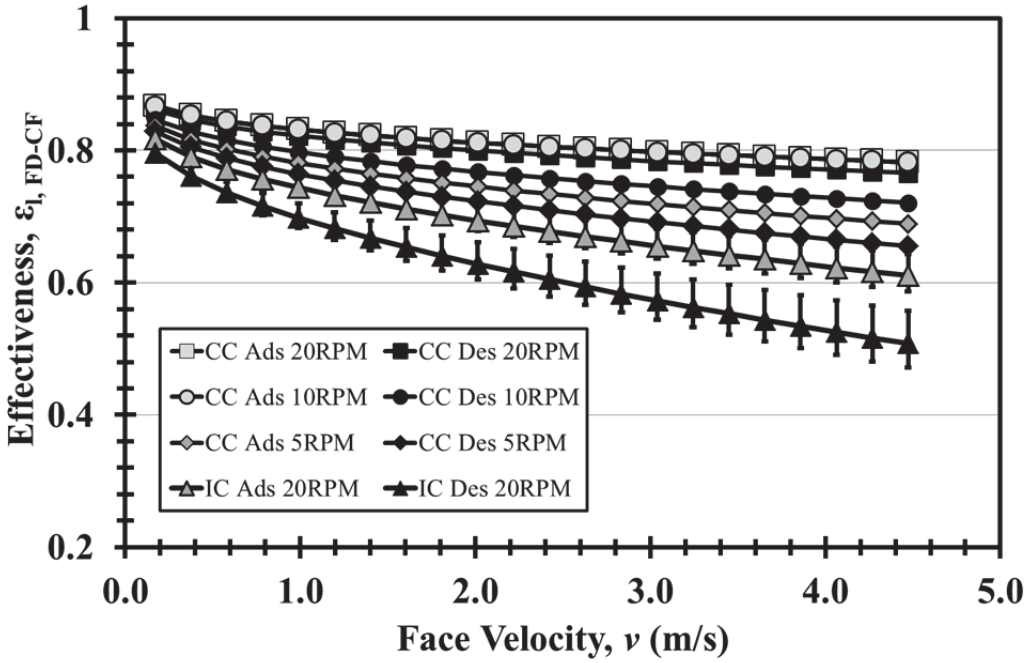

Figure 5.6: **Latent** effectiveness as a function of face velocity (m/s), *v*, as found from the **humidity desorption** and **adsorption** response results for only the **CC** coating at various energy wheel operating rotation speeds in rpm as compared to the IC coating at 20 rpm.

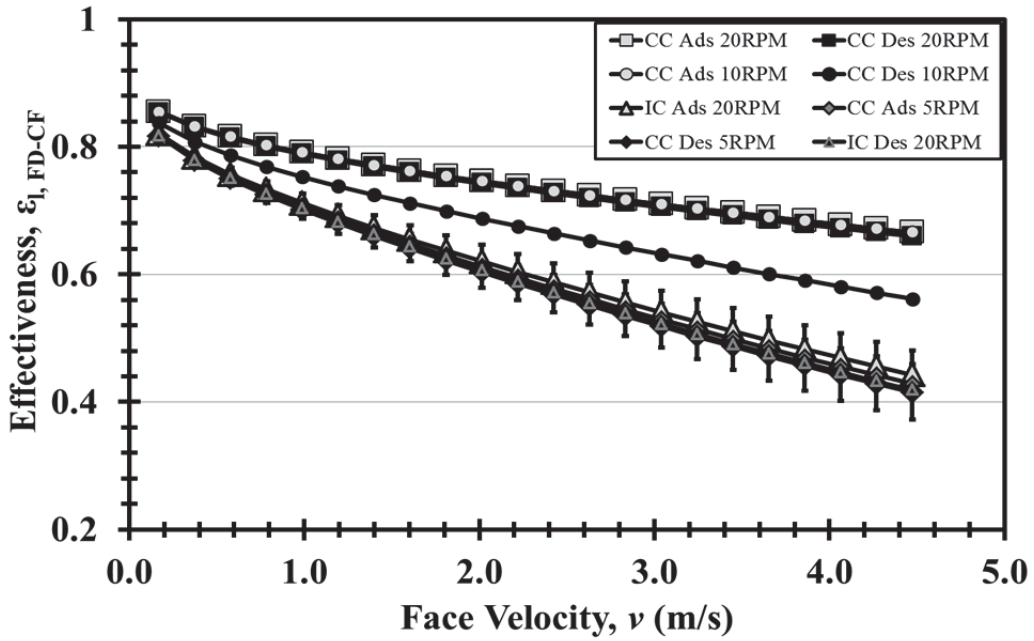

Figure 5.7: **Latent** effectiveness as a function of face velocity (m/s), *v*, as found from the **temperature desorption** and **adsorption** response results for only the **CC** coating at various energy wheel operating rotation speeds in rpm as compared to the IC coating at 20 rpm.

Figures 5.6 & 5.7 show the coarse agglomerate coatings at 3 different rpm speeds and the IC at the typical speed of 20 rpm. At low face velocities the effectiveness of all three coatings remains quite high, but by increasing the face velocity the effectiveness starts to decrease. For the humidity response in Figure 5.6 all three wheel speeds offer a much higher effectiveness profile, especially at greater face velocities which are discussed later in this section. The IC at 20 rpm gives around the same effectiveness curve as that for CC at 5 rpm for the temperature response in Figure 5.7. Meaning either slow the wheel down (5 rpm in either situation) to save energy or with very humid air to dry air conditions in an energy conservation scenario it may be more favorable to have the greater effectiveness as means to save energy, the engineer installing the system would be able assess each scenario for best improvement.

Then the effectiveness of the FC was looked at for both humidity and temperature response and compared to the IC response for both cases, as shown below in Figure 5.8 and Figure 5.9,

respectively below. Again, in these figures for the fine agglomerate coating at 3 different rpm speeds and the IC at the typical speed of 20 rpm at low face velocities, the effectiveness of all three coatings remains quite high and similar. As the face velocity is increased the effectiveness starts to spread out for the different coatings and wheel speeds, however, just increasing the wheel speed of an IC coating would not have a desired effect as will be discussed later in this section; therefore, it was not examined at any other speed than the 20 rpm. For the humidity response in Figure 5.8 all three wheel speeds of the FC offer a much higher effectiveness profile when looking at the adsorption and desorption as separate effectiveness. This is due to the fact that the FC and IC have a much greater discrepancy between the adsorption and desorption for the humidity than it did for the temperature response or that of the CC for either response. The IC at 20 rpm for both sorptions give a better effectiveness than that of the FC at 5 rpm. However, at 10 rpm something more interesting occurs, as seen in Figure 5.9, although the desorption curves the 10 rpm FC and 20 rpm IC are about the same, the adsorption curves vary quite significantly as the 10 rpm FC would give a much higher latent effectiveness. So at 10 rpm the overall FC would probably be much better than the IC at 20 rpm. Although even if the benefits of the adsorption occurring much more rapidly for this scenarios the FC would still be at least as good as the IC at half the rotation speed (10 and 20 rpm respectively). Meaning the wheel can be slowed down (to 10 rpm in the lowest situation) to save energy or, as discussed before with very humid air to dry air conditions in an energy conservation scenario, it may be more favorable to have the greater effectiveness at the same 20 rpm wheel speed.

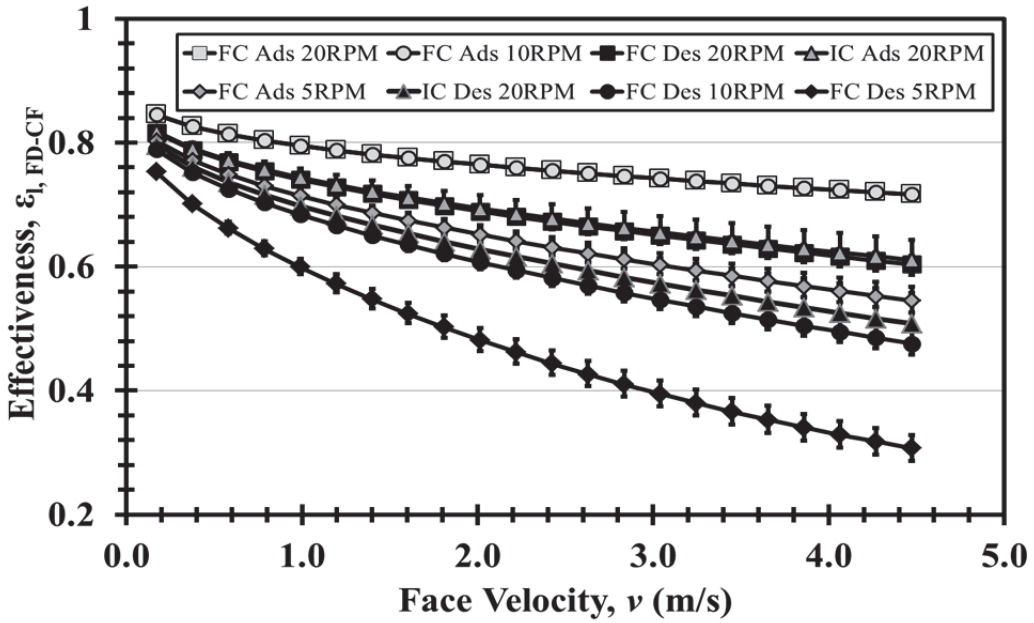

Figure 5.8: **Latent** effectiveness as a function of face velocity (m/s), *v*, as found from the **humidity desorption** and **adsorption** response results for only the **FC** coating at various energy wheel operating rotation speeds in rpm as compared to the IC coating at 20 rpm.

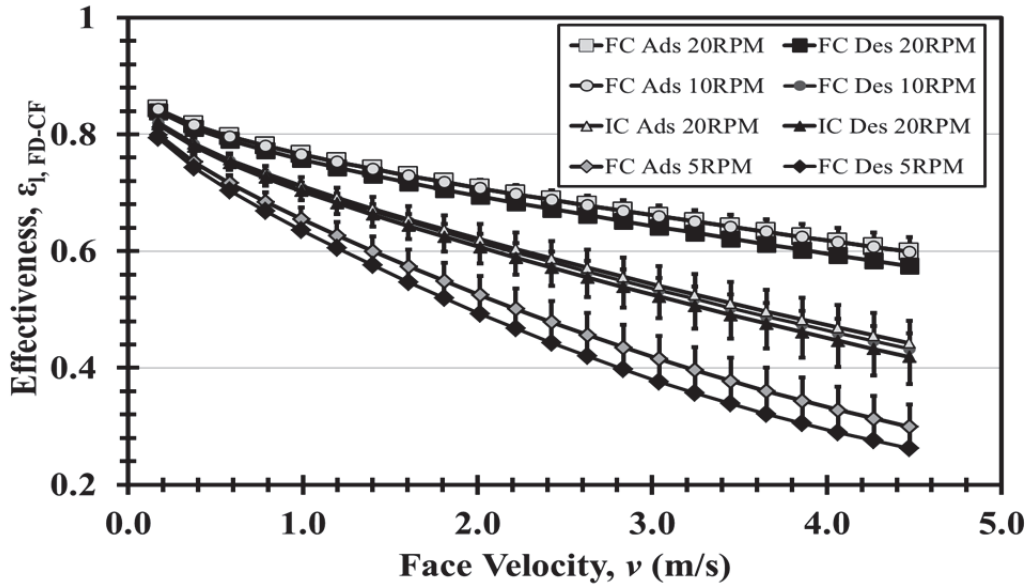

Figure 5.9: **Latent** effectiveness as a function of face velocity (m/s), *v*, as found from the **temperature desorption** and **adsorption** response results for only the **FC** coating at various energy wheel operating rotation speeds in rpm as compared to the IC coating at 20 rpm.

It should also be noted that the slower face velocities are not typically seen in energy wheel applications, as they usually range from at least 1 m/s to 5 m/s or greater depending on the overall air changes per hour and the size of the building and energy recovery system. So even

though all the Figures 5.6 to 5.9 have very similar effectiveness at the low face velocities, they tend to differ significantly as the face velocity increases to actual building operating conditions. Therefore, these similarities at the low face velocities would not matter due to most building operating conditions and as we increase the face velocities the various coatings will drop in effectiveness at different rates, according to the time constants and equations obtained throughout this research.

Also, although the rotation speed of the wheel has the opposite effect as it increases, their effectiveness, in theory, will increase. However, at too fast of rpm the leakage and carry over affects from the wheel turning become too great, that is why it is not possible to realistically gain effectiveness by increasing the wheel speed. In Figure 5.2 it is shown that the effectiveness is a function of both the wheel speed and time constant. Therefore, by increasing the time constant the same results as increasing the wheel speed are obtained without any of the negative carry over and air leakage affects that may actually lead to a decrease in effectiveness; especially if these effects become too great and overwhelm the energy exchange that is occurring within the wheel between the two air streams.

5.3 Effectiveness Uncertainty and Sensitivity Study

Although a confidence level of 95% was used in determining all the errors above, a confidence level is only accurate for predicting the mean of the data. This means that 95% of the time the calculated mean of the effectiveness should fall within the confidence bands used represented as error bars. But the actual individual results obtained would follow a 95% prediction band which tend to have a much a wider band width than the confidence bands. Looking at the equations for predicting the time constant from the face velocity the 95% confidence interval was always within $\pm 10\%$. Due to very small sample size for the collection

of this data it was not possible to calculate the actual prediction interval that a given sample may fall. But it is probably reasonable to assume that 95% of the time the actual time constant at a given face velocity should fall within $\pm 50\%$ or that the mean of the sampling is more important to energy wheel operation as most of the time an energy wheel's operating conditions should average out.

For the variation due to humidity response, the equation is of the following form:

$$\tau_m^* = Av^{-0.9} \qquad 5.3\text{–}1$$

Or, for the variation due to temperature response, the equation is of the following form:

$$\tau_m^* = Av^{-1.2} \qquad 5.3\text{–}2$$

Where A=constant dependent of the specific coating usually between [2,50].

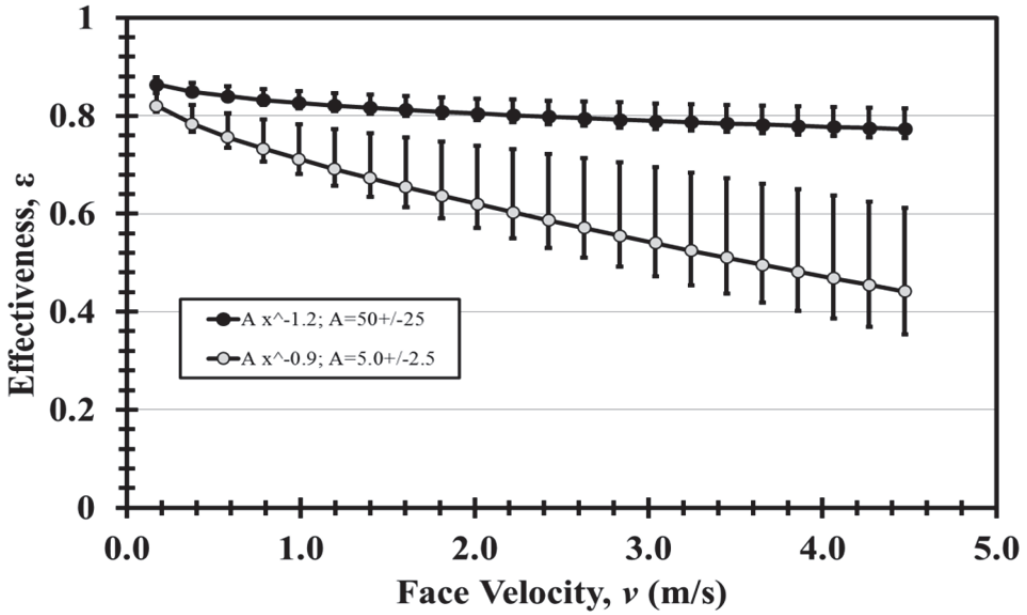

Figure 5.10: Effectiveness as a function of face velocity (m/s), *v*, assuming a 50% error in the calculated time constant. At an operating wheel speed of 20 rpm.

In Figure 5.10 it is clear that 50% error time constant does not mean that the effectiveness error is as large. Two things should be noted here, the error in general tends to be less on the bottom side of the effectiveness and that it tends to increase with an decrease in effectiveness, meaning the lower the time constants the more uncertain the results. The error on the bottom side

also signifies that the overall latent effectiveness should be significantly less than what is calculated here. In Figure 5.11 it is clear how the error will vary as a function of effectiveness giving two different errors in time constants one at 10% and the other 50% uncertainty. However, when the time constant remains high, even at 50% uncertainty in the time constant which was much greater than the deviations given for the time constants, the uncertainty in effectiveness remains quite low. In general, the results gathered in this section are still above the 0.5 effectiveness line which means that at most the absolute error in the results would not exceed 35%.

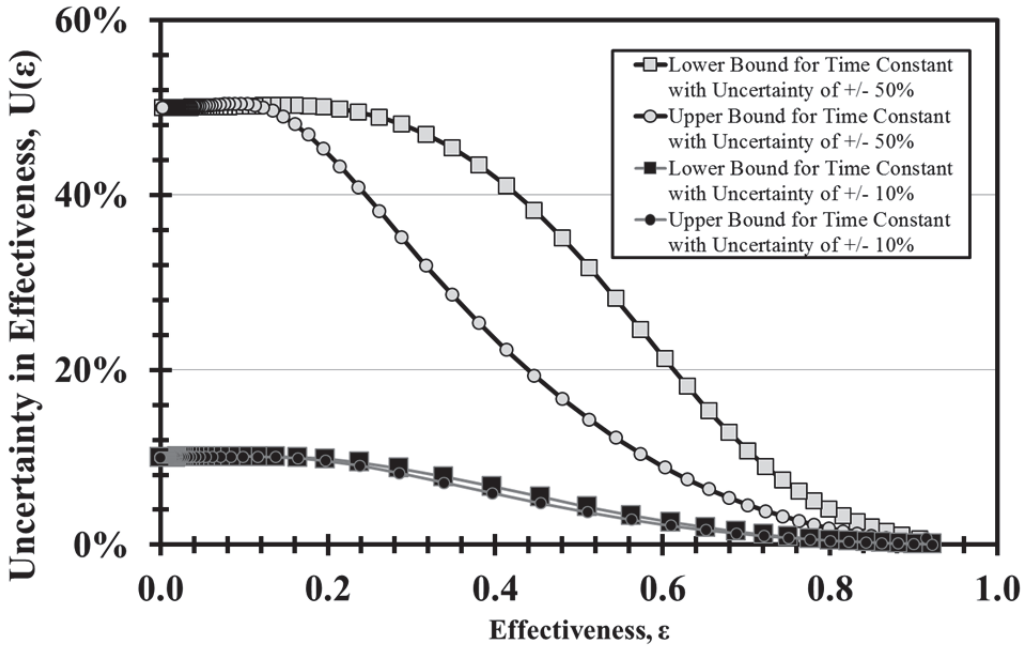

Figure 5.11: Effectiveness as a function of face velocity (m/s), *v*, assuming a 50% error in the calculated time constant. At an operating wheel speed of 20 rpm.

5.4 CHAPTER SUMMARY

This Chapter applies the theoretical relationship between step response time constants and effectiveness. Methods were derived from past research papers that are quoted. Both counter flow and parallel flow heat exchanger theoretical effectiveness calculations were shown as

function of the time constant multiplied by the angular velocity for a specific energy wheel arrangement and the appropriate assumptions were then stated. The humidity and temperature response data taken from the previous chapter is then used to form effectiveness curves for the coarse coating (CC), the fine coating (FC) and the industrial coating (IC) at 20 rpm and then again varying rpms for the CC and the FC. It was found that the IC operating at 20 rpm (the industry standard) is theoretically outperformed by both a CC wheel at greater than or equal to 5 rpm looking at both temperature sorptions and both humidity sorption responses. Also, when comparing these effectiveness curves, for the IC operating at 20 rpm to an FC wheel (with a third of the coating mass of both CC and IC) it was found in the least favorable case for the FC that this IC condition is equal to the FC operating at 10 rpm.

The uncertainty was then explained and a sensitivity study for a 95% confidence level was calculated and shown. The uncertainty of the effectiveness tends to decrease significantly as the effectiveness (or the time constants) increases in magnitude. Therefore, for the results shown, it is assumed they are at least relatively accurate in describing the effectiveness, especially for the comparison purposes of this chapter.

CHAPTER 6 :
SUMMARY, CONCLUSIONS & RECOMMENDATIONS

6.1 THESIS SUMMARY AND CHAPTER SUMMARIES

The purpose of this thesis is to present the making of two novel desiccant coatings; and compare and test them versus current desiccant coating system used in HVAC applications, more specifically energy (or enthalpy) wheels. Chapter one starts out by outlining past work done with micron sized particulate, desiccant coatings and HVAC air-to-air energy recover systems in order to gain a fuller grasp of the concepts done in this paper; and a purpose and outline to the paper is also presented. Chapter 2 then outlines the more specific materials (including silica gel agglomerates) and experimental methods used to make and test the coatings used throughout this work. In Chapter 3 the equilibrium and steady state results are presented, these include primarily the isotherm results of the coatings and the pressure readings taken at steady state for some of the transient testing. The experimental results are then presented, including the measured response in both humidity and temperature, and how the moisture time constant, τ_m^*, can be calculated from these responses; and a correlation is presented with how these time constants vary with the face velocity for each of the coatings in the same exponential manner. From these experimental results it is found that the new coatings, consisting of agglomerated particles and latex paint, give much higher calculated time constants than both latex paint and a currently used industrial coating, consisting of silica gel and a coating agent. Then the theoretical results are presented and explained, primarily consisting of how these coatings might function in an actual energy wheel's HVAC application; the higher time constant coatings including (FC and CC) are calculated to give a higher theoretical effectiveness than current coatings (IC). Finally the last chapter provides a complete summary of the research that is being done, as well as the

experimentally and theoretically supported conclusions; and finishes by illustrating the future work that could help to further the research at hand.

6.1.1 CHAPTER 1: INTRODUCTION

The first chapter provides current knowledge regarding energy wheels and explains the benefit of further research. It references several studies which give the basis of theory and methods used in the experiment and research study. The introduction then went on to explain how these past studies help to understand the current research done for this thesis. It explains the general (e.g. describing general particulate and desiccant behavior or how energy wheels transfer heat and moisture between exhaust and supply air) area and the need for more research because current knowledge and practice is not good enough (e.g. explains wheel effectiveness and why it should be higher.)

6.1.2 CHAPTER 2: EXPERIMENTAL METHODS

Chapter 2 begins by listing all of the equipment used during this research. The equipment is specified by manufacturing company or construction method, and details the purpose of each piece. It then continues to describe how it is possible to fabricate the agglomerated particles that are the pinnacle of this research and how they can be applied in a coating agent to form a desiccant coating utilized for HVAC purposes. The methodology for preparing the equilibrium isotherms is then discussed in detail. The chapter finishes by presenting a method for transient moisture sorbance testing, for both temperature and humidity response of a step change in relative humidity across a testing cell containing parallel sheets of desiccant coated aluminum foil substrate.

6.1.3 Chapter 3: Particle Agglomerates, Coating Equilibrium Isotherms and Pressure Drop Data at Steady State Conditions

This chapter presents the data at analysis obtained from equilibrium isotherm and steady state pressure readings. First particles are prepared to make agglomerates, and then applied to a substrate. The coatings are examined using laser sizing analysis for the size distribution of both the particles in the agglomerates and the agglomerates themselves. Then the rates of sorption and moisture capacity of the available surfaces are tested using the special apparatus, thus creating the isotherms. The steady state pressure readings from the transient testing apparatus are taken and examined for increased pressure drop due to the friction factor, for the CC, FC and IC coatings, all having various degrees of surface roughness.

6.1.4 Chapter 4: Results & Discussion for Time Constant Data

In this chapter response data is analyzed to determine the time constants for test cells containing the different coatings. The results from the various coatings are normalized for both the humidity response and the temperature response. The normalized transient data is then evaluated and the time constants are obtained from nonlinear regression curve fits that can obtain unknown variables (time constants and sometimes weighting factors) and their respective uncertainty. Finally the chapter concludes by presenting equations used to correlate the moisture or sensible time constants to the face velocity and comparing these results amongst one another.

6.1.5 Chapter 5: Results & Discussion for Implied Effectiveness

This Chapter applies the theoretical relationship between step response time constants and effectiveness. Methods derived from research from Shang and Besant (2005a, 2005b, 2006a, 2006b, 2008, 2009a, 2009b, 2009c), Wang et al. (Wang, 2005; 2005; 2006), and Abe et. al (Abe, 2005; 2006a, 2006b; 2006a, 2006b; 2006) provide a theoretical difference in effectiveness. The

assumptions necessary in this experiment prevent an accurate direct prediction of effectiveness on an actual energy wheel, but allow for a comparison of various coatings. Both counter flow and parallel flow heat exchanger theoretical effectiveness calculations are shown as functions of the time constant multiplied by the angular velocity for a specific energy wheel arrangement as it was developed in past transient testing work. The humidity and temperature response data from all coatings are assessed in the previous chapter and a correlation between the time constants and the face velocities are developed for of the coatings. These correlations are used to help extrapolate the data for the potential in effectiveness that is possible from these relationships. The uncertainty is discussed and the confidence of the results is calculated to the 95^{th} percentile. The cost savings analysis using the comparisons shows the potential benefit of the tested coatings. The uncertainties in effectiveness are calculated in terms of how they might be compared between these transient tests and those from ASHRAE Standard 84 (2008) steady state testing once applied to an energy wheel.

6.2 Analytical Conclusions

Desiccant Agglomerates for coatings in HVAC applications can be made using a combination of starch, fine silica gel particulate, water and an agglomerating device (as seen in Section 2.2)

Coating isotherms show that the moisture sorption of the coatings at equilibrium on a per mass basis shows that both agglomerated coatings (CC, and FC) perform similarly while the blank and the industrial coating tend to yield similar results as well. In general, CC and FC tend to be able to reach a higher moisture content almost as much as just the desiccant silica gel can alone and much greater than both the latex paint, BC, and the IC.

Steady state pressure readings imply that a coarser coating in an energy wheel will yield much higher time constants due to the increase in both heat and mass transfer from the potentially turbulent flow.

From the transient response data taken in Chapter 4, in general the following conclusions can be made:

- Time constants are an exponential function of face velocity for the both sorption processes, as they will decrease exponentially with an increase in face velocity.
- Time constants vary with different energy wheel as a function of the type of coating and although they are also a function of many other variables; but all of the other variables were maintained constant during the testing so no note can be made on how these (i.e. energy wheel configuration, or coating thickness) may affect the time constants.
- Adsorbance is faster than desorbance, time constants are greater for adsorbance therefore, this process is happening much faster; meaning that after a switch there is a much greater delay in showing the outlet air stream as responding to an increase in inlet humidity due to an increased sorption rate than there was for the opposite scenario.
- Both of the agglomerated particle coatings (CC and FC) had a much higher time constant relation to face velocity than the IC coating. This means they outperformed the IC substantially, which was the overall goal of this thesis to prove that by making an agglomerated particle that could be put into an energy wheel coating significant improvement might be obtainable.

- When half of the sheets of the FC were tested, a very substantial decrease in the time constants was observed, meaning that the total mass of the coating plays an extremely important factor in overall coating performance, and if the FC had a mass closer to that of the IC and CC a substantial improvement would have been seen; therefore, further testing of the FC coating is needed.

6.3 THEORETICAL CONCLUSIONS

From the expected efficiencies (as calculated from response data) explained in Chapter 5, in general the following conclusions can be made:

- The coating from the industrial coated wheel taken from this research operated at 20 rpm would be theoretically outperformed by both a CC wheel at greater than or equal to 5 rpm and a FC wheel (with a third of the coating mass of both CC and IC) at greater than or equal to 10 rpm. These apply to both adsorption and desorption and are calculated relative the same regardless of whether transient humidity data or transient temperature data is used to obtain the time constant correlation with face velocity.
- Most energy wheel configurations have a much greater face velocity than those measured during this research; therefore, from extrapolation at these higher face velocities as the face velocity increases so does the difference between the IC and the agglomerated coatings (i.e. they tend to perform much better as v increases).

6.4 RECOMMENDATIONS FOR FUTURE RESEARCH

Some recommendations for the pursuit of future knowledge are given below. It is the aim of this research that these findings may result in the potential actions and help to further the knowledge and overall benefit of society.

6.4.1 Coating Weight

The coatings mass applied for each of the coatings with their agglomerates are not equal, in fact the fine coating weighed less than both the blank coating and industrial coating (both of which almost had identical total mass) by almost half, and was composed of about a third of the mass of the coarse coating. In order to obtain a better understanding of these coatings it would be interesting to compare similar masses of coatings for each. If the fine coating had the same amount of silica gel as the coarse coating, the fine coating may be observed outperforming the latter. Looking at the coatings in the given test cell of equal masses may give future researchers a more consistent baseline to compare these as well as other future coatings that could be developed.

6.4.2 Further Pressure Readings, look into Turbulent versus Laminar

Only a limited amount of data was collected when examining the pressure drops across the test cell at steady state. It would be interesting for future researchers to not only gather more pressure data with a similar test cell, but also if these coatings are to be applied to actual fully manufactured energy wheels if an even greater effect of the turbulent flow due to rough surface is detected that was only partially observed during this research.

6.4.3 Real Life Application

There has been enough proof with this research as to the potential of both the coarse and the fine coatings that they should be further explored. One interesting way to further test these coatings would be to manufacture them onto actual desiccant drying or energy wheels. Once they are in wheel form similar transient tests can be performed to compare them to what the current market offers, and it also lends to the possibility of furthering the transient testing method by comparing those potential transient results with ASHRAE standardized testing in a steady state

facility, to further reinforce the coatings as well as the testing procedure done during this research.

6.4.4 Investigate other Coatings, Bonding Agents and Types of Agglomerates

Only a single type of coating agent was used to secure the silica gel agglomerates to the substrate (aluminum foil), but further research may find it useful to examine other methods of adhering or to look at a different coating agent altogether. The advantages that might be found in using a more rapidly absorbing coating agent may lead to even further improvement on the coating itself. Also with other methods of adhering the agglomerates to the actual substrate, potential a coating agent may not be needed at all (i.e. electrostatic coating methods) further improving the coating by limiting the mass and energy dampening effects of the coating agent itself.

Also the agglomerates themselves may be looked at for improvement by either utilizing different desiccants (i.e. molecular sieve) or by changing the bonding agent that holds them together (i.e. different types of starch, or something other than starch). This may lead to a further improvement in the coating by increasing the rate of adsorption or increase the capacity for which the desiccants are able to hold moisture content.

Starch also sorbs water, therefore, it is also important to examine the how much of a role the starch plays in increasing the effectiveness of the coating, and if it is possible to differentiate between the extent that each, the silica gel and the starch, might contribute to increasing the effectiveness of the coating.

6.4.5 Models That Better Explain some of the Phenomenon

The effect of the height of the peaks found during the temperature response analysis has never been correlated as to how it affects the performance of the wheels. Generating better theoretical models that may take this into account could prove to be an invaluable resource tool for future researchers and should definitely be looked into further.

6.4.6 Optimize Future Coatings

Examining all the criteria laid out in this research could lead to potential optimization of coatings prior to implementation. This combined with further research as to the fundamental mechanics underlying this problem could lead to very optimized coatings that could potential save money and energy, both valuable resources.

6.4.7 Implementation, Distribution, and Cost Analysis

Finally the overall future goal of this research is to actual implement the coatings into real life. Once the coatings have been further proved to be significantly superior in quality then those currently available, marketing and distribution will be of vital importance. It is only with this implementation that actual benefits could be applied to today's society, and help to reduce overall energy consumption. Of course with any product the production cost is of vital importance if it is to be commercially viable, therefore examining the potential manufacturing cost increases or decreases with these new types of coatings needs to examined prior to implementation. But, it was a goal of this research that this coating may be seen in various new industrial and commercial applications if proven viable.

REFERENCES

Abe, O. O. (2005). *Effectiveness of Energy Wheels from Transient Measurements.* M.Sc., University of Saskatchewan, Saskatoon, SK.

Abe, O. O., Simonson, C. J., & Besant, R. W. (2006a). Relationship between Energy Wheel Speed and Effectiveness and Its Transient Response , Part I. Mathematical Development of the Characteristic Time Constants and Their Relationship with Effectiveness. *ASHRAE Transactions, 112*(2), 90-102.

Abe, O. O., Simonson, C. J., & Besant, R. W. (2006b). Relationship between Energy Wheel Speed and Effectiveness and Its Transient Response , Part II. Comparison Between Mathematical Model Predictions and Experimental Measurements and Uncertainty Analysis. *ASHRAE Transactions, 112*(2), 103-115.

Abe, O. O., Simonson, C. J., Besant, R. W., & Shang, W. (2006a). Effectiveness of energy wheels from transient measurements. Part I: Prediction of effectiveness and uncertainty. *International Journal of Heat and Mass Transfer, 49*(1-2), 52-62.

Abe, O. O., Simonson, C. J., Besant, R. W., & Shang, W. (2006b). Effectiveness of energy wheels from transient measurements. Part II: Results and verification. *International Journal of Heat and Mass Transfer, 49*(1-2), 63-77.

Abe, O. O., Wang, Y. H., Simonson, C. J., & Besant, R. W. (2006). Transient Temperature Measurements and Characteristics for Temperature Sensors and Energy Wheels. *ASHRAE Transactions, 112*(2), 76-88.

ASHRAE. (2008). *ANSI/ASHRAE Standard 84-2008 Method of Testing Air-to-Air Heat/Energy Exchangers*. Atlanta, GA, USA: American Society of Heating, Refrigerating and Air-Conditioning Engineers, Inc.

ASHRAE. (2009). *ASHRAE 2009 Fundamentals Handbook SI Units*. Atlanta, GA, USA: American Society of Heating, Refrigerating and Air-Conditioning Engineers, Inc.

ASHRAE. (2011a). *ANSI/ASHRAE Standard 62.1-2010 Ventilation for Acceptable Indoor Air Quality*. Atlanta, GA, USA: American Society of Heating, Refrigerating and Air-Conditioning Engineers, Inc.

ASHRAE. (2011b). *ANSI/ASHRAE Standard 62.2-2010 Ventilation and Acceptable Indoor Air Quality in Low-Rise Residential Buildings*. Atlanta, GA, USA: American Society of Heating, Refrigerating and Air-Conditioning Engineers, Inc.

Bond, F. C. (1958). Grinding ball size selection. *Mining Engineering, Transactio*(May), 592-595.

Choi, W. (2001). Applications of grinding kinetics analysis to fine grinding characteristics of some inorganic materials using a composite grinding media by planetary ball mill. *Powder Technology, 115*(3), 209-214.

Colebrook, C. F., & White, C. M. (1937). Experiments with Fluid Friction in Roughened Pipes. *Proceedings of the Royal Society of London. Series A - Mathematical and Physical Sciences, 161*(906), 367-381.

Huang, Q., Zhang, H., & Zhu, J. (2009). Experimental study on fluidization of fine powders in rotating drums with various wall friction and baffled rotating drums. *Chemical Engineering Science, 64*(9), 2234-2244.

Huang, Q., Zhang, H., & Zhu, J. (2010). Onset of an innovative gasless fluidized bed - comparative study on the fluidization of fine powders in a rotating drum and a traditional fluidized bed. *Chemical Engineering Science, 65*(3), 1261-1273.

Incropera, F. P., Bergman, T. L., & Lavine, A. S. (2011). *Fundamentals of heat and mass transfer*. Hoboken, NJ: John Wiley.

Kano, J., & Saito, F. (1998). Correlation of powder characteristics of talc during Planetary Ball Milling with the impact energy of the balls simulated by the Particle Element Method. *Powder Technology, 98*(2), 166-170.

Mi, G. (1997). Mechanochemical synthesis of tobermorite by wet grinding in a planetary ball mill. *Powder Technology, 93*(1), 77-81.

Naumov, S. (2009). *Hysteresis Phenomena in Mesoporous Materials.* Doctor rerum naturalium Dissertation, University of Leipzig, Leipzig, Germany.

Rhodes, W. H. (1981). Agglomerate and Particle Size Effects on Sintering Yttria-Stabilized Zirconia. *Journal of the American Ceramic Society, 64*(1), 19-22.

Shang, W., & Besant, R. W. (2005a). Determining Flow Channel Size Variations Using a Pressure Probe for a Typical Regenerative Wheel. *ASHRAE Transactions: Research, 111*(2), 243-257.

Shang, W., & Besant, R. W. (2005b). Effects of Pore Size Variations on Regenerative Wheel Performance. *Journal of Engineering for Gas Turbines and Power, 127*(1), 121.

Shang, W., & Besant, R. W. (2006a). Effects of Manufacturing Tolerances on Regenerative Exchanger Number of Transfer Units and Entropy Generation. *Journal of Engineering for Gas Turbines and Power, 128*(3), 585-598.

Shang, W., & Besant, R. W. (2006b). Impacts of manufacturing tolerances on the effectiveness-Ntu method for regenerative exchanger design. *ASHRAE Transactions, 112*, 111-122.

Shang, W., & Besant, R. W. (2008). Theoretical and Experimental Methods for the Sensible Effectiveness of Air-to-Air Energy Recovery Wheels. *HVAC&R Research, 14*(3), 373-397.

Shang, W., & Besant, R. W. (2009a). Effectiveness of Desiccant Coated Regenerative Wheels from Transient Response Characteristics and Flow Channel Properties - Part I. Development of Effectiveness Equations. *HVAC&R Research, 15*(2), 329-346.

Shang, W., & Besant, R. W. (2009b). Effectiveness of Desiccant Coated Regenerative Wheels from Transient Response Characteristics and Flow Channel Properties - Part II. Predicting and Comparing the Latent Effectiveness of Dehumidifier and Energy Wheels Using Transient. *HVAC&R Research, 15*(2), 346-366.

Shang, W., & Besant, R. W. (2009c). Performance and Design of Dehumidifier Wheels. *HVAC&R Research, 15*(3), 437-461.

Simonson, C. J., & Besant, R. W. (1998). Heat and Moisture Transfer in Energy Wheels During Sorption, Condensation, and Frosting Conditions. *Journal of Heat Transfer, 120*(3), 699-708.

Sun, J., & Besant, R. W. (2005). Heat and mass transfer during silica gel-moisture interactions. *International Journal of Heat and Mass Transfer, 48*, 4953-4962.

Ulrich, G. D., & Vasudevan, P. T. (2004). *Chemical Engineering Process Design and Economics: A Practical Guide*. Lee, NH, USA: Process Publishing.

Wang, Y. H. (2005). *Transient Characteristics of Humidity Sensors and Their Application to Energy Wheels.* M.Sc., University of Saskatchewan, Saskatoon, SK.

Wang, Y. H., Besant, R. W., & Simonson, C. J. (2005). Transient Humidity Measurements for Flow Through an Energy Wheel. *ASHRAE Transactions, 111*(2), 353-369.

Wang, Y. H., Besant, R. W., Simonson, C. J., & Shang, W. (2006). Application of humidity sensors and an interactive device. *Sensors and Actuators B: Chemical, 115*(1), 93-101.

Webb, R. L., & Kim, N. H. (2005). *Principles of Enhanced Heat Transfer* (2nd edition ed.). New York, NY, USA: Taylor & Francis.

Whistler, R. L., & Daniel, J. R. (2000). Starch *Kirk-Othmer Encyclopedia of Chemical Technology* (pp. 18). Purdue University, West Lafayette, IN, USA John Wiley & Sons, Inc.

Yao, W., Guangsheng, G., Fei, W., & Jun, W. (2002). Fluidization and agglomerate structure of SiO 2 nanoparticles. *Powder Technology*(124), 152 - 159.

Zhang, H., Faghri, M., & White, F. M. (1996). A New Low-Reynolds Number k-e Model for Turbulent Flow Over Smooth and Rough Surfaces. *Journal of Fluid Engineering - Transactions ASME, 118*(2), 5.

Zhang, L.-Z., Liang, C.-H., & Pei, L.-X. (2008). Heat and moisture transfer in application scale parallel-plates enthalpy exchangers with novel membrane materials. *Journal of Membrane Science, 325*(2), 672-682.

Zhang, L.-Z., & Xiao, F. (2007). Simultaneous heat and moisture transfer through a composite supported liquid membrane. *International Journal of Heat and Mass Transfer, 51*, 2179-2189.

APPENDIX A:
RAW DATA

One Short Sample of Raw Data taken from file named:

'100LPM - 75% RH - Coarse Coating - Tue, Aug 02, 2011.txt'

Below:

Time	RH1	RH2	RH3	RH4	T1	T2	T3	T4	Voltage source	Volts RH1	Volts RH2	Volts RH3	Volts RH4
85.04	4.067	22.443	76.532	77.236	22.05	20.4	22.339	22.509	1.041	1.613	3.284	3.304	4.96
87.04	4.08	22.294	76.531	77.248	22.047	20.358	22.416	22.506	1.041	1.608	3.283	3.305	4.96
1.001	4.082	22.039	76.528	77.251	22.012	20.403	22.381	22.471	1.042	1.6	3.283	3.305	4.96
3.002	4.093	21.856	76.511	77.273	22.012	20.482	22.341	22.511	1.042	1.594	3.283	3.306	4.96
5.002	4.093	21.695	76.533	77.272	22.047	20.478	22.376	22.506	1.042	1.589	3.283	3.306	4.96
8.001	4.116	21.471	76.55	77.295	22.01	20.48	22.378	22.509	1.043	1.582	3.284	3.306	4.96
10.001	4.092	22.163	76.564	69.604	21.97	20.68	22.418	22.389	1.042	1.603	3.284	3.069	4.959
12.002	4.129	27.729	76.528	49.055	22.05	21.158	22.378	22.27	1.043	1.775	3.283	2.433	4.96
15.001	4.161	38.203	76.53	29.152	22.055	22.079	22.423	22.275	1.044	2.098	3.283	1.817	4.96
17.001	4.176	44.781	76.51	21.426	22.005	22.706	22.334	22.185	1.044	2.3	3.283	1.578	4.96
19.002	4.191	50.33	76.518	16.426	22.008	23.343	22.416	22.188	1.045	2.469	3.283	1.424	4.96
22.001	4.205	56.599	76.49	12.023	22.012	23.983	22.381	22.233	1.045	2.661	3.282	1.287	4.96
24.001	4.212	59.601	76.506	10.283	22.012	24.379	22.341	22.233	1.046	2.752	3.283	1.233	4.96
26.002	4.223	61.74	76.5	9.108	22.015	24.619	22.304	22.275	1.046	2.816	3.283	1.197	4.96
29.001	4.24	63.777	76.509	8.017	21.973	24.933	22.381	22.233	1.046	2.878	3.282	1.163	4.96
31.002	4.252	64.566	76.488	7.54	22.015	24.975	22.304	22.315	1.047	2.902	3.283	1.149	4.96
34.002	4.251	65.228	76.513	7.054	22.052	25.131	22.341	22.233	1.047	2.921	3.283	1.133	4.96
37.002	4.271	65.554	76.525	6.769	21.973	25.21	22.381	22.272	1.047	2.931	3.283	1.125	4.96
39.002	4.283	65.628	76.514	6.644	22.057	25.254	22.346	22.277	1.048	2.933	3.283	1.121	4.96
41.002	4.296	65.711	76.513	6.526	22.015	25.291	22.383	22.235	1.048	2.936	3.283	1.117	4.96
44.001	4.293	65.751	76.49	6.426	21.973	25.21	22.381	22.272	1.048	2.938	3.282	1.114	4.96
46.001	4.303	65.811	76.522	6.367	22.057	25.175	22.426	22.237	1.048	2.939	3.283	1.112	4.96
⋮	⋮	⋮	⋮	⋮	⋮	⋮	⋮	⋮	⋮	⋮	⋮	⋮	⋮

Rest on CD or will forward upon request to email: john.bolster@usask.ca

APPENDIX B:
TRANSIENT TIME CONSTANT DATA

Tabulated Data from curve fits, Sample Graphical fit, rest on CD or will forward upon request to email: john.bolster@usask.ca

Table B.1: Moisture time constant, τ_m^*, obtained from the transient **humidity** response data of all the coatings obtained from MatLab™ curve fits and the respective known face velocity of the air flowing across the sheets for the **adsorption** process.

Coating Type →			Blank Coating		Industrial Coating		Fine Coating Half Sheets		Fine Coating		Coarse Coating	
Volumetric Flowrate (L/min)	Face Velocity (m/s)	Reynolds Number (Re)	Time Constant τ_m	95% Pred. Bound error(τ_m)	Time Constant τ_m	95% Pred. Bound error(τ_m)	Time Constant τ_m	95% Pred. Bound error(τ_m)	Time Constant τ_m	95% Pred. Bound error(τ_m)	Time Constant τ_m	95% Pred. Bound error(τ_m)
12	0.041	18	86	16	130	43	191	16	191	16	752	12
16	0.055	24	191	26	113	28	#N/A	#N/A	299	11	558	21
20	0.068	30	126	12	46	16	122	9	297	8	660	4
30	0.102	45	107	9	#N/A	#N/A	#N/A	#N/A	#N/A	#N/A	465	4
40	0.137	60	69	18	#N/A	#N/A	#N/A	#N/A	#N/A	#N/A	#N/A	#N/A
50	0.171	75	#N/A	#N/A	69	9	#N/A	#N/A	91	6	382	1
60	0.205	90	48	9	25	5	37	2	48	3	224	4
70	0.239	105	#N/A	#N/A	31	4	#N/A	#N/A	70	4	207	3
80	0.273	119	31	7	#N/A	#N/A	#N/A	#N/A	#N/A	#N/A	#N/A	#N/A
90	0.307	134	#N/A	#N/A	#N/A	#N/A	#N/A	#N/A	46	4	194	3
100	0.341	149	23	8	26	3	27	6	27	6	138	3
110	0.376	164	#N/A	#N/A	#N/A	#N/A	#N/A	#N/A	#N/A	#N/A	#N/A	#N/A
120	0.410	179	#N/A	#N/A	17	4	#N/A	#N/A	20	2	#N/A	#N/A
130	0.444	194	#N/A	#N/A	17	2	#N/A	#N/A	#N/A	#N/A	157	6
140	0.478	209	8	8	31	2	#N/A	#N/A	48	4	141	9
150	0.512	224	#N/A	#N/A	29	4	#N/A	#N/A	#N/A	#N/A	105	2
160	0.546	239	#N/A	#N/A	#N/A	#N/A	#N/A	#N/A	#N/A	#N/A	100	4
170	0.581	254	26	25	40	4	#N/A	#N/A	39	3	121	4
180	0.615	269	#N/A	#N/A	#N/A	#N/A	#N/A	#N/A	#N/A	#N/A	110	6
190	0.649	284	#N/A	#N/A	#N/A	#N/A	#N/A	#N/A	17	8	152	9
200	0.683	299	9	6	21	7	17	8	24	4	94	2

Table B.2: Moisture time constant, τ_m^*, obtained from the transient **humidity** response data of all the coatings obtained from MatLab™ curve fits and the respective known face velocity of the air flowing across the sheets for the **desorption** process.

Coating Type →			Blank Coating		Industrial Coating		Fine Coating Half Sheets		Fine Coating		Coarse Coating	
Volumetric Flowrate (L/min)	Face Velocity (m/s)	Reynolds Number (Re)	Time Constant τ_m	95% Pred. Bound error(τ_m)	Time Constant τ_m	95% Pred. Bound error(τ_m)	Time Constant τ_m	95% Pred. Bound error(τ_m)	Time Constant τ_m	95% Pred. Bound error(τ_m)	Time Constant τ_m	95% Pred. Bound error(τ_m)
12	0.041	18	81	5	78	9	91	5	91	5	442	3
16	0.055	24	117	8	54	5	#N/A	#N/A	96	4	506	8
20	0.068	30	68	6	31	4	55	6	119	7	465	5
30	0.102	45	38	4	#N/A	#N/A	#N/A	#N/A	#N/A	#N/A	391	3
40	0.137	60	31	2	#N/A	#N/A	#N/A	#N/A	#N/A	#N/A	#N/A	#N/A
50	0.171	75	#N/A	#N/A	26	4	#N/A	#N/A	45	3	249	3
60	0.205	90	16	1	28	6	23	3	31	3	184	2
70	0.239	105	#N/A	#N/A	22	3	#N/A	#N/A	35	3	185	2
80	0.273	119	16	6	#N/A	#N/A	#N/A	#N/A	#N/A	#N/A	#N/A	#N/A
90	0.307	134	#N/A	#N/A	#N/A	#N/A	#N/A	#N/A	26	2	139	6
100	0.341	149	16	5	22	4	16	4	16	4	109	5
110	0.376	164	#N/A	#N/A	#N/A	#N/A	#N/A	#N/A	#N/A	#N/A	#N/A	#N/A
120	0.410	179	#N/A	#N/A	11	5	#N/A	#N/A	12	1	#N/A	#N/A
130	0.444	194	#N/A	#N/A	19	4	#N/A	#N/A	#N/A	#N/A	78	3
140	0.478	209	11	5	23	3	#N/A	#N/A	18	1	85	4
150	0.512	224	#N/A	#N/A	11	12	#N/A	#N/A	#N/A	#N/A	70	3
160	0.546	239	#N/A	#N/A	#N/A	#N/A	#N/A	#N/A	#N/A	#N/A	62	3
170	0.581	254	10	5	21	6	#N/A	#N/A	21	3	64	4
180	0.615	269	#N/A	#N/A	#N/A	#N/A	#N/A	#N/A	#N/A	#N/A	61	4
190	0.649	284	#N/A	#N/A	#N/A	#N/A	#N/A	#N/A	13	4	61	3
200	0.683	299	#N/A	#N/A	18	3	13	4	9	1	55	3

Table B.3: Moisture time constant, τ_m^*, obtained from the transient **temperature** response data of all the coatings obtained from MatLab™ curve fits and the respective known face velocity of the air flowing across the sheets for the **adsorption** process.

Coating Type →			Blank Coating		Industrial Coating		Fine Coating Half Sheets		Fine Coating		Coarse Coating	
Volumetric Flowrate (L/min)	Face Velocity (m/s)	Reynolds Number (Re)	Time Constant τ_m	95% Pred. Bound error(τ_m)	Time Constant τ_m	95% Pred. Bound error(τ_m)	Time Constant τ_m	95% Pred. Bound error(τ_m)	Time Constant τ_m	95% Pred. Bound error(τ_m)	Time Constant τ_m	95% Pred. Bound error(τ_m)
12	0.041	18	306	69	216	23	142	8	555	15	874	7
16	0.055	24	247	42	203	16	#N/A	#N/A	440	12	764	8
20	0.068	30	191	23	39	2	85	5	154	4	496	7
30	0.102	45	#N/A	#N/A	#N/A	#N/A	#N/A	#N/A	#N/A	#N/A	225	5
40	0.137	60	148	15	#N/A	#N/A	#N/A	#N/A	#N/A	#N/A	#N/A	#N/A
50	0.171	75	#N/A	#N/A	23	1	#N/A	#N/A	62	3	160	4
60	0.205	90	37	4	21	1	29	1	52	3	100	4
70	0.239	105	#N/A	#N/A	19	1	#N/A	#N/A	53	2	222	10
80	0.273	119	28	3	#N/A	#N/A	#N/A	#N/A	#N/A	#N/A	#N/A	#N/A
90	0.307	134	#N/A	#N/A	#N/A	#N/A	#N/A	#N/A	26	1	48	2
100	0.341	149	16	1	15	1	13	2	19	0	51	2
110	0.376	164	#N/A	#N/A	#N/A	#N/A	#N/A	#N/A	#N/A	#N/A	#N/A	#N/A
120	0.410	179	#N/A	#N/A	#N/A	#N/A	#N/A	#N/A	29	4	#N/A	#N/A
130	0.444	194	#N/A	#N/A	17	1	#N/A	#N/A	#N/A	#N/A	44	2
140	0.478	209	53	16	19	1	#N/A	#N/A	29	2	38	1
150	0.512	224	#N/A	#N/A	19	1	#N/A	#N/A	#N/A	#N/A	43	1
160	0.546	239	#N/A	#N/A	#N/A	#N/A	#N/A	#N/A	#N/A	#N/A	50	3
170	0.581	254	4	1	17	2	#N/A	#N/A	11	1	23	1
180	0.615	269	#N/A	#N/A	#N/A	#N/A	#N/A	#N/A	#N/A	#N/A	28	1
190	0.649	284	#N/A	#N/A	#N/A	#N/A	#N/A	#N/A	#N/A	#N/A	23	1
200	0.683	299	30	13	9	0	17	1	14	0	41	2

Table B.4: Moisture time constant, τ_m^*, obtained from the transient **temperature** response data of all the coatings obtained from MatLab™ curve fits and the respective known face velocity of the air flowing across the sheets for the **desorption** process.

Coating Type →			Blank Coating		Industrial Coating		Fine Coating Half Sheets		Fine Coating		Coarse Coating	
Volumetric Flowrate (L/min)	Face Velocity (m/s)	Reynolds Number (Re)	Time Constant τ_m	95% Pred. Bound error(τ_m)	Time Constant τ_m	95% Pred. Bound error(τ_m)	Time Constant τ_m	95% Pred. Bound error(τ_m)	Time Constant τ_m	95% Pred. Bound error(τ_m)	Time Constant τ_m	95% Pred. Bound error(τ_m)
12	0.041	18	210	27	213	18	131	6	574	16	885	10
16	0.055	24	158	12	166	13	#N/A	#N/A	320	9	554	6
20	0.068	30	134	12	181	15	92	5	241	6	445	5
30	0.102	45	76	7	#N/A	#N/A	#N/A	#N/A	#N/A	#N/A	274	3
40	0.137	60	45	7	#N/A	#N/A	#N/A	#N/A	#N/A	#N/A	#N/A	#N/A
50	0.171	75	#N/A	#N/A	22	1	#N/A	#N/A	70	2	155	3
60	0.205	90	35	4	29	2	41	3	57	2	121	3
70	0.239	105	#N/A	#N/A	29	2	#N/A	#N/A	39	2	123	2
80	0.273	119	20	1	#N/A	#N/A	#N/A	#N/A	#N/A	#N/A	#N/A	#N/A
90	0.307	134	#N/A	#N/A	#N/A	#N/A	#N/A	#N/A	43	2	81	2
100	0.341	149	11	1	31	5	14	1	37	1	83	2
110	0.376	164	#N/A	#N/A	#N/A	#N/A	#N/A	#N/A	#N/A	#N/A	#N/A	#N/A
120	0.410	179	#N/A	#N/A	#N/A	#N/A	#N/A	#N/A	30	2	#N/A	#N/A
130	0.444	194	#N/A	#N/A	13	1	#N/A	#N/A	#N/A	#N/A	46	2
140	0.478	209	4	1	13	1	#N/A	#N/A	25	1	42	1
150	0.512	224	#N/A	#N/A	#N/A	#N/A	#N/A	#N/A	#N/A	#N/A	49	1
160	0.546	239	#N/A	#N/A	#N/A	#N/A	#N/A	#N/A	#N/A	#N/A	35	1
170	0.581	254	18	2	9	1	#N/A	#N/A	19	1	30	1
180	0.615	269	#N/A	#N/A	#N/A	#N/A	#N/A	#N/A	#N/A	#N/A	28	1
190	0.649	284	#N/A	#N/A	#N/A	#N/A	#N/A	#N/A	#N/A	#N/A	25	2
200	0.683	299	21	9	18	1	7	1	12	1	30	1

Table B.5: Sensible time constant, τ_s, obtained from the transient **temperature** response data of all the coatings obtained from MatLab™ curve fits and the respective known face velocity of the air flowing across the sheets for the **adsorption** process.

Coating Type →			Blank Coating		Industrial Coating		Fine Coating Half Sheets		Fine Coating		Coarse Coating	
Volumetric Flowrate (L/min)	Face Velocity (m/s)	Reynolds Number (Re)	Time Constant τ_s	95% Pred. Bound error(τ_s)	Time Constant τ_s	95% Pred. Bound error(τ_s)	Time Constant τ_s	95% Pred. Bound error(τ_s)	Time Constant τ_s	95% Pred. Bound error(τ_s)	Time Constant τ_s	95% Pred. Bound error(τ_s)
12	0.041	18	322	73	227	24	165	9	645	17	1108	8
16	0.055	24	264	45	219	17	#N/A	#N/A	529	14	913	9
20	0.068	30	206	25	42	2	102	5	183	4	669	8
30	0.102	45	405	168	#N/A	#N/A	#N/A	#N/A	#N/A	#N/A	323	6
40	0.137	60	161	16	#N/A	#N/A	#N/A	#N/A	#N/A	#N/A	#N/A	#N/A
50	0.171	75	#N/A	#N/A	28	2	#N/A	#N/A	70	3	237	5
60	0.205	90	39	4	24	1	37	2	69	3	142	5
70	0.239	105	#N/A	#N/A	22	1	#N/A	#N/A	60	2	348	13
80	0.273	119	30	3	#N/A	#N/A	#N/A	#N/A	#N/A	#N/A	#N/A	#N/A
90	0.307	134	#N/A	#N/A	#N/A	#N/A	#N/A	#N/A	29	1	92	3
100	0.341	149	17	1	17	1	20	3	26	1	70	2
110	0.376	164	#N/A	#N/A	#N/A	#N/A	#N/A	#N/A	#N/A	#N/A	#N/A	#N/A
120	0.410	179	#N/A	#N/A	#N/A	#N/A	#N/A	#N/A	38	5	#N/A	#N/A
130	0.444	194	#N/A	#N/A	19	1	#N/A	#N/A	#N/A	#N/A	76	2
140	0.478	209	57	17	23	2	#N/A	#N/A	40	2	63	2
150	0.512	224	#N/A	#N/A	23	2	#N/A	#N/A	#N/A	#N/A	68	2
160	0.546	239	#N/A	#N/A	#N/A	#N/A	#N/A	#N/A	#N/A	#N/A	82	4
170	0.581	254	4	1	20	2	#N/A	#N/A	15	1	47	3
180	0.615	269	#N/A	#N/A	#N/A	#N/A	#N/A	#N/A	#N/A	#N/A	50	1
190	0.649	284	#N/A	#N/A	#N/A	#N/A	#N/A	#N/A	#N/A	#N/A	47	2
200	0.683	299	32	13	11	0	21	2	20	1	67	2

Table B.6: Sensible time constant, τ_s, obtained from the transient **temperature** response data of all the coatings obtained from MatLab™ curve fits and the respective known face velocity of the air flowing across the sheets for the **desorption** process.

Coating Type →			Blank Coating		Industrial Coating		Fine Coating Half Sheets		Fine Coating		Coarse Coating	
Volumetric Flowrate (L/min)	Face Velocity (m/s)	Reynolds Number (Re)	Time Constant τ_s	95% Pred. Bound error(τ_s)	Time Constant τ_s	95% Pred. Bound error(τ_s)	Time Constant τ_s	95% Pred. Bound error(τ_s)	Time Constant τ_s	95% Pred. Bound error(τ_s)	Time Constant τ_s	95% Pred. Bound error(τ_s)
12	0.041	18	230	30	230	19	155	7	684	19	1245	12
16	0.055	24	175	13	180	14	#N/A	#N/A	383	10	833	8
20	0.068	30	148	13	200	16	109	6	296	7	646	6
30	0.102	45	84	8	#N/A	#N/A	#N/A	#N/A	#N/A	#N/A	403	4
40	0.137	60	47	8	#N/A	#N/A	#N/A	#N/A	#N/A	#N/A	#N/A	#N/A
50	0.171	75	#N/A	#N/A	25	1	#N/A	#N/A	78	3	242	3
60	0.205	90	38	4	32	3	50	3	74	2	199	4
70	0.239	105	#N/A	#N/A	32	2	#N/A	#N/A	47	2	200	3
80	0.273	119	22	1	#N/A	#N/A	#N/A	#N/A	#N/A	#N/A	#N/A	#N/A
90	0.307	134	#N/A	#N/A	#N/A	#N/A	#N/A	#N/A	49	2	147	3
100	0.341	149	13	2	33	5	20	1	52	1	134	3
110	0.376	164	#N/A	#N/A	#N/A	#N/A	#N/A	#N/A	#N/A	#N/A	#N/A	#N/A
120	0.410	179	#N/A	#N/A	#N/A	#N/A	#N/A	#N/A	40	3	#N/A	#N/A
130	0.444	194	#N/A	#N/A	16	1	#N/A	#N/A	#N/A	#N/A	86	3
140	0.478	209	4	1	17	2	#N/A	#N/A	36	1	83	2
150	0.512	224	#N/A	#N/A	#N/A	#N/A	#N/A	#N/A	#N/A	#N/A	86	2
160	0.546	239	#N/A	#N/A	#N/A	#N/A	#N/A	#N/A	#N/A	#N/A	68	2
170	0.581	254	20	3	11	1	#N/A	#N/A	27	1	63	3
180	0.615	269	#N/A	#N/A	#N/A	#N/A	#N/A	#N/A	#N/A	#N/A	58	3
190	0.649	284	#N/A	#N/A	#N/A	#N/A	#N/A	#N/A	#N/A	#N/A	60	4
200	0.683	299	22	9	21	1	9	1	18	1	60	1

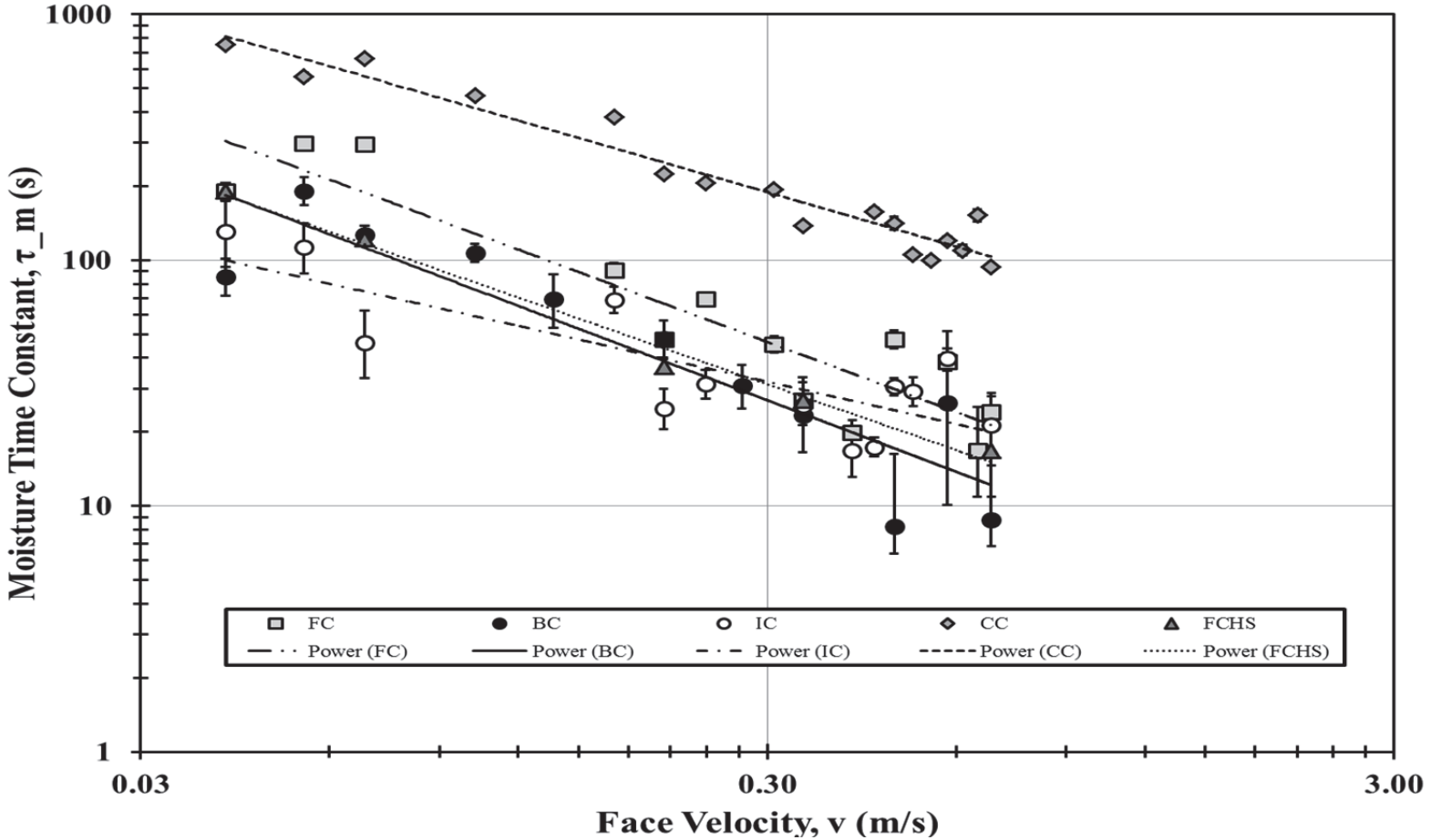

Figure B.1: Moisture time constant, τ_m^*, obtained from the transient **humidity** response data of all the coatings obtained from MatLab™ curve fits plotted against the known face velocity, *v*, of the air flowing across the sheets for the **adsorption** process. The best fit lines are power fits obtained through Excel™.

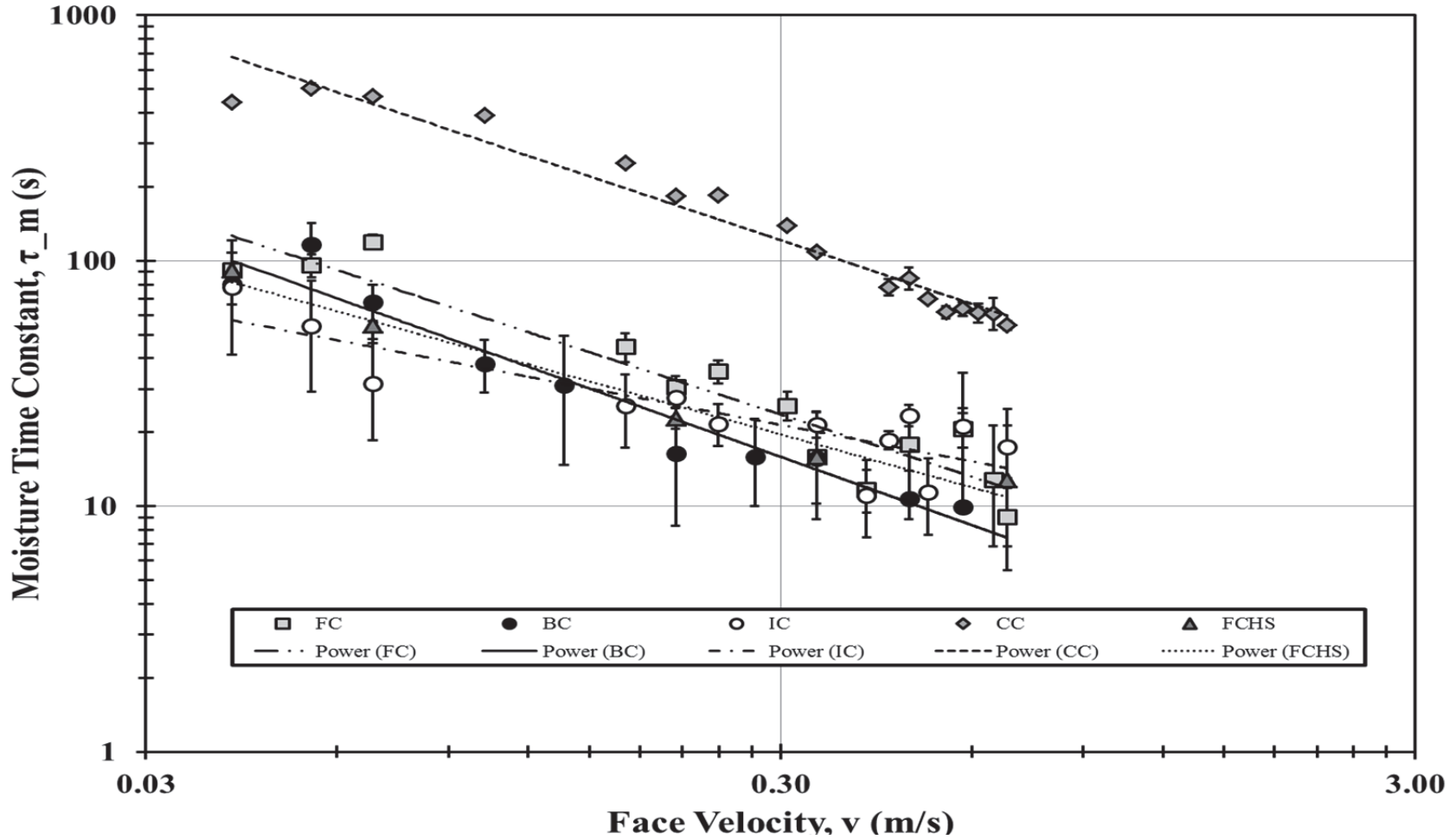

Figure B.2: Moisture time constant, τ_m^*, obtained from the transient **humidity** response data of all the coatings obtained from MatLab™ curve fits plotted against the known face velocity, *v*, of the air flowing across the sheets for the **desorption** process. The best fit lines are power fits obtained through Excel™.

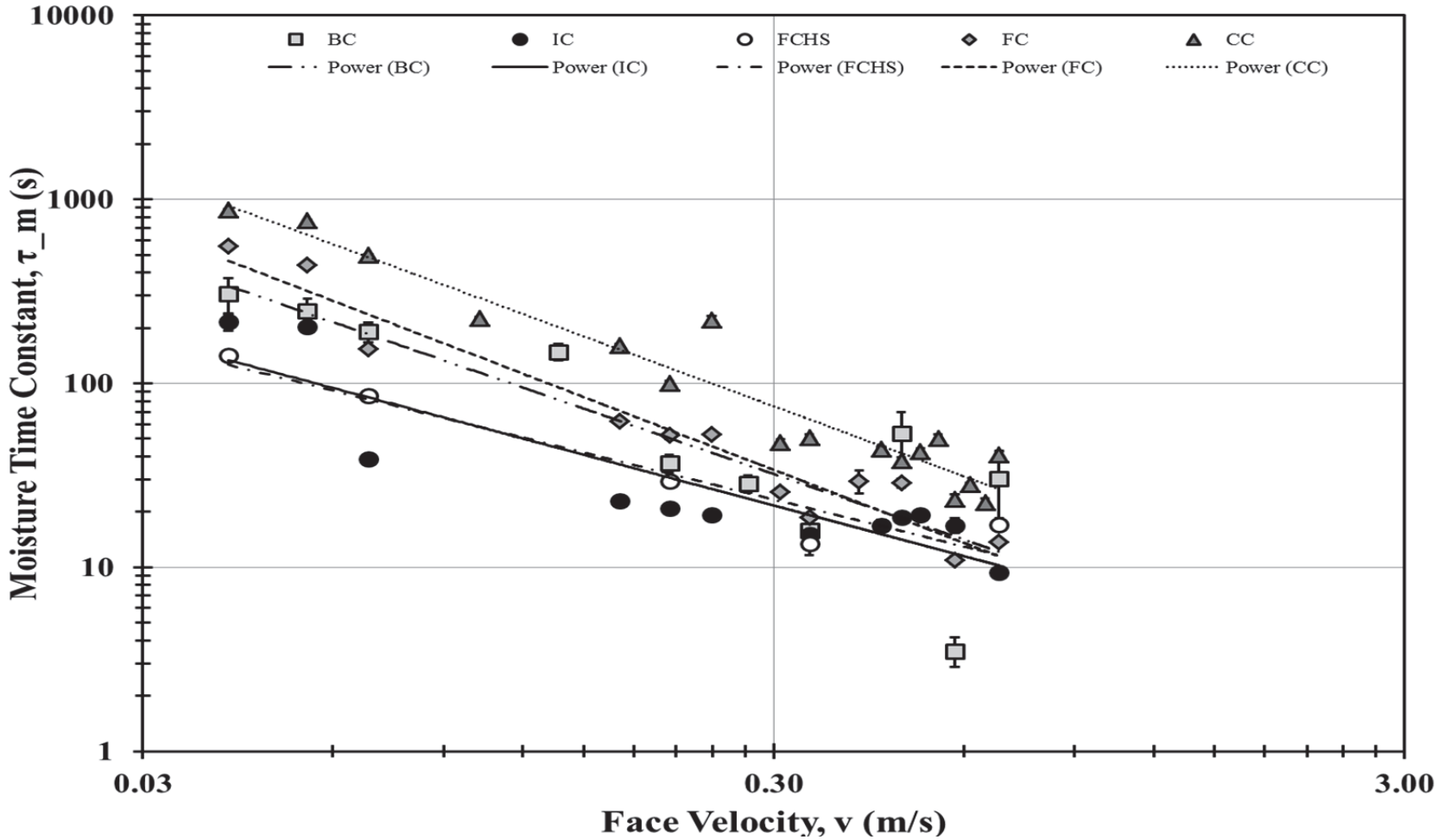

Figure B.3: Moisture time constant, τ_m^*, obtained from the transient **temperature** response data of all the coatings obtained from MatLab™ curve fits plotted against the known face velocity, *v*, of the air flowing across the sheets for the **adsorption** process. The best fit lines are power fits obtained through Excel™.

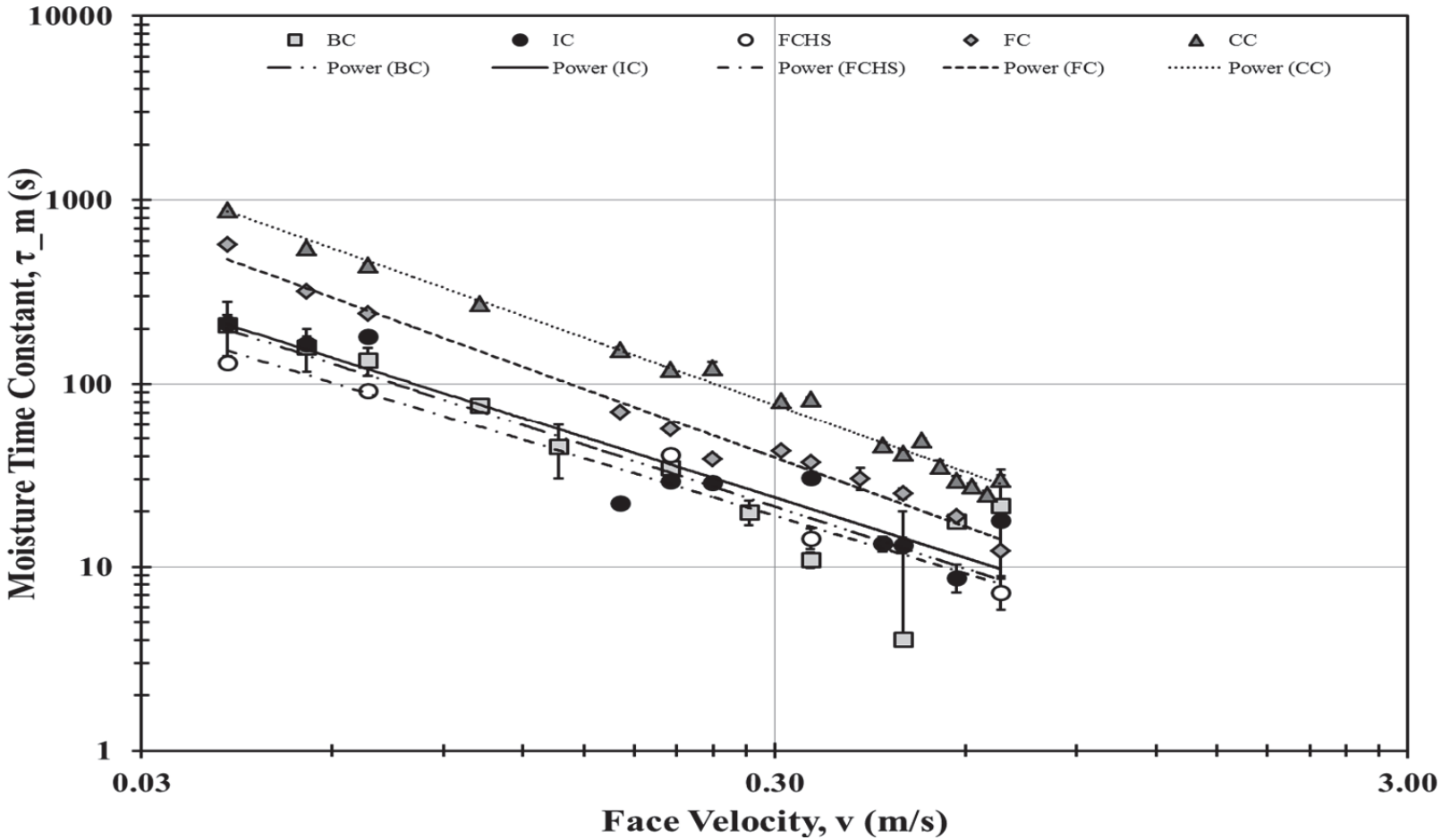

Figure B.4: Moisture time constant, τ_m^*, obtained from the transient **temperature** response data of all the coatings obtained from MatLab™ curve fits plotted against the known face velocity, *v*, of the air flowing across the sheets for the **desorption** process. The best fit lines are power fits obtained through Excel™.

Table B.7: Overall moisture time constants, τ_m^* in seconds, presented as power functions of the face velocity, *v*, in m/s, as taken from **adsorption moisture** response data. Least squared approximations taken from Excel™ in Figure B.1.

CC:	$\tau_m^* = 77.983v^{-0.734}$	$R^2 = 0.943$	B–1
FC:	$\tau_m^* = 14.876v^{-0.946}$	$R^2 = 0.855$	B–2
FCHS:	$\tau_m^* = 10.73v^{-0.888}$	$R^2 = 0.989$	B–3
IC:	$\tau_m^* = 16.074v^{-0.734}$	$R^2 = 0.677$	B–4
BC:	$\tau_m^* = 8.409v^{-0.966}$	$R^2 = 0.825$	B–5

Table B.8: Overall moisture time constants, τ_m^* in seconds, presented as power functions of the face velocity, *v*, in m/s, as taken from **desorption moisture** response data. Least squared approximations taken from Excel™ in Figure B.2.

CC:	$\tau_m^* = 42.934v^{-0.863}$	$R^2 = 0.958$	B–6
FC:	$\tau_m^* = 8.587v^{-0.842}$	$R^2 = 0.898$	B–7
FCHS:	$\tau_m^* = 8.274v^{-0.717}$	$R^2 = 0.975$	B–8
IC:	$\tau_m^* = 11.831v^{-0.494}$	$R^2 = 0.748$	B–9
BC:	$\tau_m^* = 5.228v^{-0.924}$	$R^2 = 0.944$	B–10

Table B.9: Overall moisture time constants, τ_m^* in seconds, presented as power functions of the face velocity, *v*, in m/s, as taken from **adsorption temperature** response data. Least squared approximations taken from Excel™ in Figure B.3.

CC:	$\tau_m^* = 16.454v^{-0.935}$	$R^2 = 0.935$	B–11
FC:	$\tau_m^* = 6.937v^{-1.316}$	$R^2 = 0.945$	B–12
FCHS:	$\tau_m^* = 8.425v^{-0.847}$	$R^2 = 0.912$	B–13
IC:	$\tau_m^* = 7.205v^{-0.915}$	$R^2 = 0.801$	B–14
BC:	$\tau_m^* = 7.735v^{-1.182}$	$R^2 = 0.728$	B–15

Table B.10: Overall moisture time constants, τ_m^* in seconds, presented as power functions of the face velocity, *v*, in m/s, as taken from **desorption temperature** response data. Least squared approximations taken from Excel™ in Figure B.4.

CC:	$\tau_m^* = 17.704v^{-1.219}$	$R^2 = 0.988$	B–16
FC:	$\tau_m^* = 8.453v^{-1.251}$	$R^2 = 0.985$	B–17
FCHS:	$\tau_m^* = 5.413v^{-1.043}$	$R^2 = 0.968$	B–18
IC:	$\tau_m^* = 6.415v^{-1.093}$	$R^2 = 0.897$	B–19
BC:	$\tau_m^* = 5.535v^{-1.120}$	$R^2 = 0.944$	B–20

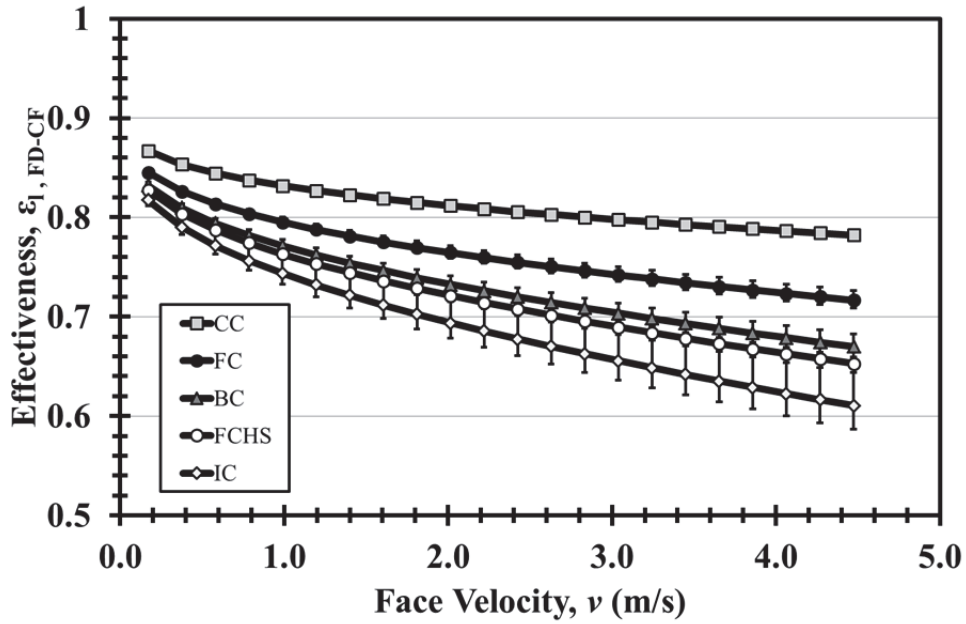

Figure B.5: Latent effectiveness as a function of face velocity (m/s), v, as found from the **humidity adsorption** response results for all of the coatings CC, FC, FCHS, IC and BC. At an operating wheel speed of 20 rpm.

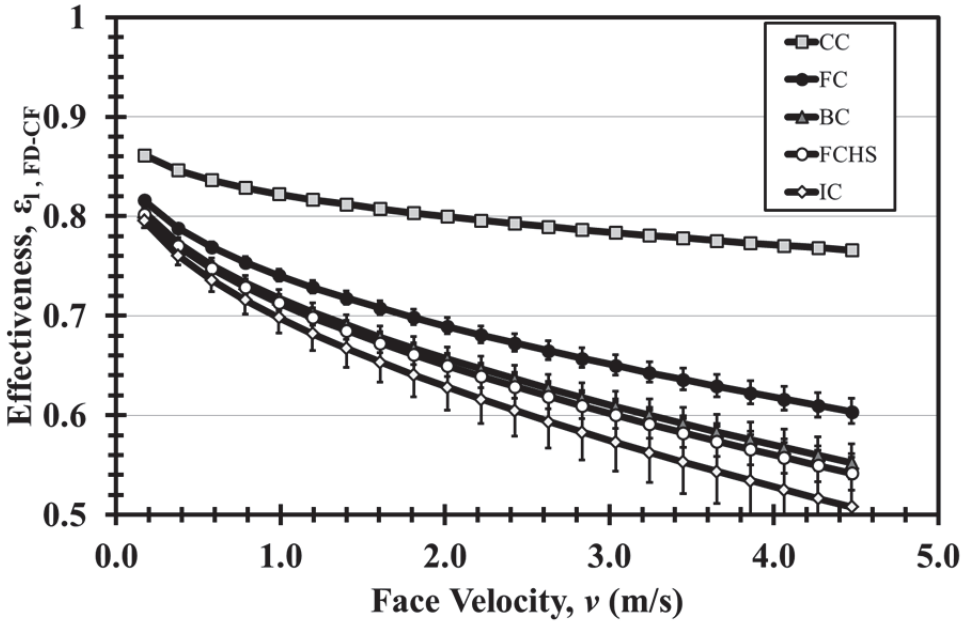

Figure B.6: Latent effectiveness as a function of face velocity (m/s), v, as found from the **humidity desorption** response results for all of the coatings CC, FC, FCHS, IC and BC. At an operating wheel speed of 20 rpm.

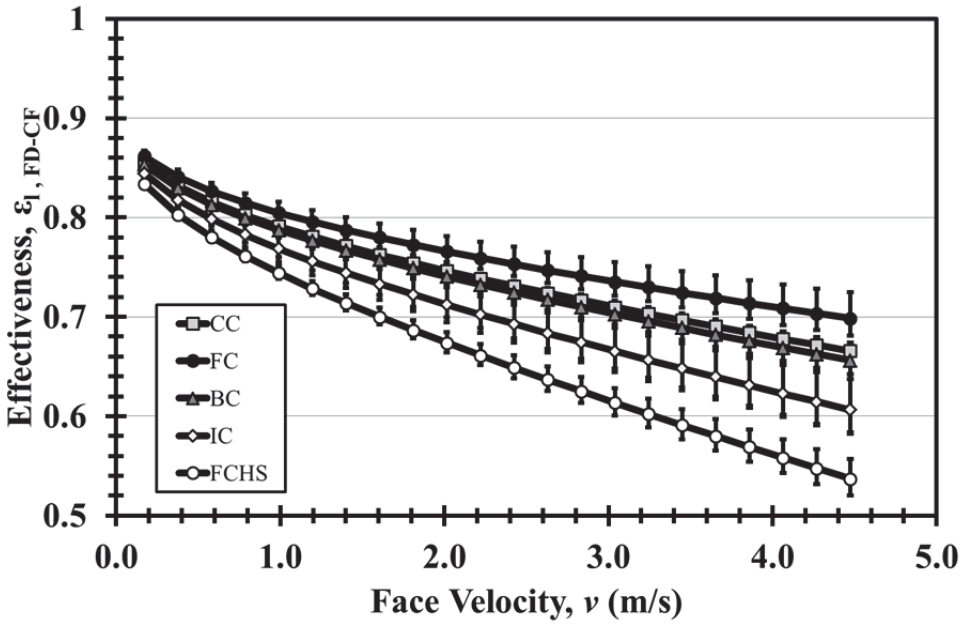

Figure B.7: Latent effectiveness as a function of face velocity (m/s), v, as found from the **temperature adsorption** response results for all of the coatings CC, FC, FCHS, IC and BC. At an operating wheel speed of 20 rpm.

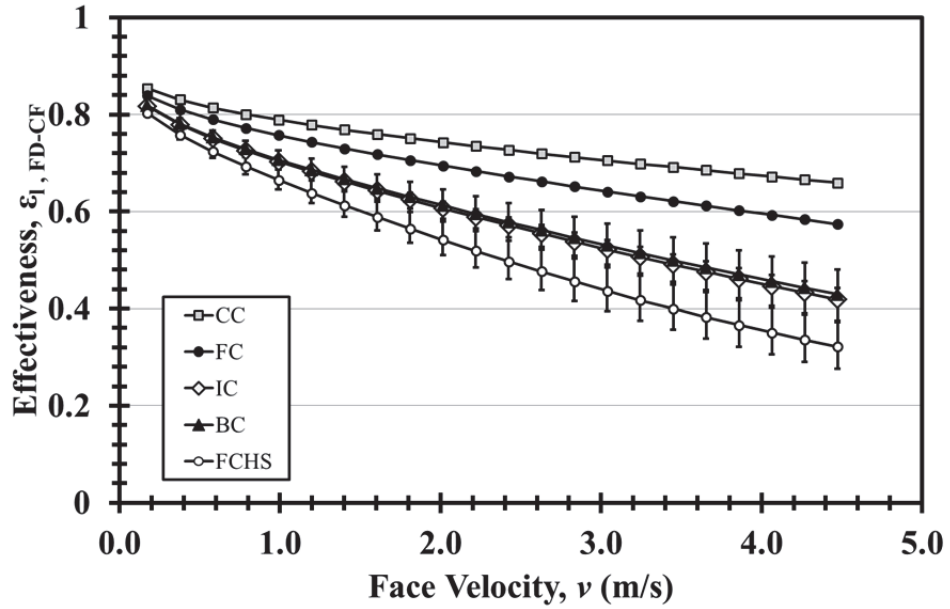

Figure B.8: Latent effectiveness as a function of face velocity (m/s), v, as found from the **temperature desorption** response results for all of the coatings CC, FC, FCHS, IC and BC. At an operating wheel speed of 20 rpm.

APPENDIX C:
INSTRUMENTATION INFORMATION AND CALIBRATION

Table C.1: Environment chamber data collection used for sensor calibration.

RH %	Temp. 1 ºC	RH 1 Volts	Temp. 2 ºC	RH 2 Volts	Temp. 3 ºC	RH 3 Volts	Temp. 4 ºC	RH 4 Volts	Power Supply Volts
10.00	23.91	1.23	23.92	1.20	23.73	1.22	24.02	1.21	5.00
20.00	23.88	1.53	23.91	1.50	23.70	1.51	23.97	1.50	5.00
30.00	23.81	1.85	23.85	1.81	23.64	1.82	23.90	1.81	5.00
40.00	23.83	2.16	23.82	2.12	23.63	2.13	23.88	2.12	5.00
50.00	23.79	2.50	23.80	2.44	23.59	2.46	23.89	2.45	5.00
60.00	23.78	2.85	23.81	2.79	23.57	2.81	23.83	2.79	5.00
70.00	23.75	3.19	23.79	3.12	23.53	3.14	23.85	3.13	5.00
80.00	23.72	3.52	23.78	3.45	23.49	3.47	23.83	3.46	5.00
90.00	23.67	3.84	23.78	3.76	23.43	3.79	23.82	3.78	5.00
95.00	23.65	3.98	23.72	3.90	23.37	3.93	23.78	3.92	5.00

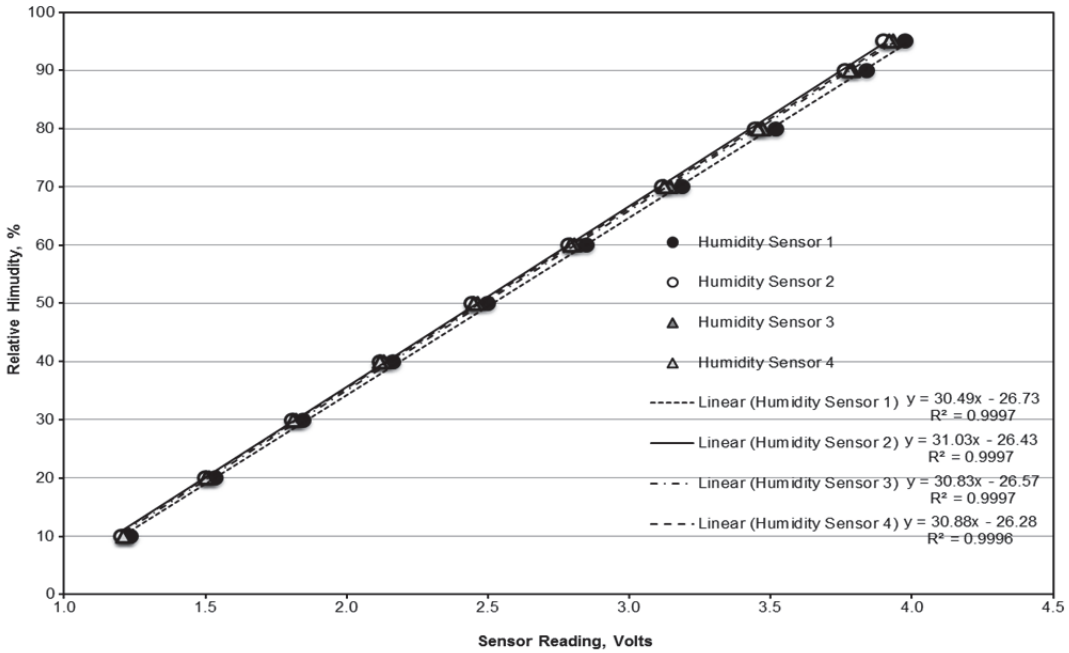

Figure C.1: Calibration for raw transient humidity data in voltage at various set relative humidities within a well regulated environment chamber at a specified 24ºC.

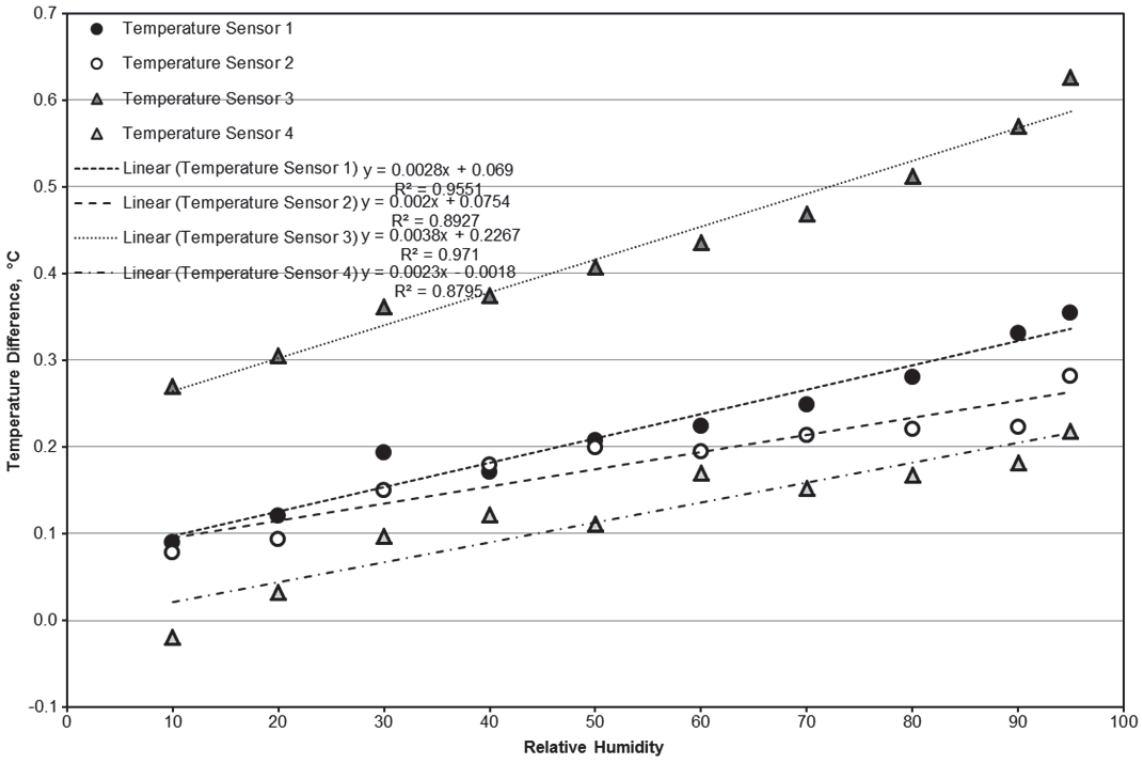

Figure C.2: Calibration for temperature correction in ºC due to change in humidity at various set relative humidities within a well regulated environment chamber at a specified 24ºC.

APPENDIX D:
PERMISSION FROM PUBLISHERS TO USE FIGURES

The following printout of the emails outlines the permission from ASHRAE:

Gmail by Google

John Bolster <john.bolster@gmail.com>

Permission to reproduce Figures

Harr, Julie <JHarr@ashrae.org> Thu, Jun 28, 2012 at 7:46 AM
To: "john.bolster@gmail.com" <john.bolster@gmail.com>
Cc: "Phillips, Michshell" <mphillips@ashrae.org>, "Michaels, Cindy" <CMichaels@ashrae.org>

Dear Mr. Bolster:

Thank you for your inquiry. Permission is granted without royalty fee for the use of the 4 figures from ASHRAE Transactions & the Research Journal.

Conditions of use are as follows:

- Use of this material is limited to one-time use as stated in attached request.
- ASHRAE copyright notice must appear. (see below)
- Use of this ASHRAE content may not be done in a way that will state or imply ASHRAE endorsement.
- No additional distribution or reproduction may be made without the permission of ASHRAE.
- The licensee may not sell the individual reprints.
- This permission should not be construed that ASHRAE is waiving any copyright protection or other rights entitled to its intellectual property.
- If the requestor modifies the content in any way, the credit line must note that the information has been modified or is based on the original ASHRAE content.

Transactions Copyright notice to read:

©ASHRAE www.ashrae.org. ASHRAE Transactions, (Vol #), (Part #), (month), (year).

HVAC&R Research Journal Copyright notice to read:

©ASHRAE www.ashrae.org. HVAC&R Research, (Vol #), (Part #), (month), (year).

Best regards,

Julie Harr

Julie Harr, Administrative Assistant
ASHRAE
1791 Tullie Cir. Atlanta, GA 30329
Direct Line: 678-539-1217 Fax: 678-539-2217 eMail: JHarr@ashrae.org Web: www.ASHRAE.org

From: Michaels, Cindy
Sent: Thursday, June 28, 2012 9:44 AM
To: Harr, Julie
Subject: FW: Permission to reproduce Figures

Hey, Julie. Below is the request for permissions I received yesterday. Thanks!! Cindy

Cindy Michaels, Managing Editor of Special Publications

Extension: 1131 eMail: CMichaels@ashrae.org

From: John Bolster [mailto:john.bolster@gmail.com]
Sent: Wednesday, June 27, 2012 4:06 PM
To: Michaels, Cindy
Subject: Fwd: Permission to reproduce Figures

Michahell is out of the office so I was hoping you may be able to help.

Thank you so much,

John Bolster

——— Forwarded message ———
From: John Bolster <john.bolster@gmail.com>
Date: Wed, Jun 27, 2012 at 1:49 PM
Subject: Permission to reproduce Figures
To: mphillips@ashrae.org

Dear Michshell Phillips,

I am currently writing my M.Sc. Thesis at the University of Saskatchewan and am seeking to obtain permission to reprint 4 figures from the ASHRAE journals Transactions: Research and HVAC&R.

The figures I am wanting to reproduce are as follows:

Figure 1:

Reprinted from "Transient Humidity Measurements for Flow Through an Energy Wheel." Wang, Y. H., Besant, R. W., and Simonson, C. J. 2005. ASHRAE Transactions: Research no. 111 (2):353-369. Copyright 2005 ASHRAE. Reprinted with permission.

Figures 3, 4, 5:

Reprinted/Adapted from "Effectiveness of Desiccant Coated Regenerative Wheels from Transient Response Characteristics and Flow Channel Properties - Part I. Development of Effectiveness Equations." Shang, W., and Besant, R. W. 2009. HVAC&R Research no. 15 (2):329-346. Copyright 2009 ASHRAE. Reprinted/Adapted with permission.

The figures will be properly cited and credited as outlined above.

Thank you,

John Bolster

End of ASHRAE email.